Development and verification of nuclear calculation methods for light-water reactors

Forskningscenter Risø, Roskilde

Publication date:
1970

Document Version
Publisher's PDF, also known as Version of record

Risö Report No. 235

Risö Report No. 235

Danish Atomic Energy Commission

Research Establishment Risö

Development and Verification of Nuclear Calculation Methods for Light-Water Reactors

by K.E. Lindstrøm Jensen

December, 1970

Sales distributors: Jul. Gjellerup, 87, Sölvgade, DK-1307 Copenhagen K, Denmark

Available on exchange from: Library, Danish Atomic Energy Commission, Risö, DK-4000 Roskilde, Denmark

U. D. C.
621.039.51 :621.039.524.44

December, 1970 Risø Report No. 235

Development and Verification of Nuclear Calculation Methods for Light-Water Reactors

by

K. E. Lindstrøm Jensen

Danish Atomic Energy Commission
Research Establishment Risø
Reactor Physics Department

Abstract

The nuclear calculation methods for light-water reactors developed in the *TWODIM SYSTEM of programmes* are described. Several methods for unit cell, assembly and over-all reactor burn-up investigations are available. The true irradiation history may thus be followed with respect to local flux spectrum and power changes where the leakage influence from the surrounding lattice on the local unit cell calculation is accounted for. A new accurate method is introduced for the control rod treatment. The applicability of the various computation methods is verified by means of a great number of detailed calculations that are compared with available measurements.

This report was written in partial fulfilment of the requirements for obtaining the Ph. D. (lic. techn.) degree.

ISBN 87 550 0061 4

CONTENTS

Page

1. INTRODUCTION

Nuclear calculation methods for accurate prediction of depletion and build-up of isotopes in fuel that undergoes burn-up, and for the associated influences on reactivity characteristics and power distributions of nuclear reactors are increasingly more important from physics and economic points of views as nuclear power becomes economically competitive. From a physics point of view the knowledge of the fuel isotopic composition and its distribution in a reactor is necessary for accurate prediction of the power distribution as the fuel burn-up proceeds. This is important for design and analysis of power reactors to ensure safe and stable operation. From an economic point of view, it is essential to correctly predict core lifetime, energy generation of given fuel charges and production of plutonium as these are important factors in the cost of nuclear power. Accurate investigations are also necessary to achieve economic reactor design and operation by means of selected fuel and control management strategies.

In the last few years there has been an increasing interest in light-water reactors at Risö, and as the nuclear calculation methods for light-water reactors had not been thoroughly investigated, the present project was initiated with the primary objective of developing and investigating the various computation methods in connection with a subsequent experimental verification.

A foreign unit cell burn-up programme was implemented at Risö for increased knowledge of the nuclear physics and the current unit cell calculation methods for light-water reactors.

A general investigation of the two-dimensional multi-energy group diffusion equation and its solution was performed with emphasis on different convergence accelerating methods for the flux solution.

This flux solution was used in a fast, approximative burn-up method for the whole reactor that employs an interpolation in tabulated macroscopic cross sections.

The one-dimensional multi-energy group collision probability equation and convergence accelerating methods for the flux solution were investigated for later application to arbitrary space and energy condensation of cross sections.

This flux solution was also applied in a fast unit cell burn-up method where the coupled partial differential equations for the isotopic chains are solved by a fast, purely numerical method.

A combined unit cell and over-all calculation method that solves the complex local - global burn-up problem where the influence from the surrounding lattice on the local calculation is accounted for was finally developed.

These calculation methods constitute the fundamental principles in the TWODIM SYSTEM of programmes for nuclear light-water reactor calculations.

The programme system was experimentally verified by means of detailed unit cell, single assembly and over-all reactor burn-up calculations that were compared with measurements for the first and second cores of the Yankee reactor, the lifetime of which was directly simulated.

The various programmes were mostly run in on the GIER computer at Risö and later transferred to the IBM 7094 computer at NEUCC (Northern Europe University Computing Centre) at the Technical University of Denmark in Lyngby where also the calculations were performed.

2. THE TWODIM SYSTEM OF PROGRAMMES FOR NUCLEAR LIGHT-WATER REACTOR CALCULATIONS

The TWODIM SYSTEM of programmes for nuclear light-water reactor calculations is shown in fig. 1 where also the magnetic tape file transfer of data between the programmes is indicated. The system covers a wide range of nuclear light-water reactor calculation methods from the unit cell to the assembly and the over-all reactor treatments. Integral transport theory and diffusion theory are applied for the stationary flux solution, and the time-dependent irradiation is followed in the quasistationary approach by means of various burn-up methods.

The transfer of data is normally from programmes with many groups and poor spatial dissolution to programmes with fewer groups and better spatial dissolution.

It originates in the LASER unit cell burn-up programme that was used as the primary source of nuclear cross section data throughout the project on account of the built-in multi-group cross section libraries. The CROSS MACRO data processing programme may provide macroscopic and homogenized cross sections for direct application in over-all reactor calculations with the two-dimensional diffusion equation programmes TWODIM for the stationary flux solution and DBU and CDB for time-dependent burn-up investigations. The CELL cross section condensation programme and the HECS gamma-matrix calculation programme determine equivalent cross sections and boundary conditions for proper representation of for example control regions in over-all diffusion theory calculations respectively. The CROSS MICRO data processing programme provides microscopic cross section libraries for the fast unit cell burn-up programme CEB and for the treatment of the individual fuel rods in the combined unit cell and over-all reactor CDB programme.

The overlay structures of the various programmes are shown in figs. 2 through 8, and the functions of the indicated subroutines and procedures are explained in the appendix.

The fundamental physical and mathematical methods developed and employed in these programmes and the associated physical consequences are now described and discussed in the subsequent sections.

3. THE LASER - CROSS COMPLEX FOR NUCLEAR CROSS SECTION DATA

In the beginning of the project the LASER unit cell burn-up programme developed by Westinghouse was implemented at Risö for increased knowledge of the nuclear physics of light-water reactors and the associated current unit cell burn-up calculation methods used in the United States. The programme was the primary source of nuclear cross section data throughout the project. It may be coupled to the cross section data processing programme CROSS.

3.1. The LASER Unit Cell Burn-up Programme

The LASER programme determines the time-dependent variation in the spatial distribution of the neutron flux spectrum and the fuel composition within a heterogeneous reactor lattice cell by means of a one-dimensional (cylindric), 85 energy group treatment in the range 0-10 MeV. In the thermal range 0 - 1.855 eV the calculation is based on a modified version of the thermalization transport theory programme THERMOS (ref. 1) that solves the one-dimensional, 35 group integral transport equation subjected to isotropic scattering. The energy meshes give accurate representations of the 0.30 eV Pu^{239} and the 1.056 eV Pu^{240} resonances. In the fast energy range 1.855 eV - 10 MeV a modified version of the slowing-down programme MUFT (ref. 2) solves the homogeneous B-1 transport equation approximation in 50 energy groups.

The LASER programme is consistent and independent in the sense that multi-group cross sections for most elements that occur in nuclear reactor physics calculations are provided by the programme. The thermal cross section library is on tape, while the fast library is on cards and forms an integral part of the programme.

The reader interested in further details concerning the LASER programme is referred to refs. 3 and 4.

The various calculation methods and basic nuclear cross section data that constitute the LASER programme have been verified in several investigations (refs. 3, 5, 6, and 7).

The LASER programme is written in FORTRAN 4, and the overlay structure is shown in fig. 2. The additional subroutines THER and FAST at each time step couple the LASER calculation with a magnetic tape file to the data processing programme CROSS described in the following section.

3.2. The CROSS Data Processing Programme

Two nearly identical versions of the CROSS programme exist. The CROSS MACRO version provides arbitrary energy-condensed multi-group, macroscopic and homogenized cross sections for later application in overall reactor investigations. The CROSS MICRO version determines optional energy-condensed multi-group microscopic cross sections for later use in unit cell calculations.

The CROSS programme is written in FORTRAN 4, and the overlay structure is shown in fig. 3.

3.2.1. Macroscopic, Homogenized Cross Sections

The detailed space-dependent flux spectrum within the fuel cell determined by means of LASER is at each time step applied for space and arbitrary energy condensation to provide macroscopic, homogenized cross sections in less than 85 groups for the unit cell as a function of irradiation.

The slowing-down calculation in LASER is based on the slowing-down density concept, and the elastic transfer cross sections between the groups therefore do not occur explicitely in the programme. For 2 and 3 group problems with the energy boundaries 0 - 1.855 eV - 5.53 keV - 10 MeV the transfer cross section from one group to the group just below it is obtained from a neutron conservation principle. For multi-group problems the CROSS MACRO programme calculates the detailed multi-group elastic transfer cross sections by a conventional method (ref. 8).

In the thermal range the LASER programme provides free gas scattering (Wigner-Wilkins) kernels (ref. 9) for all elements. For light water the bound proton scattering kernel of Nelkin (ref. 10) and for heavy water the Honeck extension (ref. 11) are furthermore provided.

In the fast and the thermal ranges the anisotropic scattering is accounted for by transport-corrected self-scattering cross sections

$$\Sigma_T^{g,g} = \Sigma^{g,g} - \bar{\mu}_o \Sigma^g_{\text{elastic}} , \qquad (3.1)$$

where $\Sigma^{g',g}$ is the transfer cross section from group g to group g', and $\Sigma^g_{\text{elastic}}$ is the total elastic scattering cross section in group g. $\bar{\mu}_o = \frac{2}{3A}$, where A is the atomic mass, is the average cosine of the scattering angle per collision in the laboratory system.

For the light- and heavy-water Nelkin kernels in the thermal range the above transport correction is replaced by

$$\Sigma_T^{g,g} = \Sigma_o^{g,g} - \Sigma_1^g , \qquad (3.2)$$

where $\Sigma_o^{g,g}$ is the isotropic scattering kernel, and Σ_1^g is the first-order coefficient in the Legendre expansion of the scattering cross section (ref. 12).

The large transport correction has thus been applied that leaves the off-diagonal transfer cross sections unchanged.

The various space and energy cross section condensation methods in the CROSS MACRO programme are similar to the methods employed in the CELL programme described in section 6.

3.2.2. Microscopic Cross Section Libraries

The CROSS MICRO programme version determines arbitrary energy-condensed multi-group microscopic cross section libraries for later application in the various unit cell treatments.

A library consists of the absorption cross section, the scattering matrix and the production and the fission cross sections for U^{235}, U^{236}, U^{238}, Pu^{239}, Pu^{240}, Pu^{241}, Pu^{242}, and the fission spectrum. Then follows the absorption cross section and the scattering matrix for Xe^{135}, Sm^{149}, fission product and O_2 or Al for the fuel region of the unit cell, succeeded by stainless steel, Al or Zr for the clad region and H_2O or D_2O and B^{10} for the moderator region.

4. TWODIM, A GENERAL PURPOSE TWO-DIMENSIONAL MULTI-GROUP DIFFUSION EQUATION FLUX SOLUTION PROGRAMME

The standard tool for solving of two-dimensional multi-group diffusion problems at Risö has for some years been the English CRAM programme (ref.13). It covers a wide range of practically occurring problems and its advantages are the possibilities of handling very big problems, different kinds of criticality and source problems, and moreover, it has a special output compiler. In fact, it is a huge and complicated programme unfortunately written in the old FORTRAN 2 language, which in itself makes the programme rather slow. Furthermore the special language makes it very sensible to the tape quality used which results in many failed runs. In the numerical treatment the convergence is only partially accelerated. A 30 x 30 mesh point, 2 energy group problem normally requires 50-100 iterations and about 10 minutes on the IBM 7094 computer.

For the solving of two-dimensional, multi-group, time-dependent nuclear reactor physics problems a faster programme was definitely needed. A normal burn-up calculation in the quasistationary approach requires about 50 time steps. Total running time for such a calculation will be of the order of 10 hours if the available programme is used, which is not realistic for production purposes.

To overcome this difficulty a general investigation of the multi-group diffusion equation and its solution were initiated, and a computer programme, TWODIM, about 10 times as fast as CRAM, was worked out.

This section describes the general multi-group diffusion equation and the solution of the associated finite difference equations. This involves solution of an eigenvalue problem as well as inversion of a large matrix. Different accelerating methods which greatly improve convergence and thereby reduce the necessary computer time are presented. Finally a general description of the TWODIM programme is given with optional features and typical running times.

4.1. The Multi-Group Diffusion Equation

The multi-group neutron diffusion equation has the following form:

$$-D^g(r)\nabla^2\varphi^g(r) + S^{g,g}(r)\varphi^g(r) = \sum_{\substack{g'=1 \\ g'\neq g}}^{ng} S^{g,g'}(r)\varphi^{g'}(r) + \lambda X^g(r)\sum_{g'=1}^{ng} F^{g'}(r)\varphi^{g'}(r) + Q^g(r), \quad (4.1)$$

where

$$Q^g(r) = \begin{cases} 0 \text{ for reactivity calculations,} \\ -\varkappa P^g(r)\,\varphi^g(r) \text{ for poison calculations,} \\ \alpha P^g(r) \text{ for source calculations,} \end{cases} \tag{4.2}$$

$$S^{g,\,g'}(r) = \begin{cases} \Sigma^{g' \to g}(r) \text{ for } g' \neq g\,, \\ \Sigma_a^g(r) + \sum\limits_{\substack{g''=1 \\ g'' \neq g}}^{ng} \Sigma^{g'' \to g}(r) \text{ for } g' = g\,, \end{cases} \tag{4.3}$$

$$F^g(r) = \nu\Sigma_f^g(r)\,,$$

$$\lambda = \frac{1}{k_{eff}}\,;$$

the remaining signs are used as follows:

$1 \leq g \leq ng$	energy group index
r	position vector
∇^2	Laplacian operator
$D^g(r)$	diffusion coefficient
$\varphi^g(r)$	neutron flux
$\Sigma_a^g(r)$	absorption cross section
$\Sigma^{g' \to g}(r)$	scattering cross section from group g' to g
$\nu\Sigma^g(r)$	neutron production cross section
$X^g(r)$	neutron fission spectrum
k_{eff}	effective multiplication factor
$P^g(r)$	poison cross section or finite source
$\varkappa$	eigenvalue for poison calculations
α	normalization factor for source calculations.

The boundary conditions which have to be satisfied can be of the con-

ventional type

$$I^g(r) = -D^g(r)\nabla\varphi^g(r) = \lambda^g_{ex}(r)\,\varphi^g(r)\,, \tag{4.4}$$

the usual logarithmic boundary condition, or of an extended type

$$I^g(r) = \sum_{g'=1}^{ng} \gamma^{g-g'}(r)\,\varphi^{g'}(r)\,, \tag{4.5}$$

the gamma-matrix condition. This is similar to the usual one except for the off-diagonal terms, where the detailed up- and down-scattering can be accounted for.

Equation (4.1) is for a non-uniform, rectangular mesh approximated with a five-point difference formula at the mid-points of intersection of the mesh lines (fig. 9) to a set of finite difference equations by means of the method described in ref. 13. This discrete approximation to the original problem results in the following set of algebraic equations for five adjacent, rectangular, homogeneous blocks:

$$a^g_{i,j}\varphi^g_{i,j} - b^g_{i-1,j}\varphi^g_{i-1,j} - b^g_{i,j}\varphi^g_{i+1,j} - c^g_{i,j-1}\varphi^g_{i,j-1} - c^g_{i,j}\varphi^g_{i,j+1} = V_{i,j}\sum_{\substack{g'=1\\ g'\neq g}}^{ng} S^{g,g'}_{i,j}\varphi^{g'}_{i,j} + \lambda\chi^g_{i,j}V_{i,j}\sum_{g'=1}^{ng} F^{g'}_{i,j}\varphi^{g'}_{i,j} + V_{i,j}Q^g_{i,j}\,, \tag{4.6}$$

where

$$a^g_{i,j} = b^g_{i-1,j} + b^g_{i,j} + c^g_{i,j-1} + c^g_{i,j} + S^{g,g}_{i,j}V_{i,j}\,, \tag{4.7}$$

$$b^g_{i,j} = \frac{\dfrac{D^g_{i+1,j}}{\Delta x_{i+1}}}{1 + \dfrac{D^g_{i+1,j}\Delta x_i}{D^g_{i,j}\Delta x_{i+1}}} \times 2A_{i+1,j}\,, \tag{4.8}$$

$$c^g_{i,j} = \frac{\dfrac{D^g_{i,j+1}}{\Delta y_{j+1}}}{1 + \dfrac{D^g_{i,j+1}\Delta y_j}{D^g_{i,j}\Delta y_{j+1}}} \times 2A_{i,j+1} \; ; \qquad (4.9)$$

the remaining signs are used as follows:

$1 \leq i \leq mx$	horizontal mesh index
$1 \leq j \leq my$	vertical mesh index
$V_{i,j}$	volume of mesh i, j
$A_{i+1,j}$	right surface area of mesh i, j
Δx_i	horizontal mesh width of mesh i, j
Δy_j	vertical mesh width of mesh i, j .

For the outer boundaries and for interior meshes where a boundary condition is used, the boundary conditions for the original problem are complied with if the following constraints are applied to the set of equations for boundary meshes:

$\varphi^g_{i+1,j} = 0$	a boundary condition is
$\Delta x_{i+1} = 1$	used for mesh i+1, j (fig. 10)
$D^g_{i+1,j} = \frac{1}{2}\lambda^g_{ex,\, i+1,\, j}$	

If a gamma-matrix condition is utilized, the diagonal terms will go through a similar treatment. The off-diagonal terms will be accounted for as a scattering contribution in the neighbour mesh from the relationship on the interface (fig. 11):

$$-I^g_{i+b,j} A_{i+1,j} = -A_{i+1,j} \sum_{\substack{g'=1 \\ g' \neq g}}^{ng} \gamma^{g \leftarrow g'}_{i+1,j} \varphi^{g'}_{i+b,j} =$$

$$= V_{i,j} \sum_{\substack{g'=1 \\ g' \neq g}}^{ng} \Sigma^{g \leftarrow g'}_{i,j} \varphi^{g'}_{i,j}. \qquad (4.10)$$

where $I^{g}_{i+b,j}$ and $\varphi^{g}_{i+b,j}$ are taken on the boundary. In case of a small width for the neighbour mesh $\varphi^{g}_{i+b,j} \sim \varphi^{g}_{i,j}$ gives

$$\Sigma^{g\to g'}_{i,j} \sim -\frac{A_{i+1,j}}{V_{i,j}} \gamma^{g\to g'}_{i+1,j} \quad \text{for } g' \neq g\,, \tag{4.11}$$

The above derivations all refer to XY geometry. However, only minor modifications are necessary for the extension to RZ and Rθ geometry.

4.2. Solution of the Difference Equations

The finite difference equations (4.6) are now given a form which is more convenient for further treatment. If the Q term which necessitates a special treatment of the problem given in a later section is neglected, these equations can in matrix notation be written

$$A\varphi = S\varphi + \lambda F\varphi\,, \tag{4.12}$$

where A represents the leakage, the absorption and out-scattering from the individual energy groups. S contains the transfer cross sections and F the fission spectrum and neutron production. By introducing

$$M = A - S \tag{4.13}$$

in equation (4.12) we obtain the equation

$$M\varphi = \lambda F\varphi \tag{4.14}$$

or

$$M^{-1}F\varphi = \left(\frac{1}{\lambda}\right)\varphi\,. \tag{4.15}$$

4.2.1. The Eigenvalue Problem

Equation (4.15) has the form of a usual eigenvalue problem. The largest eigenvalue for the $M^{-1}F$ matrix is real and positive (ref. 14) and the whole problem consists in finding this eigenvalue and its associated eigenvector. This is done by the following sequence of approximate flux

vectors:

$$\varphi_j = \lambda_{j-1} M^{-1} F \varphi_{j-1} , \tag{4.16}$$

where

$$\lambda_{j-1} = \frac{E^T M \varphi_{j-1}}{E^T F \varphi_{j-1}} , \tag{4.17}$$

j is the iteration index and E^T a transposed unit vector. These are the outer iterations for the power method, and they converge to the eigenvalue of largest magnitude $(1/\lambda)$ for $M^{-1}F$.

The inversion of the M matrix requires special attention. It has dimensions of the order of ng × mx × my, which for a 20 energy group, 25 × 25 mesh problem will comprise about 150 mill. numbers for a full matrix. Direct inversion methods are impossible owing to the limited core store capacity of present-day computers. Furthermore it seems impractical since it has a huge amount of zero entries. Instead a band-matrix treatment is applied, where M is inverted by an iterative method called the inner iterations.

4.2.2. The Block Successive Overrelaxation Scheme

The inner iteration problem for inversion of M is tantamount to solving of the system of equations

$$A \varphi = k , \tag{4.18}$$

where A is symmetric with positive diagonal elements and non-positive off-diagonal elements. Furthermore the A matrix is irreducibly diagonally dominant, and there exists a splitting of A that leaves A block-tridiagonal

$$A = A_D - A_L - A_U , \tag{4.19}$$

where A_D is a tridiagonal matrix and A_L and A_U strictly lower and upper triangular matrices.

With the partitioned matrix A equation (4.18) is transformed to

$$A_D \varphi = (A_L + A_U)\varphi + k, \tag{4.20}$$

from which follows the block Jacobi iterative method

$$\varphi_j = \underbrace{A_D^{-1}(A_L + A_U)}_{B}\varphi_{j-1} + A_D^{-1} k , \tag{4.21}$$

B is the block Jacobi matrix.

Similarly the block successive overrelaxation iterative method is defined by (ref. 14)

$$\varphi_j = \underbrace{(I - \omega A_D^{-1} A_L)^{-1}\left\{\omega A_D^{-1} A_U + (1-\omega) I\right\}}_{L_\omega}\varphi_{j-1} +$$

$$\omega (I - \omega A_D^{-1} A_L)^{-1} A_D^{-1} k , \tag{4.22}$$

where L_ω is the block successive overrelaxation matrix. I is the unit matrix and ω the relaxation factor $0 < \omega < 2$. When $1 < \omega$ ($\omega < 1$), the iteration scheme (4.22) is referred to as overrelaxation (underrelaxation).

4.2.3. The Optimum Relaxation Factor

The fundamental convergence accelerating method for the inner iterations is that of finding the value of $\omega = \omega_b$ that maximizes the rate of convergence, or in other words minimizing of the largest eigenvalue, the spectral radius $\bar{\mu}(L_\omega)$, for the L_ω matrix relating successive error vectors.

$$\varepsilon_j = L_\omega \varepsilon_{j-1} \tag{4.23}$$

with

$$\varepsilon_j = \varphi_j - \varphi_{j-1} . \tag{4.24}$$

A is a consistently ordered 2-cyclic matrix, and the relationship between any eigenvalue $\mu(L_\omega)$ for the L_ω matrix and its associated eigenvalue $\mu(B)$ for the Jacobi matrix B is as follows:

$$(\mu(L_\omega) + \omega - 1)^2 = \mu(L_\omega)\,\omega^2\,\mu^2(B) \tag{4.25}$$

with the solution

$$\mu(L_\omega) = \left[\frac{\omega\mu(B)}{2} \pm \sqrt{\frac{\omega^2\mu^2(B)}{4} - (\omega-1)}\right]^2 . \tag{4.26}$$

The eigenvalues $\mu(B)$ of B are real and bounded by the spectral radius $\bar{\mu}(B) < 1$. The value of $\omega = \omega_b$ which minimizes the maximum value of $|\mu(L_\omega)|$ is now sought. The solution to this minimax problem happens for $\sqrt{\quad} = 0$, which gives

$$\omega_b = \frac{2}{1 + \sqrt{1 - \bar{\mu}^2(B)}} , \tag{4.27}$$

where

$$\bar{\mu}(L_{\omega_b}) = \omega_b - 1 . \tag{4.28}$$

Different methods exist for determination of the optimum relaxation factor from equation (4.27) and an estimated $\bar{\mu}(B)$ (ref. 14)

Common for most of these techniques is an a priori numerical method for estimation of $\bar{\mu}(B)$ through some iterations before the actual iteration scheme.

To escape these initial iterations, which leave the original problem untouched, a non a priori method is used, where the actual iterative progress determines improved estimates of $\bar{\mu}(B)$. This was done although Varga in ref. 14 says that these methods are computing art rather than real science!

If $\bar{\mu}(B)$ is known, then equation (4.27), as a monotonic increasing function of $\bar{\mu}(B)$, determines the optimum relaxation factor $1 < \omega_b < 2$. Furthermore, for every ω equation (4.25) gives a relationship between any $\mu(L_\omega)$ and its corresponding $\mu(B)$. These dependencies can be seen in fig. 12, where $\mu(L_\omega)$ is plotted as a function of ω for different $\mu(B)$ values. Inspection of this figure suggests the following iterative

method for determination of the optimum relaxation factor, ω_b.

A value of $\omega = \omega_1$ lower than the anticipated ω_b is chosen. With this relaxation factor applied in the original inner iterative problem, the iterative scheme (4.23), which is the usual power method for the eigenvalue problem

$$\mu(L_{\omega_1})\ \varepsilon = L_{\omega_1}\ \varepsilon\ , \tag{4.29}$$

will determine the largest eigenvalue, the spectral radius $\tilde{\mu}(L_{\omega_1})$, for the L_{ω_1} matrix.

From the real eigenvalue $\tilde{\mu}(L_{\omega_1})$, where $\omega_1 < \omega_b$, its associated positive real eigenvalue $\mu(B)$ is deduced from equation (4.25). An improved estimation of the optimum relaxation factor is deduced from equation (4.27) where $\omega_1 < \omega_2 < \omega_b$. This relaxation factor will, applied to the original inner iterative problem, give a new determination of $\tilde{\mu}(L_{\omega_2})$, the whole process converging against the optimum relaxation factor ω_b.

4.2.4. The Extrapolation Method

For improvement of the convergence rate of the outer iterations they are accelerated by means of an extrapolation procedure. From equations (4.23) and (4.24) it follows that when a uniform convergence rate is discovered, it is possible to estimate the true solution for the flux vector from two successive flux iterates

$$\varphi = \varphi_j + \frac{\varphi_{j+1} - \varphi_j}{1 - \tilde{\mu}(L_\omega)}\ . \tag{4.30}$$

This flux vector is then applied to the fission source for the subsequent outer iteration.

The relationship between the estimated true flux vector and two flux iterates as stated in equation (4.30) serves furthermore as a powerful tool for deciding whether or not a problem has converged. This decision is very important since a loose criterion will result in a probably false solution and a firm one in a sometimes too high degree of accuracy, which consumes too much computer time.

Commonly used criteria relate to successive flux vectors or in more loose cases successive eigenvalues. The convergence rate is not regarded in these criteria.

A method which takes the convergence rate into account may be de-

duced from equation (4.30):

$$\frac{\| \varphi - \varphi_j \|}{\| \varphi_j \|} = \frac{\| \varphi_{j+1} - \varphi_j \|}{\| \varphi_j \| \, (1 - \tilde{\mu}(L_\omega))} < \varepsilon_{crit} , \tag{4.31}$$

where $\| \quad \|$ denotes the usual norm and ε_{crit} the specified criterion for convergence. The convergence rate appears here as the term $1 - \tilde{\mu}(L_\omega)$.

4.2.5. Source and Poison Calculations

For source calculations equation (4.12) will have the following form:

$$E\varphi = \alpha P , \tag{4.32}$$

where

$$E = A - S - \lambda F , \tag{4.33}$$

giving the usual inhomogeneous system of equations, which is solved by the inner iterations. The normalization constant α accelerates the convergence by rebalancing the left and the right sides of equation (4.32) for each iteration.

A direct eigenvalue method may be used to calculate the necessary critical poison corresponding to a given effective multiplication factor. For these problems equation (4.12) has the form

$$A\varphi = S\varphi + \lambda F\varphi - \varkappa_{max} P\varphi + \alpha P\varphi , \tag{4.34}$$

where

$$\varkappa_{max} = \alpha + \varkappa \tag{4.35}$$

is an estimated upper bound for $\varkappa$. The new quantity α is now treated as an eigenvalue which makes equation (4.34) nearly similar to equation (4.14). For the inner iterations the problem is to solve a set of equations similar to equation (4.18) except for the appearance of the matrices F and P with non-zero diagonal entries.

4.3. The TWODIM Programme

The fundamental methods outlined above form the basic principles in the two-dimensional (XY, RZ, R θ), multi-group (maximum ~ 20 groups for 25 x 25 meshes) finite difference equation computer programme TWODIM. The programme was especially designed for the detailed determination of flux and power distributions in light-water fuel element assemblies with a detailed treatment of control rods and water gaps as shown in fig. 13.

A flux representation where the fluxes were assigned to the mid-points instead of the intersections of the mesh lines was chosen. This is enormously advantageous for particular multi-group problems, where the scattering terms in equation (4.6) have smaller storage requirements. Reaction rates are determined quite exactly by means of this English method, whereas the leakage seems to be less precisely determined than with the American one. Furthermore, the leakage constitutes only part of the total neutron balance.

Boundary conditions either in the shape of full gamma matrices or the conventional diagonal terms may be obtained from the HECS programme (ref. 15).

A successive overrelaxation method, SOR, or a successive line over-relaxation method, SLOR, is applied for the inner iterations with the best relaxation factor found. In the SLOR method blocks of horizontal or vertical lines of mesh points may be solved simultaneously in a numerically stable way by means of a tridiagonal forward elimination and backward substitution method. This direct method for the subproblem implies no appreciable further arithmetic efforts compared with the usual point relaxation scheme and it generally gains a factor of $\sqrt{2}$ in convergence rate. More impressive gains can be achieved, especially in problems with non-uniform mesh spacings.

The extension of the method to greater blocks of subproblems is described in ref. 16. The spectral radius for the block Jacobi iterative matrix does indeed decrease as more points are improved simultaneously, which gives a greater (asymptotic) convergence rate (per iteration). However, the increased computational efforts per iteration and associated numerical difficulties due to dangerous accumulation of rounding-off errors seem to make the method less advantageous.

As the spectral radius $\tilde{\mu}(B)$ for the block Jacobi matrix approaches unity, the accurate determination of ω_b becomes more important as can

be seen from the slope of the contours near ω_b in fig. 12. For these slowly converging cases the number of iterations required with successive overrelaxation with ω_b is of the order of magnitude of the square root of the iterations required to obtain the same accuracy with the block Jacobi iterative method.

MacMillan has in ref.17 demonstrated that problems in RΘ geometry are best solved by vertical line relaxation (in the Θ-direction). In other geometries line relaxation parallel to the side where the meshes have smaller or unequal increments has to be preferred.

Inversion of M in equation (4.15) is made by inner iterations. However, numerical experience has shown that normally a single inner iteration is sufficient for many problems, in which case the neutron balance or Equipoise method is applied.

In TWODIM every problem is initiated with one single inner iteration per outer iteration, by which additional inner iterations not always necessary are avoided. If, as the iterations proceed, the problem in some way shows a divergent tendency due to an insufficient inversion of M, the number of inner iterations per outer iteration is doubled, resulting in an always converging method.

The successive overrelaxation method as well as the extrapolation procedure require a set of decision parameters for the different convergence schemes involved. An optimum set, which is built into the programme as a standard option, was determined by numerical experience.

The extrapolation method has shown itself to be a particularly powerful tool for improvement of the convergence rate. The method was extended to treat negative eigenvalues $\bar{\mu}(L_\omega)$ for the successive overrelaxation matrix L_ω as well as the positive ones, which results in a general procedure for extrapolation through equation (4.30).

A mesh-doubling facility is provided in the TWODIM programme where an initial, fast, coarse mesh calculation with a set of doubling factors allows an increasingly finer mesh representation. This initial partial solution of the problem has the same effect as the various rebalancing methods (refs. 16 and 18). Slowly converging problems, which for example may occur with highly non-uniform mesh spacing, large changes in the diffusion constant or with loosely coupled cores, may be greatly accelerated by means of this coarse mesh-doubling facility.

For most problems TWODIM only uses the fast memory store for the iterations. However, if during the calculation the problem exceeds the fast memory store capacity, the programme will automatically shift to a half

as fast magnetic tape version, where a two-tape flip-flop arrangement is used for the intermediate groupwise storage. No drums or discs are available on the IBM 7094 installed at the Technical University of Denmark in Lyngby, which is used for the calculations described throughout this report.

For big problems where the tape version is necessary, it is then an advantage to perform a fast-memory-stored, coarse mesh calculation before the original problem.

Adjoint calculations can be performed simply by transposing of the scattering matrix and interchanging of the neutron fission spectrum and the neutron production cross section in the input to the programme.

The TWODIM programme is written in the ILLINOIS-ALGOL language for the IBM 7094 computer, and the dynamic overlay feature (ref. 19) is used. The link structure is shown in fig. 6.

As for the present status of the programme it can be mentioned that for more than a year it has been used as a standard tool for solving of two-dimensional multi-group diffusion problems at the Reactor Physics Department, Risø.

The programme has been verified by recalculation of several previous CRAM runs.

More than 1000 different problems have been solved during that time with a problem-solving range extending from wind field determination round tall chimneys and sky-scrapers to flux and power distributions in fuel element assemblies, and the over-all behaviour of light- and heavy-water reactors.

One-dimensional problems are solved within a couple of iterations by means of the SLOR method. With the built-in decision parameters for acceleration of the convergence, two-dimensional problems are normally solved within 20-25 iterations.

A typical 20 × 20 mesh, 5 group (2 thermal) fuel assembly calculation for the Yankee reactor (ref. 20) with a detailed mesh description of the two adjacent control rods surrounded by water gaps thus requires 18 iterations and a running time of 60 seconds.

5. DBU, A TWO-DIMENSIONAL MULTI-GROUP DIFFUSION BURN-UP PROGRAMME

With the intention of performing two-dimensional multi-group over-all burn-up calculations the TWODIM programme was used as a standard block for the flux solution in a diffusion burn-up programme, DBU. The long-term irradiation of the whole reactor is followed in the quasistationary approach by means of a fast approximative interpolation burn-up method.

This method as well as the extension to treatment of spatial xenon-induced power oscillations will be described in the following section. A general description of the programme is given with available options and running times. The programme has been used for studying of spatial xenon oscillations for the BHWR-800 NORDIC STUDY (ref. 21) of which a summary is given.

5.1. The Interpolation Burn-up Method

A fast, approximative method for over-all burn-up analysis is the interpolation burn-up method. It has been used to a great extent in the Scandinavian countries (ref. 22) as well as in England (ref. 23), whereas it seems seldom used in, for example, the United States.

The time-dependent problem is treated in the quasistationary approach by splitting of the problem into a number of time steps during which the power density distribution is assumed constant in space.

The fundamental idea of this method is now that the detailed depletion of the single fuel rod or bundle of fuel rods is avoided in the over-all calculation by the use of a tabulation of few-group macroscopic cross sections as a function of irradiation.

The conventional calculation procedure for the interpolation burn-up method is applied (ref. 23). Each time step is initiated by an over-all diffusion theory calculation giving a local incremental irradiation determined from the local power density and the time step used. The macroscopic cross sections corresponding to the local actual accumulated irradiation are then simply obtained by interpolation of the tabulated cross sections, and a new time step is taken. The tabulated burn-up calculation for the asymptotic rods placed in a regular lattice can then be obtained once and for all with a usual cell or point multi-group depletion programme.

The method accounts for changes in isotopic contents as well as spectrum effects and variation of thermal disadvantage factors during irradi-

ation. This is due to xenon, samarium and other fission product build-up and of course the usual uranium to plutonium conversion.

Asymptotic rods all go through the same stages of irradiation in which case the method is exact. However, a lot of fuel rods are situated in geometric asymptotic regions, but do not really have asymptotic behaviour.

This is for example the case for the inner fuel rods in fuel assemblies placed at different positions in the over-all picture. These rods behave in a similar way when they are situated in the same geometric surroundings far from thermalizing water gaps and absorbing control rods. However, the rods may have a considerably different local power level. An increase by a factor of two in power level will immediately increase U^{238} and Pu^{240} capture owing to the Doppler effect. Slower effects are the increased moderator temperature and especially the increased xenon concentration, which together will harden the thermal spectrum and thus decrease the local reactivity by about one per cent.

The combined power effects can be accounted for in an approximative way by extension of the one-dimensional tabulation to a two-dimensional one with the macroscopic cross sections as a function of burn-up as well as power density.

For asymptotic fuel rods at different, but constant power levels during irradiation the outlined method will be correct.

In PWR fuel assemblies the usual number of fuel rods is about 200-300. The lattice is very tight with narrow water gaps and zirconium followers are used to replace the control rods when they are withdrawn. Surface and corner fuel rods adjacent to water gaps and control rods constitute only about 10% of the total number of fuel rods, indicating that most rods behave as if they were asymptotic. If furthermore the local power density does not vary too much with irradiation, the interpolation burn-up method seems to be acceptable for treatment of the assembly as a whole.

For BWR fuel assemblies the situation is more difficult owing to the highly inhomogeneous lattice. Each assembly consists of about 50-60 fuel rods surrounded by large water gaps with no use of power flattening zirconium followers. In this case the corner and surface fuel rods constitute about 50% of all fuel rods, and an asymptotic treatment of the whole assembly is unsatisfactory. Instead a more accurate method for the homogenization of the assembly should be applied, resulting in equivalent cross sections for the whole assembly.

Strictly speaking, the interpolation burn-up method involves that fuel rods with equal power density and accumulated burn-up will have the same

set of cross sections, regardless of the way in which the values have been obtained. Nevertheless, it seems to be adequate for a lot of burn-up problems, especially for regular or homogeneous lattices, where most fuel rods can be considered asymptotic. The method is, however, insufficient for regions where flux spectrum, power density or spacewise composition change much since the actual cross sections are almost independent of the true, previous irradiation history.

5.2. Treatment of Non-Equilibrium Xenon

The method outlined above will treat the equilibrium xenon concentration in a fairly good manner, always assuming that the associated transients have damped out, and that an equilibrium situation has been established. However, these power transients may become very dangerous in modern reactors, and special attention is required.

For economic reasons the current design of commercial power reactors requires (1) high power densities and low fuel enrichments, (2) low peak-to-average power distributions and (3) high total thermal power output. The first of these requirements results in a high thermal neutron flux level; the second leads to flattened power shapes; and the last one encourages the design of large reactors. Each of these conditions leads toward reactors in which it is possible to sustain xenon-induced spatial power oscillations.

These transients can be accounted for by solving of the space- and time-dependent differential equations for Xe^{135} and its precursor I^{135} (fig. 20):

$$\frac{dn_I}{dt} = -\lambda_I n_I + \gamma_I \Sigma_f \varphi \ , \tag{5.1}$$

and

$$\frac{dn_{Xe}}{dt} = -\lambda_{Xe} n_{Xe} - \sigma_{a,Xe} \varphi n_{Xe} + \lambda_I n_I + \gamma_{Xe} \Sigma_f \varphi \tag{5.2}$$

with the solutions

$$n_I = \frac{\gamma_I \Sigma_f \varphi}{\lambda_I} + \left(n_I^o - \frac{\gamma_I \Sigma_f \varphi}{\lambda_I} \right) e^{-\lambda_I t} \tag{5.3}$$

$$n_{Xe} = \frac{(\gamma_I + \gamma_{Xe})\,\Sigma_f \varphi}{\lambda_{Xe} + \sigma_{a,Xe}\varphi} + \frac{\lambda_I n_I^o - \gamma_I \Sigma_f \varphi}{\lambda_{Xe} - \lambda_I + \sigma_{a,Xe}\varphi} e^{-\lambda_I t} +$$

$$\left[n_{Xe}^o - \frac{(\gamma_I + \gamma_{Xe})\Sigma_f \varphi}{\lambda_{Xe} + \sigma_{a,Xe}\varphi} - \frac{\lambda_I n_I^o - \gamma_I \Sigma_f \varphi}{\lambda_{Xe} - \lambda_I + \sigma_{a,Xe}\varphi} \right] e^{-(\lambda_{Xe} + \sigma_{a,Xe}\varphi)\,t} \quad , \quad (5.4)$$

where the absorption term in equation (5.1) has been neglected. n is the time- and space-dependent concentration after a time step of the length t; n^o the concentration at the beginning of the time step. λ is the radioactive decay constant, and γ the fission yield. σ_a is the microscopic absorption cross section, and $\sigma_a \varphi$ is supposed to include summation over all energy groups. Similarly $\gamma \Sigma_f \varphi$ includes summation over all fissile nuclei and groups. Equations (5.3) and (5.4) were deduced with the assumption that φ and Σ_f are constant during the time step. The first term in equation (5.4) is the asymptotic or equilibrium value which will be obtained for $t \to \infty$.

Introduction of these equations in the two-dimensional over-all calculation will permit investigations of xenon-induced spatial power oscillations. The physical reason for their existence will be illustrated by a practical example.

Imagine that the flux in a region of the reactor is suddenly decreased by, for example, insertion of a control rod. This will leave the production of Xe^{135} nearly unchanged since it is mostly produced by β-decay of I^{135}, whereas the absorption is lowered, thereby increasing the Xe^{135} concentration. The increased poison will again decrease the flux and so on. This development will continue, and when the I^{135} concentration has decreased so much that the production of Xe^{135} is equal to the amount disappearing by absorption and β-decay, the whole situation will change. Now a decrease in Xe^{135} concentration will follow and increase the flux and so on. If a constant power level is maintained, different regions will contribute out of phase to the over-all oscillation.

Major feedback mechanisms associated with xenon oscillations are spatial effects due to local Doppler effect, local moderator temperature and local xenon concentration. For BWR's the usually strong negative void reactivity effect will damp such oscillations. It seems therefore that the xenon-induced spatial power oscillations are more expressed for especially large PWR's, of which a lot of investigations (refs. 24 and 25) give evidence.

5.3. The DBU Programme

The interpolation burn-up method as well as the special treatment of non-equilibrium xenon form the fundamental principles in the two-dimensional multi-group diffusion burn-up programme DBU, where TWODIM constitutes the standard block for the over-all flux solution. The programme serves as an efficient tool for over-all burn-up investigations if it is provided with appropriate macroscopic cross sections for homogenized regions of the reactor.

A three-dimensional interpolation between depletion, power density and flux spectrum is used, and the non-linear xenon, samarium and Doppler effects are thus taken into account besides spectrum changes due to water gaps and control rods. As mentioned in section 5.1 it is the general opinion that the method will be insufficient for the detailed depletion of the single assembly owing to the strongly associated heterogeneities near water gaps and movable control rods.

It seems, therefore, that the spectrum interpolation should be replaced by void content for over-all BWR investigations. For practical reasons an interpolation is applied instead of a polynomial representation, allowing the use of the direct output from a cell depletion programme as input.

The cross section tabulations can be in either card or magnetic tape form depending on the output from the generating cell depletion programme.

Different types of fuel can be treated in the programme, which thus allows varying fuel compositions (enrichment) and unit cell geometries.

During burn-up loading, unloading and shuffling of fuel elements as well as control rod movements can be performed.

These manipulations should be followed by some iterations with time steps of zero length, which are necessary to establish the proper (converged) effect and flux spectrum conditions.

Space-dependent xenon-induced power oscillations can be investigated with the programme according to the method described in section 5.2.

A special routine can move the control rods until criticality by an iterative method always searching for the lowest form factor. Furthermore, the method can be used for investigations of different control management procedures of spatial xenon oscillations.

The DBU programme is, as the TWODIM flux solution part, written in the ILLINOIS-ALGOL language for the IBM 7094 computer. Dynamic overlay (*ref. 19*) is used with the link structure shown in fig. 7.

The programme has been used for almost a year for e.g. studying of spatial xenon oscillations for the BHWR-800 NORDIC STUDY.

Verification of the over-all burn-up method will be given in section 11, where over-all depletion calculations for the first core of the Yankee reactor (ref. 20) will be compared with experiments.

Macroscopic cross sections as a function of burn-up, power density and flux spectrum can be provided by means of the LASER-CROSS MACRO complex.

A typical 30 x 30 mesh,2 group quarter core over-ail depletion calculation for the Yankee reactor with a direct representation of control rods and followers requires about 40 seconds per time step.

5.4. Study of Spatial Xenon Oscillations

A summary of xenon-induced spatial power oscillation studies for the BHWR-800 NORDIC STUDY (ref. 21) is given.

RZ and XY geometry calculations were performed with an early version of the DBU programme in the modified one-energy group approximation.

It was observed that time step lengths of the order of one hour or less were required for adequate accuracy. Furthermore, the use of a flux convergence criterion of 10^{-5} was required instead of 10^{-4}, which is normally used in static problems, to ensure sufficient accuracy of the calculated xenon stability characteristics.

Criticality was maintained by use of the eigenvalue poison search that distributes the poison uniformly over the core.

It was demonstrated that a flat power distribution was mostly exposed to xenon oscillations due to the small interior leakage.

The axial free-running mode oscillation induced by insertion of four control rod rings is given in fig. 14. The power densities are damped and convergent. Fig. 16 shows a power density map three hours after insertion of four control rod rings, where the power maximum, owing to xenon effect, is in its upper position.

The azimuthal free-running mode oscillation induced by control rod insertion is shown in fig. 15. The power densities oscillate harmonically and are divergent with a period of 36 hours. However, these oscillations can be controlled with control rods. Power densities at different times after the perturbation appear from figs. 17 through 19.

6. CELL, A GENERAL ONE-DIMENSIONAL MULTI-GROUP CROSS SECTION CONDENSATION COLLISION PROBABILITY PROGRAMME

A constantly recurring problem in reactor physics is the proper determination of effective or homogenized, macroscopic, few-group cross sections for sometimes complicated geometries with a great variation in spatial flux spectrum. These equivalent cross sections are later used in, for example, diffusion theory for over-all calculations.

A usual procedure for these problems is that of using a sufficient number of energy groups for the whole problem. Sometimes this method requires a lot of groups and takes up much computer time.

Instead the problem can be split into subproblems, where the space and especially the detailed energy-dependent flux distribution is calculated once and for all that provides space-dependent few-group cross sections for application in the original over-all problem.

The prescribed method ensures that the few-group cross sections are determined with the correct shielding and, as far as spectrum conditions are concerned, in surroundings that correspond to the actual surroundings in the over-all picture.

For treatment of regions with strong flux gradients and large absorptions, which occur in, for example, control rods, a diffusion theory treatment is insufficient, and a more exact integral transport theory calculation is required.

This section describes the cross section condensation programme CELL. By means of a one-dimensional, multi-group collision probability method it solves the detailed space-dependent flux spectrum problem, which in its turn is applied for arbitrary space and energy condensation to fewer groups. Furthermore the standard flux solution procedure SOLU and the employed convergence accelerating methods are described.

6.1. The Collision Probability Equation

The multi-group collision probability equation has the following form for the thermal range (ref. 26):

$$\Sigma_i^g V_i \varphi_i^g = \sum_{j=1}^{nr} P_{i,j}^g \left(\sum_{g'=1}^{ng} \Sigma_j^{g,g'} V_j \varphi_j^{g'} + V_j S_j^g \right) ; \qquad (6.1)$$

the remaining signs are used as follows:

$1 \leq g \leq ng$	energy group index
$1 \leq i \leq nr$	one-dimensional mesh index
V_i	volume
φ_i^g	neutron flux
S_i^g	source density distribution from fast-energy range
Σ_i^g	total cross section
$\Sigma_i^{g,g'}$	scattering cross section from group g' to g
$P_{i,j}^g$	first collision probability in region i per source neutron in region j.

The scattering cross section $\Sigma_i^{g,g'}$ as well as the total cross section

$$\Sigma_i^g = \Sigma_{a,i}^g + \sum_{g'=1}^{ng} \Sigma_i^{g',g}$$

where $\Sigma_{a,i}^g$ is the absorption cross section, should be transport-corrected by means of the method in section 3.

If the whole spectrum is considered, the source density distribution is:

$$S_j^g = \lambda X_j^g \sum_{g'=1}^{ng} F_j^{g'} \varphi_j^{g'} \qquad (6.2)$$

$$F_j^g = \nu\Sigma_{f,j}^g$$

$$\lambda = \frac{1}{k_{eff}} \quad ;$$

the remaining signs are used as follows:

X_j^g	neutron fission spectrum
$\nu\Sigma_{f,j}^g$	neutron production cross section

k_{eff} effective multiplication factor .

6.2. SOLU, A Standard Flux Solution Procedure

Equation (6.1) represents a set of inhomogeneous linear equations, and in the conventional matrix notation they have the form:

$$M\varphi = k , \tag{6.3}$$

where M contains the transport and transfer terms and k the fixed source. These equations are very suitable for solution by an iterative method. M is not necessarily symmetric, but has positive diagonal elements and non-positive off-diagonal elements. Furthermore, M is strictly diagonally dominant and thus has spectral radii for the associated point Jacobi and Gauss-Seidel matrices lower than one. Therefore these matrices are convergent. These two splittings are shown for equation (4.18) in equations (4.21) and (4.22) for $\omega = 1$.

Thus an iterative solution method for equation (6.3) is equivalent to the inner iteration problem in section 4.2. However, another method must be used for determination of the optimal relaxation factor.

A "trial and error" method always searching for a relaxation factor which minimizes the spectral radius $\bar{\mu}(L_\omega)$ of the point successive relaxation matrix L_ω is applied throughout the iteration progress.

The extrapolation procedure outlined in section 4.2 allowing negative values of $\bar{\mu}(L_\omega)$ serves as an efficient convergence accelerating method especially for slowly convergent problems.

Renormalization forces the left and right sides of equation (6.3) to balance after each iteration, and thus the convergence rate is improved.

If the whole spectrum is considered, equation (6.3) will transform into the usual eigenvalue problem, see equation (4.14),

$$M\varphi = \lambda F \varphi , \tag{6.4}$$

where F contains the fission spectrum and neutron production.

The outer iterations are solved by the usual power method employed in section 4.2.

For the multi-group unit cell problem with no leakage it appears to be an advantage to solve the inner iterative problem completely between the outer iterations. This is due to the flat resonance fluxes giving thermal

fluxes nearly independent of the fission source distribution.

Thus more than one inner iteration per outer iteration is applied in direct contrast to the usually fastest method for few-group, over-all diffusion calculations. The TWODIM programme in section 4 normally uses a single inner iteration per outer iteration.

The methods described above constitute the fundamental principles in the flux solution procedure SOLU which is used as a standard routine throughout the project for solving of collision probability problems.

Verification of the procedure has been made for a two-group, two-mesh problem, which was directly solved by manual calculation.

6.3. Cross Section Condensation

The calculated detailed flux spectrum is now applied for optional space and energy condensation to obtain homogenized few-group cross sections.

Within each of the fine energy groups a space homogenization is performed for the reaction cross sections

$$\Sigma_x^g = \frac{\sum_i \Sigma_{x,i}^g \varphi_i^g V_i}{\sum_i \varphi_i^g V_i} \quad , \tag{6.5}$$

$$\Sigma_x^g = (\Sigma_a^g, \Sigma^{g',g}, \Sigma_f^g, \nu\Sigma_f^g) \quad , \tag{6.6}$$

where the space summation is to be extended over the specified regions by the use of the principle of reaction rate conservation. Now a diffusion coefficient is deduced from the homogenized cross sections:

$$D^g = \frac{1}{3(\Sigma_a^g + \sum_{g'} \Sigma^{g',g})} = \frac{1}{3\,\Sigma^g} \, . \tag{6.7}$$

An energy condensation is then applied for the fine group cross sections:

$$\Sigma_x^h = \frac{\sum_{g \in h} \Sigma_x^g \varphi^g}{\sum_{g \in h} \varphi^g} , \qquad (6.8)$$

$$\Sigma_x^h = (\Sigma_a^h, D^h, \Sigma_f^h, \nu\Sigma_f^h) , \qquad (6.9)$$

$$\Sigma^{h,h'} = \frac{\sum_{g \in h, g' \in h'} \Sigma^{g,g'} \varphi^{g'}}{\sum_{g' \in h'} \varphi^{g'}} , \qquad (6.10)$$

where the energy summation must include all fine groups within a specified coarse group.

6.4. The CELL Programme

The methods described above were incorporated in the one-dimensional (cylinder, slab, sphere) multi-group (maximum ~ 60 groups for 14 meshes collision probability cross section condensation programme CELL that provides effective homogenized few-group cross sections for later use in, for example, over-all diffusion programmes. The programme was originally designed for proper determination of effective homogenized few-group cross sections for direct representation in diffusion theory of cruciformed control rods surrounded by water gaps.

The cylinder, slab and sphere collision probability procedures (CPM-procedures) have been provided from ref. 27 with a method suggested in ref. 26.

Homogenized condensed cross sections will be punched on cards in a form directly matching TWODIM and related programmes as well as the programme itself.

CELL is written in the ILLINOIS-ALGOL language with dynamic overlay (ref. 19). The link structure is shown in fig. 4.

Verification and the physical aspects of the described homogenization and condensation method will be given in section 11, where the method has been used for the control rod treatment of the Yankee reactor (ref. 20).

7. CEB, A CELL BURN-UP PROGRAMME

For some years the LASER programme (ref. 4) has been the standard tool at Risø for treatment of light-water reactor unit cell burn-up problems. With a fixed multi-energy (85 groups) formalism, an independent cross section representation and a combined multi-region collision probability theory and homogeneous B-1 transport equation approximation, the programme is very general, covering a wide range of criticality and burn-up problems. Furthermore, it is rather fast as it requires about 1.5 minutes per time step in computer time for usually occurring problems.

However, for performance of over-all depletion calculations with a detailed cell burn-up treatment of the single fuel rod or bundle of fuel rods, a faster method is necessary.

Similarly, if many calculations are to be performed for the same unit cell, for example if a lot of time steps are to be taken, it is the general opinion that the detailed 85 energy group calculation at each time step can be avoided. Instead a 10-20 energy group treatment is probably sufficient for many purposes, where the associated microscopic cross sections are condensed from 85 groups by the use of, for example, a middle-of-life flux spectrum.

Thus it was the intention to develop a fast unit cell burn-up programme, which in some ways is tailored to meet the requirements of efficiency.

This section describes the multi-group, one-dimensional collision probability unit cell burn-up programme CEB, with the isotopic depletion performed in the conventional quasistationary approach.

Some of the routines in the CELL programme, for example the flux solution procedure SOLU, are again used as standard blocks in the CEB programme.

The set of coupled partial differential equations for the isotopic chains is solved in the burn-up procedure BURN by means of a fast, purely numerical method, and thus calls of the time-consuming exponential function are avoided.

Finally, a general description of the programme is given with special features and typical running times.

7.1. The Isotopic Burn-up Method

Usual unit cell burn-up programmes (ref. 4) solve the time-dependent problem in the quasistationary approach by splitting the depletion problem

into a number of time steps during which the total cell power is constant. The flux spectrum, but not the level, is assumed invariant throughout the unit cell during a time step, an assumption which is quite reasonable for most depletion problems with burn-up steps of the order of 1000-1500 MWD/TU. During a time step the fissile and fertile nuclide concentrations will change and thereby change the flux level according to the requirement of constant total cell power. The larger time step is therefore subdivided into a sufficient number of smaller time steps, where a fixed flux level is applied followed by a flux normalization.

The calculation procedure is conventional for cell burn-up programmes (ref. 4). Each larger time step is initiated by a multi-group collision probability determination of the flux. The calculated space-dependent flux spectrum is now maintained during the time step, and a detailed spatial isotopic depletion is performed followed by a new flux calculation and another large time step.

Thus an accurate calculation is performed for the spatial distribution of the neutron flux spectrum and the fuel composition as a function of burn-up in the heterogeneous lattice cell.

7.2. The Burn-up Procedure BURN

The depletion of the heavy nuclide chains shown in fig. 21 is accounted for by solving of a set of coupled differential equations.

For reasons of efficiency only the U^{235}-U^{238} Pu system is considered, since it is that customarily encountered in light-water reactors. Furthermore, the usual practice is to ignore some of the reactions here that are less important for most cell burn-up calculations.

Thus the U^{235} chain is terminated by formation of U^{236} owing to the small absorption cross section of the latter.

For the U^{238}-Pu chain the beta-decay of U^{239} and Np^{239} is assumed to take place instantaneously. Therefore it is supposed that neutron capture in U^{238} will produce Pu^{239} directly, ignoring a production of about 2 o/oo Np^{240}. Except for a short time immediately after the start of the reactor, when the delay of the Pu^{239} production may be of some significance, the above assumptions are acceptable. Furthermore, this chain is normally terminated by production of Pu^{242} because of the rather small absorption cross section and usually low concentration.

The resulting, in some ways tailored, set of coupled differential equations representing the fissile and fertile heavy nuclide reactions has the form

$$\frac{dn}{dt} = -n(\sigma_a \varphi + \lambda) + n'(\sigma'_c \varphi + \lambda') + n''(\sigma''_c \varphi + \lambda'') \quad , \tag{7.1}$$

where the first term on the right hand side represents the depletion of the nuclide concentration n, and the following terms account for the production of nuclide n by capture or decay of n' and n''. σ_a and σ_c are absorption and capture cross sections and λ decay constant. $\sigma\varphi$ is supposed to include summation over all energy groups.

The equations are solved by splitting each larger time step into smaller ones, in which a fixed flux level is applied followed by a flux normalization.

The conventional procedure is now to solve equation (7.1) directly for each smaller time step by the use of an explicit analytical treatment with application of the exponential function or its expansion for smaller arguments.

The subdivision into smaller time steps for the reason of adequate flux normalization suggests solution by conversion to a finite difference form

$$\frac{dn}{dt} \rightarrow \frac{n_{t+\Delta} - n_t}{\Delta} \tag{7.2}$$

$$n \rightarrow \frac{n_{t+\Delta} + n_t}{2} \quad , \tag{7.3}$$

where Δ is the smaller time step used.

A modified implicit Euler method is employed by substitution of (7.2) and (7.3) into equation (7.1) giving

$$n_{t+\Delta} = (n_t [2 - (\sigma_a \varphi + \lambda)\Delta] + [n'_{t+\Delta} + n'_t] \times [\sigma'_c \varphi + \lambda']\Delta + [n''_{t+\Delta} + n''_t][\sigma''_c \varphi + \lambda'']\Delta)/[2 + (\sigma_a \varphi + \lambda)\Delta]. \tag{7.4}$$

A straightforward numerical treatment is then applied for U^{235}, U^{236}, U^{238}, Pu^{239}, Pu^{240}, Pu^{241}, Pu^{242}, and B^{10} at each smaller time step followed by a flux normalization before proceeding to the next one.

The customary procedure for normalizing of the flux follows from fig. 22 (ref. 28), where the employed constant fluxes in the smaller time steps will have an integrated value always less than the true one obtained for

$\Delta \to 0$. A modification was performed in fig. 23 with a guess of the average flux values within the smaller time steps to ensure a better approximation for the integrated flux. This modification reduces the number of smaller time steps per larger ones by a factor of 5 with the same accuracy.

Concerning the required number of smaller time steps per larger ones, both the finite difference approximation in equations (7.2) and (7.3) as well as the smooth change of the flux converted into a stepwise change with time must be accounted for to ensure a proper solution of the depletion problem.

After the initial large time step Xe and Sm in turn are assumed to have reached their equilibrium concentrations, a procedure which is commonly used in cell burn-up programmes (ref. 4).

$$n_{Xe} \to \frac{(\gamma_I + \gamma_{Xe})\Sigma_f \varphi}{\lambda_{Xe} + \sigma_{a,Xe}\varphi} \tag{7.5}$$

$$n_{Sm} \to \frac{\gamma_{Pm}\Sigma_f \varphi}{\sigma_{a,Sm}\varphi} \tag{7.6}$$

The reader is referred to section 5.2 for the symbols.

A single pseudo fission product is applied which is defined by one fission product produced per fission.

The methods described above constitute the basic principles in the burn-up procedure BURN.

Verification of the procedure has been made by depletion of a Yankee unit cell, for which the appropriate average fluxes and effective microscopic cross sections for each time step were provided from the LASER programme.

There is full agreement between the two depletion methods.

With larger time steps of 30 days a relative accuracy better than 10^{-4} is obtained even with a subdivision into only 10 smaller time steps.

7.3. The CEB Programme

The one-dimensional (cylinder, slab, sphere) multi-group (maximum ~ 40 groups and 6 meshes) collision probability cell burn-up programme CEB employs the burn-up procedure BURN as well as several blocks from the CELL programme including the standard flux solution procedure SOLU.

A wide range of current cell burn-up problems will be solved efficient-

ly with a detailed spatial isotopic depletion.

The programme can be provided with multi-group microscopic cross sections in either card or magnetic tape form.

Accumulated burn-up, space-dependent flux spectra and number densities as well as reactivity and homogenized few-group macroscopic cross sections for later application in, for example, diffusion theory, are printed for each time step.

The CEB programme is written in the ILLINOIS-ALGOL language with dynamic overlay and with link structure shown in fig. 5.

Verification of the programme will be given in section 10, where cell burn-up calculations for the Yankee reactor (ref. 20) will be compared with calculations performed with LASER as well as with experimental data.

With 16 group microscopic cross sections from the LASER-CROSS MICRO complex, a typical Yankee unit cell burn-up calculation requires about 3 sec per time step.

A detailed spatial fission product depletion was recently incorporated in the CEB programme (ref. 29). The FIPO procedure accounts for 166 different isotopes distributed on 68 linear chains by means of a combined analytical and numerical method without any further serious computational efforts.

8. CDB, A COMBINED CELL COLLISION PROBABILITY AND OVER-ALL DIFFUSION THEORY BURN-UP PROGRAMME

Unit cell burn-up calculations concern the accurate determination of reaction rates and fuel compositions as a function of burn-up in a unit cell representative of a given (asymptotic) portion of the core. For the long-term behaviour of reactors as regards reactivity variations (lifetime) and spatial distributions of power and fuel material inventories, multi-dimensional, over-all burn-up calculations are required.

The most common approximation in depletion studies (ref. 30) is the simplification of the problem into a local burn-up problem superimposed on a global flux problem as described in section 5. For many classes of problems, particularly those in which the reactor loading is relatively uniform and regular, this is a fairly acceptable procedure. However, there are important cases where the fundamental assumption of separability between cell and over-all events is unsatisfactory. This is especially the case for BWR assemblies owing to the heterogeneity of the lattice from the presence of water gaps, non-uniform local enrichments for power flattening and self-shielded burnable poison in the fuel. The situation is similar for fuel rods adjacent to control rods and water gaps in PWR assemblies.

Therefore it is sometimes desirable to represent the influence from the surrounding lattice on the local calculation to ensure that the single fuel rod or bundle of fuel rods is depleting in the true milieu.

This section describes a method of solving the complex local - global burn-up problem. A combined one-dimensional, multi-group collision probability unit cell and two-dimensional multi-group over-all diffusion burn-up programme, CDB, determines the long-term irradiation for assemblies or the whole reactor in the quasistationary approach in that it performs a detailed spatial isotopic depletion for the single fuel rod or bundle of similar fuel rods. The CDB programme consists mainly of routines from the cell burn-up programme CEB described in section 7 and the over-all diffusion solution programme TWODIM described in section 4.

A general description of the programme is finally given with optional features and typical running times.

8.1. The Local - Global Coupling Method

The influence from the surrounding lattice on the local calculation can be accounted for in different ways:

1) The local calculation may incorporate a term to represent neutron leakage or current over the cell boundary. In general, this is a function of neutron energy, fuel irradiation stage and history and may be determined from the over-all reactor calculation. Therefore, some form of iteration between cell and reactor calculation is implied. Alternatively, the use of many groups in the reactor calculation will obviate the need for this interaction.

2) The cell calculation is in fact a multi-cell evaluation for all cells considered. An assembly is therefore treated as a whole with appropriate boundary conditions, and in this way superposition of the local and global flux problem is avoided.

3) Iteration may be avoided if leakage information from previous global calculations is used in subsequent local calculations. This approximation will hold whenever the leakage dependence on local burn-up is not great, or when the shifts in global flux behaviour occur slowly as a function of burn-up.

Where the interpolation burn-up method relying on the fundamental assumption of separability between cell and total reactor events has been used to a great extent in England and the Scandinavian countries, the third method is very often applied in the United States (ref. 31). However, the method has also been used at Risö (ref. 32).

This method solves the combined depletion problem in that it applies the few-group (~ 2-4 groups) diffusion theory for the neutron flux shape and uses macroscopic cross sections deduced from local isotopic number densities, variable self-shielding factors and a microscopic cross section library.

The over-all flux and power shapes are used to compute the local depletion of each of the burnable isotopes over a specified time step. Within each time step both the power density and the flux spectrum over-all distributions are assumed to be invariant.

New (non-uniform) isotopic number densities are then available and permit a re-entry into the group constant calculation followed by a new flux determination repeating the whole process.

Each fuel rod or bundle of fuel rods is thus depleted by the use of the few-group over-all neutron flux combined with self-shielding factors depending on irradiation or isotopic concentrations. These factors, which account for the local and global coupling, have to be determined once and for all by means of, for example, a conventional multi-group cell burn-up

programme.

The problem with this method is the history and spatial dependence of the self-shielding factors.

A few-group treatment is usually applied for the reason of available computer running times.

The second method involves a simultaneous calculation for all cells under consideration with a detailed representation of the single cell in the multi-cell arrangement. Obviously, this seems to be the best method if transport theory in either P_n, S_n or collision probability theory is used for the entire problem.

However, for accurate determination of the spatial flux spectrum changes within the individual fuel rods as depletion proceeds the build-up of fission products and the usual uranium to plutonium conversion requires a multi-group performance (~ 10-20 groups).

For present-day computers a multi-group transport theory treatment requires long execution times at least for the over-all reactor depletion problem. Applied to the single assembly the method seems more realistic, even though it is expected to be rather time-consuming.

The first method, which treats the interaction between the surrounding lattice and the local cell in terms of neutron leakage or current over the cell boundary, was applied in the CDB programme.

The local burn-up problem is solved with the CEB programme for a detailed one-dimensional multi-group (~ 10-20 groups) collision probability cell burn-up treatment of the single fuel rod or bundle of fuel rods. The actual local power density and neutron leakage spectrum for this calculation are provided from an over-all, two-dimensional, usually few-group (2-5 groups) diffusion theory calculation with the TWODIM programme.

The calculation procedure is now described.

Each larger time step is initiated by a multi-group cell burn-up treatment, where a detailed spatial isotopic depletion within the individual fuel rods is performed. The actual power densities are determined from the local fission rate densities. The local few-group neutron leakage spectra are obtained from the leakage terms in equation (4.6) giving equivalent few-group leakage cross sections $\Sigma^g_{l,i,j}$.

$$L^g_{i,j} \quad V_{i,j} \Sigma^g_{l,i,j} \varphi^g_{i,j} \tag{8.1}$$

These few-group leakage cross sections determined by signs are dis-

tributed uniformly within the single cells, and extended to the multi-group scheme for the cell flux calculation they account for the surrounding lattice.

At the end of the time step, macroscopic homogenized few-group cross sections are determined for the individual cells from the distributions of spatial flux spectrum and isotopic number densities within the cells by means of a multi-group microscopic cross section library.

Then follows a few-group, two-dimensional diffusion theory calculation, which provides local power densities and neutron leakage spectra for the single cells during the next time step repeating the whole process.

During each time step the power density and neutron leakage over-all distributions as well as the flux spectrum within the individual cells are assumed to be invariant.

Some iterations between cell and over-all reactor calculation are usually necessary to establish the proper (converged) effect and flux spectrum conditions thus ensuring the true surroundings for the fuel rods during the irradiation.

8.2. Non-Uniform Doppler and Dancoff Effects

The heterogeneity of the lattice from the presence of water gaps, non-uniform local enrichments for power flatt-ning and self-shielded burnable poison in the fuel makes local spatial neutron spectrum variations important.

However, the applied microscopic cross sections for determination of these variations are spatially dependent.

The spatial variation in power density changes the capture rate especially in the U^{238} and Pu^{240} resonances. This non-uniform Doppler broadening effect is accounted for by means of a simple linear interpolation with microscopic absorption cross sections for U^{238} and Pu^{240} as functions of power density. The cell burn-up calculations are, therefore, at each time step provided with microscopic absorption cross sections for U^{238} and Pu^{240} depending on the previously determined local power densities.

For correct establishment of the (converged) over-all power density distribution some iterations are normally required with time steps of zero length.

The Dancoff interaction effect varies locally throughout the fuel assembly. Corner and face fuel rods near water gaps are not shielded as much as asymptotic rods by neighbouring fuel rods, and they consequently have a Dancoff factor closer to zero. This non-uniform Dancoff effect is

treated in an approximative way.

The fuel rod multi-group resonance cross sections have the following form

$$\sigma_a^g \sim RI^g = a + b\sqrt{\frac{S}{M}} \quad , \tag{8.2}$$

where σ_a^g is the U^{238} resonance absorption cross section in group g and RI^g the associated effective resonance integral in group g. For the total resonance integral the constants a and b are equal 4.15 barns and 26.6 barns $g^{1/2}\ cm^{-1}$ in *Hellstrand's original fitting* law for UO_2 fuel, where S is the effective surface area of the oxide rod and M its mass. The relationship between the effective and physical surface area is given by

$$S = S_{physical}(1 - C) \quad , \tag{8.3}$$

where the Dancoff factor C is about 0.35-0.40 for usual regular lattices and accounts for the mutual shielding of the fuel rods. C is equal to zero for an isolated fuel rod.

Since the resonance mean free path in water is about 8 mm, which is less than the usual water gap widths, it is reasonable to regard the face and corner fuel rods as completely unshielded on their outside surfaces. Approximately, the mutual shielding effects are therefore reduced in proportion to the number of missing near neighbours

$$S = S_{physical}(1 - g \times C) \quad , \tag{8.4}$$

where

$$g = \begin{cases} 1 \text{ for asymptotic rods,} \\ \frac{5}{8} \text{ for face rods,} \\ \frac{3}{8} \text{ for corner rods,} \end{cases} \tag{8.5}$$

and C is the Dancoff factor for the regular lattice.

The local U^{238} microscopic resonance absorption cross sections can then be obtained from the cross sections belonging to the regular lattice with the spatial-dependent multiplication factor

$$\frac{a + b\sqrt{\frac{S(1-gC)}{M}}}{a + b\sqrt{\frac{S(1-C)}{M}}} \sim \sqrt{\frac{1-gC}{1-C}} \quad . \tag{8.6}$$

The last approximation follows from fig. 24 , ignoring the first term on the right-hand side of equation (8.2). This correction factor is in the range 1-1.20 and thereby gives an increased plutonium production for face and corner fuel rods.

8.3. The CDB Programme

The methods described above for solving of the assembly or the over-all reactor local - global depletion problem form the fundamental principles in the combined one-dimensional, multi-group collision probability unit cell and two-dimensional multi-group over-all diffusion burn-up programme CDB. The programme serves as an efficient tool for assembly and over-all burn-up investigations. For assemblies effective, homogenized few-group macroscopic cross sections can be provided as a function of, for example, burn-up, power density and void content for later use in a BWR over-all simulator by means of, for example, nodal theory combined with the interpolation burn-up method described in section 5.

The programme can be supplied with multi-group microscopic cross sections in either card or magnetic tape form.

Non-uniform Doppler effect is accounted for with a simple interpolation method. Local Dancoff factors for the individual fuel rods are determined by the progra .me from the number of missing near neighbours.

During burn-up loading, unloading and shuffling of fuel elements or fuel rods as well as control rod movements can be performed. After these manipulations some iterations are usually necessary with time steps of zero or small length to establish the proper (converged) effect and flux spectrum conditions.

The CDB programr is, as the CEB and TWODIM subprogrammes, written in the ILLINOIS-ALGOL language for the IBM 7094 computer. Dynamic overlay (ref. 19) is used with link structure shown in fig. 8.

Verification of the programme will be given in sections 11 and 12, where single assembly and over-all burn-up calculations for the first and second cores of the Yankee reactor (ref. 20) will be compared with detailed experimental data for the individual fuel rods.

Microscopic cross sections can be provided by means of the LASER-CROSS MICRO complex.

With 10 groups for an individual spatial isotopic depletion of the 49 fuel rods in a Brown Ferry (BWR) single assembly and 15 x 15 meshes and 2 groups in the global flux determination, each time step requires a total of about 40 sec in computer time.

9. VERIFICATION; CALCULATIONS COMPARED WITH MEASUREMENTS FOR THE YANKEE REACTOR

The various computation methods that were described in the preceding sections and that constitute the fundamental blocks of subprogrammes in the TWODIM SYSTEM are now verified by detailed calculations compared with available measurements for the Yankee reactor (PWR).

A direct simulation of the true reactor lifetime was performed by means of actual operating data that include changes in reactor power level and fuel and control rod managements.

The primary objective of this reactor core follow study is to investigate the efficiency of the miscellaneous computation methods in predicting:

1) Core reactivity and core lifetime.
2) Fuel isotopic characteristics for fuel rods placed in asymptotic neutron spectra.
3) Distributions of burn-up and fuel isotopes within the assemblies and within the core, and the total core isotopic inventory.
4) Burn-up and isotopic inventories of selected fuel rods.

The calculation methods employed for these investigations were verified by measurements mainly obtained through destructive examinations of Core I fuel rod samples from the first Yankee core that went through normal burn-up during the Core I lifetime, and Core 1 fuel rod samples that have been recycled in Core II for extended burn-up.

9.1. Description of the Yankee Core

Core 1 of the Yankee power reactor (PWR) described in refs. 20 and 33 contained 76 fuel assemblies, each loaded with either 304 or 305 fuel rods arranged in a square lattice. In each assembly one fuel rod located approximately in the centre of the assembly was omitted from the lattice to provide space for the insertion of a flux wire thimble. The total number of fuel rods in the core was 23142. A general description of the first core is given in table 1.

Core II was identical to Core I except for the presence of two Core I spent fuel assemblies located in the central region of the core. Compared with Core I, Core II was operated at a higher reference power level (540 versus 392 MWt) and for a shorter burn-up (7870 versus 8470 MWD/TU).

Both batch-loaded cores consisted of 348 stainless-steel fuel tubes loaded with UO_2 pellets of 10.18 g/cm^3 density. The height of a UO_2

column was 230.05 cm and equalled the effective length of a fuel rod exclusive of stainless-steel spacer disks and thermal expansion gaps.

The arrangement of the fuel assemblies in the core and the alpha-numeric matrix notation used to describe the core location of a particular fuel assembly are shown in fig. 25. The indicated control rod positions were in turn occupied by Ag-In-Cd control rods and Zr followers during operation. Fixed Zr shim positions and stainless-steel fillers, displacing water from the recesses in the fuel assemblies, are also shown.

The normal control rod withdrawal pattern was 642351, where group 6 was withdrawn first followed by group 4 and so on. The symmetric groups 1-2 and 3-4 were periodically interchanged. Thus, with respect to the fuel loading and the location of the control rod groups when group 6 was withdrawn, the core possessed quarter-core symmetry about the E-W and N-S axes of the core.

9.2. Fuel Sample Measurements

For performance of post-irradiation analysis of spent Yankee fuel samples, 56 fuel rods from fourteen Core I fuel assemblies (Phase I) and 7 fuel rods from one (F5) of two (F5 and E6) Core I assemblies recycled in Core II for extended burn-up (Phase II) were cut into 6 axial pieces or zones Selected 4 and 6 one-pellet samples were thus provided for extensive examinations such as X-ray spectrographic, mass spectrometric and radiochemical analyses as described in refs. 34, 35 and 7. Their locations with respect to fuel assemblies and the core are shown in fig. 26.

Phase I represents the analysis of pellet samples from 191 pre-selected locations within Yankee Core I which had a burn-up range from 1300 to 1800 MWD/TU. Phase II represents the analysis of pellet samples from 28 locations in the extended burn-up Core I fuel assembly F5 with burn-ups ranging from 10000 to 31000 MWD/TU.

Measured fuel pellet isotopic inventories and burn-ups have been converted to fuel rod quantitities by the use of appropriate axial interpolation factors when pellet samples were missing as described in ref. 34.

The fuel rod data have been converted to assembly average data by means of appropriate interpolations within the assemblies when fuel rod locations were missing, and region-to-rod factors for the conversion of point data to region data.

Assumption of quarter-core and eight-core symmetry gives the total core isotopic inventory and burn-up.

The various interpolations between data points followed by appropriate reflections, as far as permitted by core and distribution symmetries which are introduced in the analytical treatment of the measured data, cause errors of gross (and/or statistical) nature.

Many sources can contribute to the statistical and systematical uncertainty in the measured fuel pellet data as discussed in refs. 34 and 35:

1) Engineering and manufacturing tolerances on core components and fuel.
2) Spectral effects due to mechanical and physical phenomena that occur during reactor operation.
3) Experimental methods, including sampling and laboratory analysis.
4) Uncertainties in assumed values of basic nuclear parameters and physical constants used in the data reduction process.

The first and the second causes of uncertainties are generally statistical in nature, while the third and the fourth causes can be of both statistical and systematical nature.

The statistical uncertainties are usually reported as a 2-standard deviation in the subsequent sections that give the precision of the measurements, while estimated systematical uncertainties, which are normally difficult to determine, were included in few cases only.

10. UNIT CELL CALCULATIONS

Microscopic burn-up physics is concerned with the accurate determination of fuel compositions, flux distributions and reaction rates as functions of fuel burn-up in a uniform lattice cell. In this calculation method the whole-reactor problem is separated into the unit cell treatment and the over-all reactor behaviour, which in an approximate way enters the unit cell calculation through a buckling term. The unit cell computation method takes into account all non-linearities and mutual connections in the system of equations for the combined energy - space - time problem, and the meth will usually provide homogenized or effective average cross sections for later use in macroscopic multi-dimensional diffusion theory burn-up calculations of the over-all reactor problem.

Unit cell burn-up calculations will usually give reasonable estimates of the initial over-all reactivity characteristics and of the continuous charge-discharge irradiation limit. Furthermore, the unit cell treatment will estimate depletion and build-up of isotopes in fuel rods located in an asymptotic neutron spectrum far from perturbing water gaps and control rods.

A separation of two diffusion lengths from perturbing heterogeneities is considered sufficient to establish this asymptotic neutron spectrum. For the Yankee reactor unit cell with L = 2 cm and a pitch of 1.0719 cm the fourth fuel rod from the control rod is in the asymptotic region.

This section describes unit cell burn-up calculations compared with measurements for asymptotically located Yankee Core I fuel rods which have been recycled in subsequent cores for extended burn-up. The LASER and CEB programmes described in sections 3 and 7 were applied in these investigations.

10.1. Unit Cell Description

A summary of Yankee fuel rod unit cell properties is given in table 2. These include cold, hot zero-power and hot full-power dimensions, temperatures and fresh-fuel isotopic number densities which were applied throughout the Yankee core study. The unit cell power and fuel mass densities besides the geometric buckling required in the unit cell burn-up calculation are also shown.

10.2. Treatment of Fission Products

The fission products in LASER and CEB are separated into Xe^{135}, Sm^{149} and all other fission products lumped into one pseudo fission product

The concentration of this pseudo fission product is, by definition, one atom per fission.

The LASER programme requires the cross section for the pseudo fission product to be represented by polynomials in the burn-up (ref. 4). The 2200 m/sec value of an equivalent 1/v cross section for the thermal range 0 - 1.855 eV and an equivalent epithermal cross section that is constant in the range 1.855 - 5530 eV must be specified as functions of burn-up.

For these cross sections to be obtained for the Yankee unit cell, the FISS program (ref. 36) was modified in collaboration with L. Mortensen, Risö, to allow for several fissile nuclides. The FISS programme determines the time-dependent fission product absorption cross section by performing a detailed calculation of the time-dependent concentrations of 166 different isotopes partitioned into 68 linear chains by means of the analytical method applied in the CINDER programme (ref. 37).

For the most important nuclides the UKNDL 78 fission product nuclide cross sections (ref. 38) were applied in the LASER 85 energy group structure (ref. 4). 85 group cross sections were constructed for the remaining isotopes from available 2200 m/sec cross sections with an assumed 1/v dependence in the thermal range and from resonance integrals based on a 1/E flux behaviour in the fast range.

An 85-energy group treatment was thus applied with thermal disadvantage factors obtained from LASER.

The UKNDL fission product cross sections give resonance integrals for some isotopes that are in poor agreement with available measurements. This is especially the case for the Pm^{147} cross section, which seems to be the greatest single source of uncertainty in fission product calculations. Appropriate λ-value were applied to fit the measurements in these cases.

The calculated variation of the thermal and epithermal fission product cross sections with burn-up for the Yankee unit cell is shown in fig. 27.

10.3. Calculation Procedure

Burn-up calculations for the Yankee unit cell were performed with LASER and CEB with the properties given in table 2 and fig. 27. Normal time step lengths of 64 days gave burn-up steps of 1200 MWD/TU, and with two initial time steps of 4 and 12 days to account for the build-up of Xe^{135} and Sm^{149} the fuel has experienced burn-up until 24300 MWD/TU.

The LASER calculations were performed with three spatial meshes in the fuel, one in the clad and three in the moderator for the heterogeneous collision probability treatment in the 35 thermal energy groups in connection

with the homogeneous B-1 transport treatment in the 50 fast groups (ref. 4).

The original cross section library inclusive of the H_2O Nelkin scattering kernel was applied.

The CEB programme requires a microscopic cross section library in an optional energy group structure with appropriately determined microscopic multi-group cross sections.

Flux spectrum averaged 10 and 16 group cross section libraries with the energy group structures shown in table 3 were processed by means of the LASER - CROSS MICRO complex described in section 3.

A unit cell burn-up calculation was performed with LASER in 85 groups until 3900 MWD/TU where the most serious flux spectrum changes due to xenon, samarium and the initial uranium to plutonium conversion have occurred.

This average 85 group flux spectrum was now used in the data processing programme CROSS MICRO for the subsequent flux spectrum microscopic cross section condensation to fewer groups for later application in the all spectrum heterogeneous collision probability treatment applied in the CEB programme.

Burn-up calculations with CEB were performed until 48300 MWD/TU with 42 time steps and about 2 minutes in total computer time for the problem.

Only one spatial mesh in the fuel, one in the clad and one in the moderator were normally applied in these calculations. The use of three meshes in the fuel, one in the clad and three in the moderator has only a minor effect; thus it never changes the effective multiplication factor k_{eff} by more than 0.2 o/oo.

10.4. Reactivity Characteristics

The uniformity of the Yankee Core I makes it possible to estimate beginning-of-life reactivities with a unit cell treatment.

Measured reactivities for different beginning-of-life reactor operation states compared with unit cell calculations performed with LASER and CEB are shown in table 4.

For determination of the effective multiplication factor k_{eff} from the measured excess reactivity ρ, the relationship $\rho = \ln k_{eff}$ was used, which is the most suitable when the total excess reactivity is obtained from a summation of small reactivity changes as described in ref. 5.

The accordance between calculations and measurements is satisfactory.

The 10 energy group collision probability treatment in CEB overestimates k_{eff} by about 7 o/oo. The deviation is however within the experimental uncertainty.

This discrepancy is mainly caused by the U^{238} resonance absorption cross sections obtained from the LASER - CROSS MICRO complex. The applied resonance cross sections are related to the average flux in the cell because of the homogeneous fast-energy treatment in LASER. The collision probability theory used in CEB requires instead the cross sections to be determined in relation to the average flux in the fuel, which causes a small increase in the resonance cross sections.

The U^{238} resonance cross sections applied in the CEB calculations are therefore underestimated by about 2-3% giving a slightly smaller Pu^{239} production and an overestimation of k_{eff} by about 7 o/oo.

The reader interested in further details about the different resonance cross section and flux relations which can be applied for the treatment of this effect, is referred to the work by J. Mikkelsen, ref. 39.

The use of cold dimensions and number densities (see table 2) in the hot, zero power and full power calculations reduces k_{eff} by about 2 o/oo.

The unit cell effective multiplication factor as a function of burn-up calculated with LASER and CEB appears from fig. 28. The continuous charge - discharge burn-up limit is about 16000 MWD/TU.

The discrepancy between the LASER and the about 40 times faster CEB 10 group calculation is within the experimental uncertainty. The use of 16 groups has only a minor effect.

10.5. Isotopic Abundances

Measured main chain uranium and plutonium isotopic abundances and Pu/U mass ratio obtained from mass spectrometric analysis in ref. 7 are now compared with a 10 group CEB unit cell calculation for verification of the employed group condensation procedure to be used later in over-all reactor and single assembly calculations.

The calculated and measured parameters are given as functions of the total accumulated fissions per initial U^{238} density (F^{tot}/N_o^{28}) determined from reduction of heavy-element isotopic compositions of spent fuel, instead of from burn-up, for elimination of bias from energy-conversion factors (MeV/fission) that are necessary for the burn-up determination.

The relationship between burn-up and F^{tot}/N_o^{28} appears from fig. 29 which approximately shows that $0.01\ F^{tot}/N_o^{28} \sim 9275$ MWD/TU.

The calculated and measured uranium and plutonium abundances (a/o) are shown as functions of total accumulated fissions in figs. 30 and 31 respectively. The agreement is excellent.

The calculated and measured Pu/U mass ratios are compared in fig. 32. The calculation is in good agreement with the measurements, although there is a small underestimation in the calculation due to the applied U^{238} resonance cross sections as discussed in section 10.4.

The scatter in the measured data is mainly caused by fuel samples that are taken from different axial zones and therefore have different irradiation histories depending on the local fuel and moderator temperatures, but also the environmental effect on the neutron flux spectrum contributes to this scatter.

10.6. Isotopic Concentrations

Measured main chain uranium and plutonium isotopic concentrations per initial U^{238} concentration (N^i/N_o^{28}) obtained from ref. 7 and given as functions of total accumulated fissions per initial U^{238} concentration (F^{tot}/N_o^{28}) are now compared with the 10 group CEB calculation.

The agreement is excellent for the uranium isotopes as can be seen from figs. 33, 34 and 35.

The over-all agreement in figs. 36 through 39 between calculation and measurements for the plutonium isotopes is good except for Pu^{239}, where there is a small underprediction in agreement with the Pu/U mass ratio calculation in fig. 32. This deviation is caused by the underestimated U^{238} resonance cross sections applied in the calculation.

At higher burn-ups there is a minor overprediction of Pu^{241}.

11. OVER-ALL CALCULATIONS

Macroscopic burn-up physics is concerned with the long-term behaviour of reactors as regards reactivity variations (lifetime), power and burn-up distributions, and total core fuel material inventories. For the treatment of the over-all light-water reactor problem, the problem is divided into a number of homogeneous regions or compositions for proper representation of reflector, structural materials, water gaps, control rods and smeared-out fuel unit cells consisting of fuel rod and cladding surrounded by an equivalent amount of moderator. As the burn-up proceeds, the unit cell treatment can be coupled more or less to the over-all behaviour as discussed in section 8.

Over-all reactor calculations can be used for the simulation of real reactor lifetimes. The different heterogeneous effects caused by the presence of thermalizing water gaps and zirconium followers, absorbing control rods and steel baffle surrounding the core as well as the outer circumscribing water reflector will be treated in this calculation. They all contribute to the over-all reactivity and spatial flux spectrum, power and burn-up distributions.

The over-all reactor problem is of course a three-dimensional one, but under certain conditions it can (or must for computational reasons) be treated in the two-dimensional approach by means of appropriate techniques.

For the BWR the important axial coupling between the void and the power distributions gives great changes in the axial void concentration that highly affects reactor properties along the coolant flow path. This imposes an over-all treatment in RZ geometry if two dimensions are applied where the cylindrical regions consist of homogenized fuel, control rods and water gaps (ref. 40).

If the axial change in the horizontal reactor compositions is small, which is definitely the case for the PWR if all control rods are either fully inserted or fully withdrawn, the over-all reactor problem can be treated in XY geometry with an appropriate axial buckling term to account for the axial leakage. Furthermore, the shape of the axial power distribution remains nearly unchanged in average during the reactor lifetime with a sinus-like shape throughout the core (ref. 41) that further justifies the XY over-all PWR treatment.

The two-dimensional XY calculation permits a rather detailed mesh description of fuel regions, control regions, structural materials, and water reflector for the representation of the core.

This section describes the average axial quarter core study of the Yankee Core I, which was simulated in detail. Calculations performed with the DBU and CDB programmes described in sections 5 and 8 are compared with available measurements as far as reactivity variations and spatial distributions of burn-ups and isotopic inventories are concerned.

11.1. Quarter Core and Assembly Descriptions

A plan view of the Yankee core with assembly and control rod identifications is shown in fig. 25. The cold dimensions applied in the average axial quarter core study with the detailed mesh representation of control rods, followers and core baffle are given in fig. 40. Number densities for associated non-fuel compositions are presented in table 5. Table 6 shows various properties employed in the average axial quarter core study of Yankee Core I.

A plan view of a Yankee fuel assembly is shown in fig. 41 with cold dimensions and fuel rod core locations. Identification number F5-SE-f5 thus refers to the fuel rod in the lower right-hand corner (f5) of the lower right-hand subassembly (SE for south east) of fuel assembly F5.

11.2. Treatment of Non-Fuel Regions

The over-all few-group diffusion theory treatment requires appropriately determined macroscopic cross sections for the homogeneous regions or meshes and boundary conditions represented by conventional extrapolation lengths or full gamma-matrices as described in section 4.

The control rods surrounded by water gaps require special attention as discussed in section 6. A multi-group transport theory treatment must be applied for determination of the space-dependent flux spectrum to obtain proper homogenized and condensed few-group cross sections.

The composition of the Yankee Ag-In-Cd control rods appears from table 7. About 40% of the total capture occurs in the fast-energy range above 1.855 eV, and Ag accounts for about 90% of this capture. The fast cross sections therefore need an accurate treatment with special emphasis on the Ag cross sections.

Fast-energy 7 group cross sections above 1.855 eV in the 16 energy group structure shown in table 3 for the control rod isotopes listed in table 7 have been determined by J. Mikkelsen, Risø, by means of the RESAB Programme System (*ref.* 39) that takes all shielding effects into account. The resonance parameters applied in the calculations give infinite dilution resonance integrals that are in good accordance with available measurements as

can be seen from table 8.

The reader interested in further details concerning these cross sections is referred to the work by J. Mikkelsen (ref. 39).

In the thermal range below 1.855 eV the cross sections for the control rod compositions were determined in the LASER 35 energy group structure on the basis of various sources.

The thermal cross sections for Ag were deduced from a 2200 m/sec cross section of 63.6 barns (ref. 42) and an assumed 1/v dependence.

The thermal cross sections for In were calculated by means of RESAB with appropriate resonance parameters for determination of the resonance shape at 1.46 eV (ref. 39).

The thermal cross sections for Cd were calculated with the SIGMA programme (ref. 43), which is the Danish version of the GALAXY programme (ref. 44) with the UKNDL cross sections (ref. 38).

In the over-all few-group diffusion theory calculation the control regions consisting of water gaps and control rods or followers were represented by either homogeneous equivalent cross sections or boundary conditions in the shape of gamma-matrices.

Macroscopic cross sections in 42 groups (35 thermal and 7 fast) for infinite medium H_2O (Nelkin scattering kernel) and fuel region consisting of smeared-out fuel rod, steel cladding and equivalent unit cell water were determined by means of the LASER - CROSS MACRO complex described in section 3. The H_2O cross sections were obtained from an unfuelled calculation, where the associated soft flux spectrum is based upon neutron slowing-down in water only.

A 42 group slab collision probability calculation was performed for a fuel region, water gap and control rod as illustrated in fig. 42 with the CELL programme described in section 6. The resulting space-dependent flux spectrum was used to determine the homogeneous equivalent 2 and 5 group cross sections for the water gap and control rod mixture. Separate water gap and control rod 5 group cross sections were converted into the equivalent 5 group gamma-matrix representing the water gap and control rod regions by means of the slab option in the collision probability programme HECS (ref. 15).

The above-described procedures ensure a correct shielding of the 1.46 eV In and 0.18 eV Cd resonances. Furthermore, the various few-group cross sections were determined in proper surroundings as regards flux spectrum conditions.

The Zr followers surrounded by water gaps went through a treatment similar to that of the control rods. The 42 group infinite medium Zr macroscopic cross sections were obtained from an unfuelled LASER-CROSS MACRO calculation.

For obtainment of proper spectrum average few-group cross sections for the core steel baffle a 16 group slab calculation was performed with CELL as shown in fig. 43. The macroscopic cross sections for SS-348 were again determined from an unfuelled LASER - CROSS MACRO calculation.

Soft spectrum few-group cross sections for the H_2O reflector were applied in the over-all investigations.

11.3. Calculation Procedure

Over-all calculations with the DBU and CDB programmes require each problem to be divided into a number of compositions for representation of the different burn-up regions and non-fuel regions. A subdivision of these homogeneous regions into smaller meshes is normally necessary for adequate accuracy in the difference equation flux solution (section 4).

In the quarter core assembly average investigations each assembly is treated as a single burn-up region as illustrated in fig. 40 and discussed in section 5. The various composition numbers and cold dimensions applied in the calculations are shown in the figure.

Detailed examinations within selected fuel assemblies are, because of limited computer storage, performed with fine burn-up region and mesh descriptions within these assemblies as indicated in fig. 44 and coarser descriptions outside them to take into account the environmental effects as shown in figs. 45, 46 and 47. The composition numbers and cold dimensions used are also shown.

The procedure outlined above for the treatment of selected fuel rods within assemblies gives absolutely determined spent-fuel inventories for the single fuel rod considered with the correct relationship to the over-all reactor lifetime.

The time step lengths and control rod patterns applied in the Phase I investigations are presented in table 9. The initial calculation as well as each control rod manipulation are followed by a time step of 0 and 2 days respectively for establishment of the proper (converged) spatial power and flux spectrum conditions due to non-uniform xenon, samarium and Doppler effects as described in section 5. These small time steps are also necessary to ensure a close coupling between the local and global calculations in

the CDB programme as discussed in section 3.

From the control rod motion history of Yankee Core I given in ref. 45 the control rod patterns applied in the investigations were determined, the criterion being that a control rod is considered as fully inserted during a time step in the XY treatment, if the tip is at least half way into the core for at least half of the time step; otherwise the control rod is considered as withdrawn.

The control rod group numbers in table 9 refer to fig. 25 and not to the composition numbers for the control regions in fig. 40.

The DBU programme was provided with 2 and 5 group homogenized unit cell macroscopic cross sections as functions of burn-up determined with the LASER - CROSS MACRO complex. A tabulation of cross sections was prepared with 15 burn-up steps in the range 0 - 14700 MWD/TU for the burn-up determination and calculated at three power densities, 32.918, 63.3037 and 100.768 W/cm^3 for treatment of the spatial xenon, samarium and Doppler effects.

The CDB programme was supplied with 10 group microscopic cross sections determined from the LASER - CROSS MICRO complex by the same procedure as described in section 10 for the CEB programme. Microscopic absorption cross sections for U^{238} and Pu^{240} were determined at the above-mentioned three power densities for the treatment of non-uniform Doppler effect.

For the over-all diffusion theory in DBU and CDB a 2 group treatment was applied if nothing else is stated.

11.4. Reactivity Conditions

Measured Yankee Core I beginning-of-life reactivities are in table 10 compared with unit cell and over-all calculations performed with LASER and DBU respectively, and the accordance is satisfactory.

The difference between the DBU and the LASER calculations for the hot, clean, full-power condition is mainly caused by the non-uniform Doppler effect and the presence of the thermalizing zirconium followers as well as the absorbing core steel baffle surrounded by the light-water reflector.

For the hot, equilibrium xenon and samarium, full-power condition, the non-uniform xenon and samarium effects give further contributions to this difference, although it is small.

The relationship between the unit cell and the over-all effective multiplication factors as functions of burn-up appears from fig. 48. The LASER unit cell burn-up calculation assumes a uniform irradiation of all fuel rods

within the core, whereas DBU determines the over-all, non-uniform irradiation. The burn-up rate for the over-all calculation is greater than for the unit cell calculation, because regions with relatively greater importance in the centre of the core undergo a greater burn-up than the core average.

The measured Yankee Core I end-of-life burn-up at normal operating conditions is in table 11 compared with unit cell and over-all calculations. The agreement between the measurement and the over-all calculation is excellent. The relationship between the unit cell and the over-all irradiation is approximately given by

$$I_{\text{over-all}} = 0.81 \times I_{\text{unit cell}} \qquad (11.1)$$

11.5. Assembly Average Burn-ups and Isotopic Inventories

Measured and calculated burn-ups normalized to core average of Yankee Core I spent fuel assemblies are presented in table 12 with the core average burn-up given in table 15.

The normalized measurements are deduced from the arithmetic mean of normalized flux-wire, isotopic and Cs^{137} data.

The assembly average burn-ups determined by means of DBU are generally in good agreement with the measurements with a deviation of about 1-2% and within the experimental uncertainty except for F4 and K5. The overestimated burn-up of F4 and F5 might be caused by an underestimated control rod group 2 residence time in the core. The pronounced scatter in the K5 measurements illustrated by 0.570 ± 0.028 (flux-wire), 0.636 ± 0.025 (isotopic) and 0.723 ± 0.030 (Cs^{137}) may account for the observed difference of about 9%.

For comparison a TURBO calculation obtained from ref. 41 is presented; it shows good accordance between the varying self-shielding factor and the interpolation burn-up methods described in sections 8 and 5 respectively.

The difference between the results obtained with the 2 energy group DBU calculation in table 12 and use of 5 energy groups is always less than about 0.3 o/oo for k_{eff} and 4 o/oo for the burn-up determination, which indicates the adequacy of the applied 2 group over-all calculation method as far as the treatment of control regions and core baffle is concerned.

The assembly average burn-ups determined with CDB are in satisfactory agreement with the measurements and in most cases within the experimental uncertainty. Comparison with the calculation where the non-uniform Doppler effect is omitted shows that this effect tends to flatten the power shape and therefore also the burn-up shape by as much as about 2%.

Measured and calculated uranium and plutonium inventories of Yankee Core 1 spent fuel assemblies are compared in tables 13 and 14. The assembly average inventories determined with CDB are normally within the experimental uncertainty except for Pu^{242}, which is underestimated.

Initial and final total core uranium and plutonium inventories of Yankee Core I spent fuel are presented in table 15.

For the final loading the calculation is in good agreement with the measurement except for Pu^{242}, which is underpredicted by about 19%. This discrepancy is mainly caused by rather unknown cross sections for Pu^{242}, which, however, only plays a minor role for the nuclear characteristics owing to its weak concentration and small cross sections.

The calculation underpredicts U^{235} by 0.4% and overpredicts U^{236} by 2.7%. For the plutonium isotopes it underpredicts Pu^{239} by 2.7%, overpredicts Pu^{240} by 3.9% and finally underpredicts Pu^{241} by 3.0%.

11.6. Isotopic Distributions Across Some Assemblies

Because of the axial variation in the power distribution a wide range of U^{235} depletions and burn-ups is exhibited for a given fuel rod. Fuel samples located in regions with high power densities and associated high fuel temperatures have a higher rate of plutonium production owing to the increased Doppler broadening of the U^{238} resonances. The U^{238} capture gives rise to formation of Pu^{239} which again can transmute to higher mass number Pu isotopes in subsequent captures.

The variation of Pu/U mass ratio with U^{235} depletion for asymptotic fuel samples appears from fig. 49. The measurements are for different axial samples from selected Phase I and Phase II fuel rods located in asymptotic regions. Each fuel rod consists of a wide range of U^{235} depletions and associated Pu/U mass ratios.

A LASER calculation with an effective resonance temperature T_{eff}^{res} = 707°C corresponding to the Core I power level of 392 MW is presented. A calculation with T_{eff}^{res} = 860°C, which corresponds to the core power level of 624 MW for simulation of assembly F5 in Core II as described later in section 12, is also shown.

Fuel rod average Phase I and Phase II TURBO calculations obtained from ref. 41 and CDB calculations described in section 12 are given for comparison.

Plutonium production in fuel rods located in flux-perturbed regions occurs at a rate different from that for fuel rods in uniform lattice regions of the core. The main reason for the dependence of the plutonium build-up

on the local flux spectrum is the resonance capture in U^{238}. Where U^{238} is mostly a fast-energy range absorber, Pu^{239}, Pu^{240} and Pu^{241} are principally thermal absorbers. These properties all contribute to high plutonium production in hardened flux spectra with great fast-to-thermal flux ratios, whereas in soft flux spectra the plutonium production is low.

The flux spectrum near water gaps and zirconium followers is soft compared with the uniform lattice spectrum, whereas the opposite is true near control rods.

Plutonium production consequently occurs at a higher rate in fuel rods near inserted control rods and at a lower rate near zirconium followers than is the case in fuel rods located in asymptotic regions.

For a given U^{235} depletion the plutonium production in terms of Pu/U mass ratio increases along the diagonal from the zirconium follower to the centre of assembly H3 as illustrated in fig. 50. The growth in the plutonium production is caused by the increasingly hardened flux spectrum.

Control rod group 6 is withdrawn during Core I operation, which leaves the zirconium follower in assembly H3 during the whole Core I lifetime.

The fuel rod average measurements are obtained from axial interpolations and volume weighting operations of axial samples for selected fuel rods. These are situated from the zirconium follower to the centre of the assembly along the diagonal passing through the centres of the follower and the zirconium shim rod. The locations of the fuel rod measurements appear from fig. 50, see fig. 41 for explanation of the matrix notation identification.

The illustrated uncertainty includes estimated systematic error.

The asymptotic unit cell calculation performed with LASER is in excellent agreement with the measurements for the asymptotic fuel rods. This confirms the applicability of the unit cell treatment for these regions.

The average axial quarter core CDB calculation with a detailed mesh description within assembly H3 as shown in figs. 44 and 46 relates the different burn-up regions in H3 to the actual over-all reactor behaviour as far as spent fuel isotopic compositions are concerned.

The calculations for the different burn-up regions are indicated in fig. 50 as 1 x 1 for the corner fuel rod, 2 x 2 for the next burn-up region, 3 x 3 for the subsequent one, and finally 2 x 2 for the last burn-up region along the diagonal from the follower to the centre of the assembly. Each burn-up region represents the average of fuel rods on the diagonal and some neighbouring fuel rods, except for the corner burn-up region, which consists of a single fuel rod.

Some Core 1 end-of-life (Phase I) CDB calculations with correct

relationship to the over-all reactor lifetime are also shown in fig. 50.

The accordance with the measurements is satisfactory and excellent for the interior fuel rods. The underestimation in the Pu/U mass ratio of about 6% for the corner fuel rod is almost within the experimental uncertainty.

The distributions of U^{235} depletion and Pu/U mass ratio across some typical Core I spent fuel assemblies, H3, J3 and F4, are shown in figs. 51 through 56. The majority of the Phase I experimental data was obtained from these assemblies for which the different over-all radial core positions cause a wide variation in experienced burn-up from about 36% above core average for F4 to about 40% below average for J3 as indicated in table 12.

The illustrated Phase I data in the figures are fuel rod average measurements, whereas each burn-up region in the average axial quarter core CDB calculation represents the average for either a corner fuel rod or for some fuel rods along the diagonal between the control rod positions.

The assembly average measurements and calculations are also shown in the figures.

The assembly diagonal distributions give information about the local flux spectrum and power variations, while the assembly average distributions give information about the global, over-all variations.

The fractional U^{235} depletion for assembly H3 in fig. 51 is 0.25 near the assembly centre and about 0.34 for the corner fuel rod in both analyses and experiment. The adjacent control rod group 6 zirconium follower was present during the entire Core I lifetime for which reason the flux spectrum across the assembly remained nearly unchanged with time. There is good accordance between the measured and the calculated diagonal distributions. The burn-up regions on either side of the diagonal have a tilt of about 8-10% owing to the transverse flux leakage towards the core periphery. The assembly average calculation is overestimated by 4.8%.

The Pu/U mass ratio for assembly H3 in fig. 52 is approximately 0.0049 in both calculation and experiment near the assembly centre, whereas the corner fuel rod measurement of about 0.0051 is underpredicted by 5%. The corner fuel rod calculation is, however, within the illustrated uncertainty that includes estimated systematic error. The scatter in the measured data for the regions with asymptotic spectrum demonstrates clearly the experimental uncertainty. The burn-up regions on either side of the diagonal show a tilt of about 4-10%. The assembly average calculation is in excellent agreement with the measurement with an underprediction of 0.2%.

The calculated diagonal U^{235} depletion and Pu/U mass ratio distributions in assembly H3 are in satisfactory agreement with the measurements. The applicability of the local - global coupling method used in the CDB programme for the treatment of the individual fuel rods in the assembly is thus demonstrated for the slowly varying flux spectrum and power conditions in assembly H3.

The non-uniform Dancoff effect accounts for about 14% of the corner fuel rod Pu/U mass ratio, which indicates the importance of an accurate determination of the Dancoff effect for corner fuel rod predictions.

However, the corner fuel rods only slightly affect the total core plutonium production since the 152 perturbed corner rods only constitute a small fraction of the 23142 fuel rods for the entire core.

The non-uniform Doppler effect contributes to the Pu/U mass ratio with about 0.2% and 1% for an assembly centre and the corner fuel rod respectively.

In assembly J3, which is located at the periphery of the core where a strong flux gradient occurs, the calculated diagonal distributions of U^{235} fractional depletion in fig. 53 and Pu/u mass ratio in fig. 54 are in excellent agreement with the measurements. This indicates that the applied procedure for the treatment of the core baffle and the surrounding light-water reflector is satisfactory as far as local power and flux spectrum conditions are concerned. The illustrated uncertainty includes estimated systematic error. The TURBO calculation from ref. 41 is shown for comparison.

The assembly average U^{235} depletion and Pu/U mass ratio are underpredicted by 1.2 and 10.4% respectively. The difference in the Pu/U mass ratio is, however, based on a small absolute value.

The U^{235} depletion in assembly F4 varies in fig. 55 from 0.33 for the corner fuel rod near control rod group 2 to 0.30 in the assembly centre and to 0.41 for the corner fuel rod near control rod group 3. The CDB calculation is in excellent accordance with the measurement for the fuel rod near control rod group 3, whereas the depletion is overestimated by about 7% near the control rod group 2 location. The assembly average U^{235} depletion is overestimated by 6.3%.

Assembly F4 was located near the core centre between control rod groups 2 and 3. In the CDB calculation group 2 was inserted (at least half way into the core) for about 39% of the core life, while group 3 was inserted for about 15% of the core life. These groups were very seldom inserted simultaneously and the associated flux gradients along the diagonal of assembly F4 therefore exhibited severe changes during the lifetime. Nevertheless, the calculated distribution of U^{235} depletion along the diagonal is in

reasonably good accrodance with the measured distribution.

Because of the local distribution and the assembly average it is evident that the depletion in F4 is slightly overestimated which was also observed in section 11.5. An underestimated control rod group 2 residence time in the core might be responsible for this overestimation.

The diagonal distribution of Pu/U mass ratio in fig. 56 is in satisfactory agreement with the measured distribution and just within the indicated uncertainty which includes estimated systematic error. The assembly average Pu/U mass ratio is only overpredicted by 0.8%.

Compared with the CDB calculation the TURBO calculation from ref. 41 further overpredicts the U^{235} depletion near the control rod group 2 location, while the Pu/U mass ratio for the corner fuel rods is pronouncedly underpredicted.

The treatment of the non-uniform Dancoff effect in the CDB programme accounts here for about 14-15% of the corner fuel rod Pu/U mass ratio.

The diagonal U^{235} depletion and Pu/U mass ratio distributions across some assemblies presented above demonstrate the applicability of the local–global coupling method used in the CDB programme for the treatment of the individual fuel rods in assemblies with greatly varying flux spectrum and power conditions.

11.7. Isotopic Inventories of Selected Fuel Rods

Measured and calculated uranium and plutonium isotopic inventories of selected Yankee Core I spent fuel rods (Phase I) are compared in table 16. The fuel rod average isotopic masses and corresponding burn-ups are given.

The CDB calculations are absolutely determined with the correct relationship to the over-all reactor lifetime. Any kind of normalization for comparison with the measurements was thus avoided. The calculated fuel rod average masses therefore include uncertainties that originate in the over-all calculation.

For core location H3-C-f6 the calculated U^{235} mass is precisely equal to that measured, while the U^{236} mass is overpredicted by 3.1%. The Pu^{239} and Pu^{240} masses are overpredicted by 0.3 and 2.6% respectively, while the Pu^{241} and Pu^{242} masses are underpredicted by 5.7 and 20.7% respectively. The latter has furthermore only minor importance for the total plutonium inventory. The burn-up is underpredicted by 0.9% compared with the heavy-element isotopic determination and overpredicted by 2.3% compared with the Cs^{137} determination. The calculated masses and burn-ups are mostly within the experimental uncertainties except for U^{236} and Pu^{242}.

For core locations G4-C-f6 and E5-C-a6 the U^{235} mass is underpredicted by about 1-3%, while the U^{236} mass is overpredicted by about 8-9%. The Pu^{239} mass is overpredicted by about 1-3%, whereas the Pu^{240} and Pu^{241} masses are overpredicted by about 9-10%. It is evident that a slight overestimation of the absolute fuel rod average depletion contributes to the deviations indicated above.

The uncertainties that originate in the over-all calculation are now avoided in the subsequent investigation.

Measured and calculated normalized uranium and plutonium isotopic inventories of selected Yankee Core 1 spent fuel rods (Phase 1) are compared in tables 17 through 19. The fuel rod average isotopic mass ratios and associated burn-ups are given.

Calculations with the Swedish cluster cell burn-up programme FLEF described in ref. 46 are also presented.

The FLEF calculations obtained from ref. 47 and the CDB calculations are normalized to the measurements with the requirement of identical U^{235}/U^{238} mass ratios.

The illustrated uncertainties for each fuel rod average calculation are caused by a displacement in the U^{235}/U^{238} mass ratio within the experimental uncertainty. The calculated deviations from the measurements and the calculated deviations caused by the uncertainty in the normalization of the U^{235}/U^{238} mass ratio are indicated.

The fuel rod average isotopic mass ratios and burn-ups of the fuel rod core locations H3-C-f6, G4-C-f6 and E5-C-a6 determined by means of CDB are in all cases within the experimental uncertainties as shown in tables 17 through 19.

The U^{236}/U^{238} mass ratio is thus overpredicted by about 3-5%. The deviation in the Pu/U mass ratio varies from about -4 to 1.5%. The Pu^{239}/Pu mass ratio is determined within 0.5%, while the Pu^{240}/Pu mass ratio is overpredicted by about 2%, which causes an underprediction of the Pu^{241}/Pu mass ratio by about 0-6%. The burn-up is underestimated by approximately 2%.

The FLEF calculations have in most cases deviations that are twice as large as the deviations determined by the CDB calculations.

12. SINGLE ASSEMBLY CALCULATIONS

In the single assembly calculation method the whole-reactor problem is divided into the single assembly treatment and the over-all reactor behaviour, which in an approximate way enters the single assembly calculation through a buckling term and suitable boundary conditions in connection with appropriate power levels during the reactor lifetime.

The single assembly computation method permits a rather detailed mesh and burn-up region description within the assembly where each unit cell is normally represented by a single burn-up region. The method allows detailed investigations of depletion and build-up of isotopes in selected fuel rods situated in asymptotic neutron spectrum regions as well as in highly non-uniform, flux-perturbed regions near water gaps and control rods.

As is the case with the unit cell calculation method, the single assembly calculation method has no direct relationship to the over-all reactor lifetime. For comparison with experiments some kind of normalization is therefore necessary.

This section describes average axial single assembly burn-up calculations performed with the CDB programme compared with measurements of selected Yankee Core I fuel rods in assembly F5 that was recycled in the subsequent Core II for extended burn-up.

12.1. Calculation Procedure

The detailed mesh and burn-up region description of assembly F5 appears from fig. 57 where the cold dimensions and composition numbers applied in the CDB investigations are shown. The locations of the measured fuel rod samples are indicated by open circles.

Further description of the assembly is given in section 11.1.

The unit cell collision probability treatment was performed in 10 groups as were the over-all calculations in section 11. The assembly diffusion theory calculation was made in 2 and 5 groups respectively. The control regions were represented by equivalent cross sections in the 2 group treatment, while gamma-matrices were employed in the 5 group case. The centre core location of assembly F5 causes a small over-all radial leakage across the assembly along the diagonal through the core centre. An outer symmetric boundary condition was therefore applied around the assembly.

The measured burn-ups of assembly F5 normalized to core average in Core I and Core II were 1.395 (table 12) and 1.18 (ref. 47) respectively.

The associated average power densities in Core I and Core II and other properties of the F5 assembly are given in fig. 20.

The time step lengths and the control rod patterns for groups 1 and 2 in the single assembly CDB calculations are illustrated in table 9.

12.2. Isotopic Distributions Across the Assembly

Measured and calculated distributions of U^{235} depletion and Pu/U mass ratio across assembly F5, which has been operated in Core I and later recycled in Core II for extended burn-up, are shown in figs. 58 and 59.

The illustrated Phase II data in the figures are fuel rod average measurements each represented by a single burn-up region in the CDB calculations that were normalized to the measurements in the asymptotic region of the assembly.

The 5 group gamma-matrix CDB calculation in fig. 58 of the diagonal U^{235} fractional depletion across assembly F5 is in excellent agreement with the measurements. The nearly symmetric distribution across the assembly varies from about 0.55 for the corner fuel rods adjacent to control rod groups 1 and 2 to about 0.49 in the assembly centre.

Control rod groups 1 and 2 were very seldom and never simultaneously inserted in Core I and Core II respectively. The associated flux gradients along the diagonal of assembly F5 therefore exhibited severe reversals during the lifetime. Nevertheless, the calculated U^{235} depletion distribution across the assembly is approximately symmetric in agreement with the experimental data.

If the control regions are represented by equivalent 2 group cross sections instead of 5 group gamma-matrices, the calculated corner fuel rod U^{235} depletion decreases by about 5% at equal depletion in the asymptotic region.

The TURBO calculation from ref. 41 is shown for comparison.

The diagonal distribution of Pu/U mass ratio in fig. 59 is in excellent agreement with the measured distribution except for the corner fuel rod mass ratios which are overpredicted by about 3 and 6% in the 2 and 5 group calculation respectively. The illustrated uncertainty includes estimated systematic error.

The Pu/U mass ratio determined with the 5 group gamma-matrix calculation varies from 0.0098 in the assembly centre to 0.0091 for the rod next to the corner fuel rod near control rod group 2.

The capture in U^{238} for subsequent formation of Pu^{239} occurs primarily on account of the high flux level when the zirconium follower is present.

Moreover, U^{238} is mainly a resonance absorber, and the above-mentioned smooth decrease in the Pu/U mass ratio from the assembly centre in the direction of the control rod position is therefore caused by the increasingly softened flux spectrum towards the zirconium follower.

When the control rod is present, the flux spectrum naturally hardens, but it has only minor importance for the Pu/U mass ratio because of the associated low flux level.

The smooth decrease in Pu/U mass ratio along the diagonal from the assembly centre towards the control rod position is then succeeded by an abrupt increase for the corner fuel rod compared with the neighbouring rod. The increase is mainly caused by the smaller Dancoff effect or shielding from the surrounding fuel rods compared with that for the regular lattice due to the adjacent water gaps and control rods or followers that separate the corner rod from neighbouring fuel rods in adjoining assemblies.

Although the Dancoff interaction effect varies locally throughout the fuel assembly, only corner and face fuel rods are treated for this non-uniform effect in the CDB programme as described in section 8.2. The excellent agreement between the calculated and measured Pu/U mass ratio for the fuel rod next to the corner rod justifies this treatment.

From the overestimated corner fuel rod Pu/U mass ratio it is evident that the corner fuel rod shielding was underestimated in the CDB calculation that treats face and corner fuel rods as completely unshielded on their outside surfaces.

Additional investigations should be initiated for a more accurate treatment of this non-uniform Dancoff effect.

The Pu/U mass ratio in the TURBO calculation is underestimated in the asymptotic region of the assembly and pronouncedly underpredicted for the corner fuel rods as shown in fig. 59.

12.3. Plutonium Build-up in Centre and Corner Rods

The fissile-plutonium build-up is of major interest for nuclear reactors since the highly enriched plutonium may be obtained by purely chemical separation methods.

The average burn-up of assembly F5 was about 20860 MWD/TU at the end of Core II lifetime. The relatively high burn-up of the Phase II measurements permits comparison of calculated and measured Pu^{239} and Pu^{241} build-ups over a range of U^{235} depletions from about 0.30 to 0.65. The dependence of Pu^{241} on Pu^{240} also makes the build-up of Pu^{240} important.

The spent Core II number densities of Pu^{239}, Pu^{240} and Pu^{241} per initial U^{238} number density (N^{49}/N_o^{28}, N^{40}/N_o^{28} and N^{41}/N_o^{28}) versus U^{235} depletion are illustrated in figs. 60 through 62 for an asymptotic fuel rod (F5-C-f6) and for a corner fuel rod (F5-SE-f5) next to control rod group 1. The fuel rod samples from the six axial positions result in a wide range of plutonium isotopic number densities and U^{235} depletions within each fuel rod. The volume-weighted average of the six axial samples for each fuel rod and the associated uncertainty, which includes estimated systematic error, are also shown in the figures.

The dashed curves are asymptotic unit cell LASER and CEB calculations, while the full curves represent the average axial single assembly CDB calculation of selected fuel rod histories what concerns power and flux spectrum changes caused by control rod movements during the reactor lifetime. The 2 group cross section treatment of the control regions was applied in this connection.

From the variation illustrated in fig. 60 of Pu^{239} concentration with U^{235} depletion it appears that the LASER calculation is in excellent agreement with the measurements for the asymptotic fuel rod, while CEB underpredicts by about 4%.

The Core II end-of-life (Phase II) CDB calculation overpredicts the U^{235} depletion for the asymptotic fuel rod by about 5%, while the Pu^{239} concentration is correctly determined. The control rod movements induce only very small perturbations in the asymptotic fuel rod Pu^{239} build-up and U^{235} depletion.

The corner fuel rod exhibits severe changes in the power level and the flux spectrum when the adjacent control rod group 1 is moved.

U^{238} is mainly a fast-energy range absorber, while Pu^{239} is mainly a thermal absorber. When control rod group 1 is inserted, the resulting hardened flux spectrum in the neighbouring corner fuel rod increases the net Pu^{239} production more than is the case in an asymptotic fuel rod. The opposite is true when control rod group 1 is withdrawn and the follower is present as illustrated in fig. 60, where the effect of the spectrum shift is demonstrated for the corner fuel rod in the CDB calculation.

At a U^{235} depletion of about 0.45 the Pu^{239} concentration decreases as the fuel rod is further depleted. The great Pu^{239} concentration before the decrease is caused by the presence of control rod group 1. As control rod group 1 is withdrawn in the subsequent depletion, the Pu^{239} concentration tends to reach the corresponding and lower soft spectrum value.

The Phase II CDB calculation for the corner fuel rod with the control

regions represented by 2 group cross sections underestimates the U^{235} depletion by about 5%, while the Pu^{239} concentration is overestimated by about 2%. The 5 group gamma-matrix calculation is in excellent agreement with the measured U^{235} depletion, while the Pu^{239} concentration is overpredicted by 5%, just within the experimental uncertainty. The TURBO calculation from ref. 41 underpredicts the Pu^{239} concentration by about 14%.

The variation in Pu^{240} concentration with U^{235} depletion is shown in fig. 61. The Pu^{240} build-up appears to be essentially the same for the corner fuel rod as for the centre rod at a given U^{235} depletion.

The LASER calculation passes directly through the measurement for the asymptotic centre fuel rod, while CEB underestimates the Pu^{240} concentration by about 2%.

The Phase II CDB calculation for the centre fuel rod overpredicts the Pu^{240} concentration by about 5%, just within the experimental uncertainty that includes estimated systematic error.

Pu^{239} is principally a thermal absorber, whereas Pu^{240} behaves as a resonance absorber because of the low-lying 1.056 eV resonance. When control rod group 1 is inserted, the hardened flux spectrum reduces the net Pu^{240} production in the corner fuel rod in comparison with an asymptotic fuel rod. If control rod group 1 is withdrawn, the opposite is true as illustrated by the corner fuel rod CDB calculation in fig. 61.

The Phase II CDB calculation for the corner fuel rod with the control regions represented by 2 group cross sections overestimates the Pu^{240} concentration by about 7%, while it is overestimated by about 9% in the 5 group gamma-matrix calculation.

From the variation illustrated in fig. 62 of Pu^{241} concentration with U^{235} depletion it appears that the LASER and CEB calculations underestimate the Pu^{241} concentration for the asymptotic centre fuel rod by about 6%.

The centre fuel rod Phase II CDB calculation overpredicts the Pu^{241} concentration by about 9%.

Pu^{240} behaves like U^{238} as a resonance absorber because of the low-lying 1.056 eV resonance, while Pu^{241} is principally a thermal absorber. The hardened flux spectrum caused by insertion of control rod group 1 increases the net Pu^{241} production in the corner fuel rod in comparison with an asymptotic fuel rod. The opposite occurs when control rod group 1 is withdrawn as illustrated in fig. 62 for the corner fuel rod in the CDB calculation.

The corner fuel rod Phase II CDB calculation with the control regions represented by 2 group cross sections underestimates the Pu^{241} concentration by about 6%, while it is overestimated by about 6% in the 5 group gamma-matrix calculation.

Both calculations are nearly within the experimental uncertainty that includes estimated systematic error. The TURBO calculation from ref. 41 underpredicts the Pu^{241} concentration by about 14%.

The above calculations of the various plutonium isotopic concentrations for the corner fuel rod indicate that the 5 group gamma-matrix treatment is preferable as it gives almost the same overestimate for all the plutonium isotopes. The overestimated plutonium production for the corner fuel rod is due to the treatment of the non-uniform Dancoff effect in the CDB programme as discussed in section 12.2.

Typical beginning-of-life unit cell leakage spectra or equivalent leakage cross sections, Σ_1, in equation 8.1 for the asymptotic fuel rod core location F5-C-f6 and the corner fuel rod core location F5-SE-f5 in the CDB calculation are illustrated in figs. 63 and 64 corresponding to inserted and withdrawn control rod group 1 and 2 positions. A positive leakage cross section is tantamount to leakage out of the unit cell, while a negative cross section accounts for leakage into the unit cell. The leakage caused by the 1.46 eV In resonance appears clearly from the figures.

12.4. Isotopic Inventories of Selected Fuel Rods

The centre and the corner fuel rod uranium and plutonium isotopic inventories determined by the 5 group gamma-matrix CDB calculation are compared with the measurements in tables 21 and 22. The fuel rod average isotopic mass ratios and associated burn-ups are given. The calculations are normalized to the measurements with the requirement of identical U^{235}/U^{238} mass ratios to prevent a bias that originates in different absolutely determined depletions in the single assembly CDB calculation.

The calculated deviations from the measurements and the calculated deviations caused by the uncertainty in the normalization of the U^{235}/U^{238} mass ratio are indicated.

The calculated fuel rod average isotopic mass ratios and burn-ups of the centre fuel rod core location F5-C-f6 are in excellent agreement with the Phase II measurements as shown in table 21. The mass ratios for Pu^{239}/Pu, Pu^{240}/Pu and Pu^{241}/Pu are thus determined within 1%.

The calculations for the corner fuel rod core location E5-SW-a5 are in satisfactory agreement with the Phase I measurements as illustrated in

table 22 and in all cases within the experimental uncertainties.

The corner fuel rod core position F5-SE-f5 that is symmetrical with E5-SW-a5 with respect to the north - south axis of the reactor core has been recycled in Core II for extended burn-up. The calculations are in good agreement with the Phase II measurements as shown in table 22.

These corner fuel rods exhibited severe changes in power and flux spectrum conditions when the adjacent control rod group 1 was moved.

Nevertheless, the Pu^{239}/Pu mass ratio is determined within 0.4%, while the Pu^{240}/Pu mass ratio is overpredicted by about 4-6%, which causes an underprediction of the Pu^{241}/Pu mass ratio of about 0-4%. The treatment of the non-uniform Dancoff effect in the CDB programme causes an overestimation of the Pu/U mass ratio of about 3-6%.

13. SUMMARY AND MAIN CONCLUSIONS

The developed TWODIM SYSTEM of programmes that includes a wide range of nuclear calculation methods for light-water reactors from the unit cell to the assembly and the over-all reactor treatments was verified by means of detailed calculations that were compared with available measurements for the Yankee reactor. The first and second cores were directly simulated by means of actual operating data that include changes in reactor power level and fuel and control rod managements for investigations of the applicability of the various nuclear calculation methods.

The fast unit cell burn-up treatment for fuel rods located in asymptotic neutron spectrum regions served as an efficient and for most investigations adequate tool for unit cell burn-up calculations of the time-dependent reactivities and fuel isotopic concentrations.

The interpolation burn-up method that relies on the fundamental assumption of separability between cell and over-all reactor events was sufficient for over-all reactor burn-up calculations. It is, however, insufficient for detailed investigations within the single fuel assembly owing to the often severe changes in flux spectrum and power distributions caused by control rod movements.

The new gamma-matrix boundary condition method was found excellent for the representation of control rods surrounded by water gaps in over-all diffusion calculations.

The developed method of coupling of the unit cell to the over-all calculations where the influence from the surrounding lattice on the local calculation is accounted for ensured that the single fuel rod was depleted in the true milieu. The applicability of this local - global coupling method for the treatment of the individual fuel rods in assemblies with greatly varying flux spectrum and power conditions was demonstrated for fuel rods situated in asymptotic neutron spectrum regions as well as in highly non-uniform, flux-perturbed regions near water gaps and control rods.

14. ACKNOWLEDGEMENTS

For stimulating discussions and valuable suggestions the author is grateful to the entire Reactor Physics Department at Risø and especially to B. Micheelsen, C. F. Højerup, J. Mikkelsen, and L. Mortensen.

The author wants to thank the staff of NEUCC and the computer group at Risø. In particular, the continuous assistance of E. Hansen in the IBM 7094 computations is gratefully acknowledged.

15. REFERENCES

1) H. C. Honeck, THERMOS - A Thermalization Transport Theory Code for Reactor Lattice Calculations. BNL-5826 (1961) 77 pp.

2) H. Bohl, Jr., E. M. Gelbard and G. H. Ryan, MUFT-4 - Fast Neutron Spectrum Code for the IBM 704. WAPD-TM-72 (1957) 34 pp.

3) C. G. Poncelet, Burnup Physics of Heterogeneous Reactor Lattices. WCAP-6069 (1965) 182 pp.

4) C. G. Poncelet, LASER - A Depletion Programme for Lattice Calculations based on MUFT and THERMOS. WCAP-6073 (1966) 104 pp.

5) C. G. Poncelet, Effects of Fuel Burnup on Reactivity and Reactivity Coefficients in Yankee Core I. WCAP-6076 (1965) 93 pp.

6) L. Bindler and C. G. Poncelet, Evaluation of Calculational Models and Thermal Cross-Section Data in the Analysis of PuO_2-UO_2-H_2O Lattices. Trans. Amer. Nucl. Soc. 8, (1965) 512-513.

7) R. J. Nodvik et al., Supplementary Report on Evaluation of Mass Spectrometric and Radiochemical Analyses of Yankee Core I Spent Fuel, Including Isotopes of Elements Thorium Through Curium. WCAP-6086 (1969) 259 pp.

8) G. D. Joanou and J. S. Dudek, GAM-I: A Consistent P_1 Multigroup Code for the Calculation of Fast Neutron Spectra and Multigroup Constants. GA-1850 (1961) 140 pp.

9) E. P. Wigner and J. E. Wilkins, Jr., Effect of the Temperature of the Moderator on the Velocity Distribution of Neutrons with Numerical Calculations for H as Moderator. AECD-2275 (1944) 17 pp.

10. M. Nelkin, The Scattering of Slow Neutrons by Water. Phys. Rev. 119, (1960) 741-746.

11. H. C. Honeck, An Incoherent Thermal Scattering Model for Heavy Water. Trans. Amer. Soc. 5, (1962) 47-48.

12. H. C. Honeck, The Calculation of the Thermal Utilization and Disadvantage Factors in Uranium Water Lattices. Nucl. Sci. Eng. 18, (1964) 49-68.

13. A. Hassitt, A Computer Program to Solve the Multigroup Diffusion Equations. TRG Report 229 (1962) 39 pp.

14) R.S. Varga, Matrix Iterative Analysis (Prentice-Hall, Inc., Englewood Cliffs, N.J., 1962) 322 pp.

15) J. Pedersen, Calculation of Heterogeneous Constants for Cylinders and Slabs. Risø-M-850 (1969) 20 pp.

16) K. Andrzejewski, FROST - A Two-Dimensional Few Group Neutron Diffusion Code. KR-133 (1969) 19 pp.

17) D.B. MacMillan, Iterative Methods for Solution of Diffusion Problems in r-θ Geometry. In: Proceedings of 19th National Conference. Association for Computing Machinery (1964) EL.3-1 - EL.3-5.

18) J.P. Dorsey and R. Froehlich, GAMBLE-5, A Program for the Solution of the Multigroup Neutron-Diffusion Equations in Two Dimensions, With Arbitrary Group Scattering, for the UNIVAC 1108 Computer. GA-8188 (1967) 78 pp.

19) E. Hansen, ILLINOIS-ALGOL Dynamic Overlay Storage Allocation Under IBJOB. SM-15, Danish Atomic Energy Commission (1969) (Internal Report).

20) H.W. Graves, R.F. Janz and C.G. Poncelet, The Nuclear Design of the Yankee Core. YAEC-136 (1961) 88 pp.

21) Danish Atomic Energy Commission 1969/70, Fourteenth Annual Report (1970) 13-14. Detailed report is to be published.

22) J. Pedersen, HEBUS, A Three-Dimensional Heterogeneous Burn-up- and Shuffling Programme. Risø-M-864 (1969) 31 pp.

23) F.R. Allen, ZADOC, A Two-Group, Two-Dimensional Fuel Management Programme for IBM 7090 or STRETCH. AEEW-R425 (1965) 58 pp.

24) C.G. Poncelet and A.M. Christie, Xenon-Induced Spatial Instabilities in Large Pressurized Water Reactors. WCAP-3680-20 (1968) 203 pp.

25) A.M. Christie et al., Control of Xenon Instabilities in Large Pressurized Water Reactors. WCAP-3680-23 (1969) 58 pp.

26) I. Carlvik, A Method for Calculating Collision Probabilities in General Cylindrical Geometry and Applications to Flux Distributions and Dancoff Factors. In: Proceedings of the 3rd International Conference on the Peaceful Uses of Atomic Energy, Geneva, 31 August - 9 September 1964, 2,(United Nations, New York, 1965) 225-233.

27) H. Neltrup, Risø, Denmark, unpublished work (1966).

28) F.W. Todt, Revised GAD, An Infinite Medium Depletion Program for Reactor Fuel Cycle Analysis. GA-6635 (1965) 137 pp.

29) L. Mortensen, Risö, Denmark, to be published as a Risö-M-Report (1971).

30) J.G. Tyror, Burn-up Predictions for Gas-Cooled, Graphite-Moderated Reactors. Fuel Burn-up Predictions in Thermal Reactors, Vienna, 10-14 April, 1967. (IAEA, Vienna, 1968) 3-14.

31) S.M. Hendley and R.A. Mangan, TURBO - A Two-Dimensional Few-Group Depletion Code for the IBM 7090. WCAP-6059 (1964) 134 pp.

32) C.F. Højerup, Risö, Denmark. A paper presented at the EAES Symposium on Advances in Reactor Theory, Karlsruhe, 27-29 June, 1966. Not generally available.

33) Directory of Nuclear Reactors 4,(IAEA, Vienna, 1962).

34) J. Jedruch and R.J. Nodvik, Experimentally Determined Burnup and Spent Fuel Composition of Yankee Core I. WCAP-6071 (1965) 131 pp.

35) R.J. Nodvik, Evaluation of Mass Spectrometric and Radiochemical Analyses of Yankee Core I Spent Fuel. WCAP-6068 (1966) 181 pp.

36) L. Mortensen, Risö, Denmark, unpublished work (1969).

37) T.R. England, Time-Dependent Fission Product Thermal and Resonance Absorption Cross Sections. WAPD-TM-333 (1962) 62 pp.

38) D.S. Norton, The UKAEA Nuclear Data Library February, 1968. AEEW-M824 (1968) 23 pp.

39) J. Mikkelsen, The Neutron Resonance Reactions in Thermal Nuclear Reactors Determined by Semi-Analytic as well as Numerical Methods. Risö Report No. 234 (1970) 167 pp.

40) G. Buffoni et al., Burn-Up of Pressurized or Boiling Water Reactors. RT/FI (67) 28 (1967) 175 pp.

41) P.G. Lacey and R.E. Radcliffe, Diffusion-Theory Depletion Analysis of the Yankee Core I. WCAP-6077 (1966) 124 pp.

42) M.D. Goldberg et al., Neutron Cross Sections, 2nd edition. BNL-325, 2B, suppl. 2 (1966) 418 pp.

43) J. Pedersen, Risö, Denmark, internal report (1969).

44) V.J. Bell et al., A User's Guide to GALAXY 3. AEEW-R-379 (1964) 59 pp.

45) C. G. Poncelet, Analysis of the Reactivity Characteristics of Yankee Core I. WCAP-6050 (1963) 139 pp.

46) I. Carlvik, Methods and Computer Codes Developed in Sweden for Reactor Physics Calculations. Tekniska Högskolan, Avd. för Teknisk Fysik, Finland, Report No. 506/1969 (in Swedish, 1969) 106 pp.

47) M. Edenius, Aktiebolaget Atomenergi, Sweden, internal report (1969).

48) W. T. Sha, An Experimental Evaluation of the Power Coefficient in Slightly Enriched PWR Cores. WCAP-3269-40 (1965) 46 pp.

49) C. G. Poncelet, Analysis of the Reactivity Characteristics of Yankee Core I. WCAP-6050 (1963) 139 pp.

50) L. LeSage and R. Sher, Measurement of Infinite Dilution Capture Resonance Integrals with a Moxon-Ray Detector. Reactor Physics in the Resonance and Thermal Regions. Proceedings of the National Topical Meeting of the American Nuclear Society San Diego, 7-9 February, 1966, 2. Edited by A. J. Goodjohn and G. C Pomraning. (MIT Press, Cambridge, Mass., 1966) 175-192.

16. APPENDIX

The description of the TWODIM SYSTEM of programmes for nuclear light-water reactor calculations on the IBM 7094 computer is expanded below. The loading sequence of the binary decks for the individual programmes is shown in figs. 65 through 71. The additional mounted scratch tapes for temporary storage and cross section library tapes used are also presented. The binary decks are read from the Risö programme library tape. A brief description of the primary functions of the various subroutines and procedures is presented:

LASER - unit cell burn-up

FAST	Fast-energy range data transfer to CROSS by magnetic tape.
THER	Thermal-energy range data transfer to CROSS by magnetic tape.

The remaining subroutines are described in ref. 4.

CROSS - data processing

MAIN	Controls the sequence of calls to the subroutines.
UPPER	Fast-energy range multi-group cross sections.
LOWER	Thermal-energy range multi-group cross sections.
FEWG	Few-group cross section condensation.

CELL - cross section condensation

CELL	Controls the sequence of calls to the procedures.
PREP	Cell data are read and prepared.
CPM	Provides collision probability matrix, see section 6.1.
SOLO	Flux solution, see section 6.2.
FLUX	Fluxes are written.
COND	Cross section condensation.

CEB - fast unit cell burn-up

CEB	Controls the sequence of calls to the procedures.
DAPA	Cell data and magnetic cross section library tape from CROSS MICRO are read.
FIDA	Fission product data are read.
STEP	Time step is read; flux is normalized; call of BURN for irradiation and preparation of macroscopic cross sections.
FIPO	Detailed fission product treatment.

BURN Burn-up of fuel isotopes, see section 7.2

SOLU Flux solution, see section 6.2.

EDIT Macroscopic editing.

The remaining procedures are as described for CELL.

TWODIM - over-all flux solution

MAIN Controls the sequence of calls to the procedures.

FLUC Composition numbers and fluxes are written; call of REAC.

REAC Reaction rates are written.

COAR Coarse mesh data are read.

FINE Fine mesh data are prepared.

COES Coefficients for flux solution, see section 4.1.

SVOR Successive vertical overrelaxation for flux solution.

SHOR Successive horizontal overrelaxation for flux solution.

COEB Tape version of COES.

BVOR Tape version of SVOR.

BHOR Tape version of SHOR.

DBU - over-all burn-up

MAIN Controls the sequence of calls to the procedures.

ROMO Control rod movement.

BUMA Burn-up map is written.

BUDA Burn-up data on magnetic cross section library tape from CROSS MACRO are read.

BUDI Time step or shuffling pattern is read; flux is normalized; irradiation and burn-up distribution are determined, see section 5.1.

REGI Region cross sections by interpolation burn-up method, see section 5.1.

XENT Non-equilibrium xenon treatment, see section 5.2.

The remaining procedures are as described for TWODIM.

CDB - combined unit cell and over-all burn-up

MAIN Controls the sequence of calls to procedures for over-all treatment.

CEDA Cell data and magnetic cross section library tape from CROSS MICRO are read.

CEBU Controls the sequence of calls to procedures for unit cell burn-up treatment.

TIMS Time step or shuffling pattern is read; over-all flux is normalized; over-all power densities and leakage cross sections are determined, see section 8.1.

MACR Unit cell macroscopic cross sections.

DEPL Unit cell flux normalization; call of BURN for depletion and preparation of macroscopic cross sections.

CEDI Unit cell inventories are written.

The remaining procedures are as described for CEB and TWODIM.

Table 1

Yankee Core I description (PWR)

Core data	
Uranium fuel loading (kg)	20908 [a]
Fuel enrichment (w/o U^{235})	3.4
Average core diameter (cm)	190.75
Active core height (cm)	233.40
Number of Ag-In-Cd control rods	24
Number of Zr shims	8
Nominal system pressure (atm)	136
Moderator temperature (°C)	268
Average clad temperature (°C)	280
Average fuel temperature (°C)	578
Number of fuel assemblies	76
Number of fuel rods	23142
Fuel rod pitch (cm)	1.0719
Fuel rod outside diameter (cm)	0.8636
Fuel rod stainless-steel cladding thickness (cm)	0.0533
Fuel pellet diameter (cm)	0.7468
Unit cell W/U [c]	2.67
Operating data	
Initial criticality	19-8-60
At power	16-1-61
Final shut-down	18-5-62
Nominal specific power (kW/kg)	18.75
Nominal power output (MWt)	392
End-of-life burn-up at normal conditions	6240 [d]
EFPH (effective full power hours at 392 MWt)	10840 [b]
Core average burn-up (MWD/TU)	8470 [b]

a) Determined from gravimetric measurements.

b) Determined from calorimetric data. Includes core extension period from 6240 to 8470 MWD/TU with decreasing core power and moderator temperature.

c) W/U implies water to equivalent uranium metal volume.

d) Obtained from ref. 5.

Table 2

Yankee unit cell description

Region type	Cold	Hot zero power	Hot full power [c]
	Outer region radius (cm)		
Fuel (UO_2)	0.3734	0.3742	0.3751
Clad (SS348 eff) [a]	0.4318	0.4337	0.4338
Mod. (H_2O)	0.6048	0.6073	0.6073
	Temperature (°C)		
Fuel average	20	268	578
Fuel eff. res. [b]	20	268	707
Clad	20	268	280
Mod.	20	268	268
	Number density (10^{24} atoms/cm^3)		
Fuel U^{235}	0.0007777	0.0007744	0.0007707
Fuel U^{236}	0.00000452	0.00000450	0.00000448
Fuel U^{238}	0.021822	0.021729	0.021625
Fuel O_2	0.045379	0.045185	0.044968
Clad SS348	0.077693	0.076000	0.076941
Mod. H_2O	0.033431	0.026193	0.026193

Effective fuel rod length, hot, full power (cm)	230.9
Power density (W/cm)	73.35
Fuel mass density (g U/cm)	3.912
Buckling B^2 (cm^{-2})	0.0007
UO_2 linear expansion coefficient (10^{-5} $°C^{-1}$)	0.794
SS linear expansion coefficient (10^{-5} $°C^{-1}$)	1.777

a) The pellet-to-clad gap was homogenized with the SS348.

b) Effective U^{238} resonance temperature for application in the LASER programme with the method described in ref. 48.

c) Properties obtained from ref. 3.

Table 3

Energy group structures

16 groups		10 groups		5 groups		2 groups	
Energy group	Upper energy boundary (eV)	Energy group	Upper energy boundary (eV)	Energy group	Upper energy boundary (eV)	Energy group	Upper energy boundary (eV)
1	10^7		10^7		10^7		10^7
2	3.678×10^6	1		1			
3	1.353×10^6					1	
4	4.978×10^5	2	4.978×10^5	2	4.978×10^5		
5	5.530×10^3	3	5.530×10^3		5.530×10^3		
6	748.4	4	748.4	3			
7	78.88						
8	1.855	5	1.855		1.855		1.855
9	1.0987	6	1.0987	4			
10	1.0137	7	1.0137				
11	0.6249	8	0.6249		0.6249		
12	0.3206					2	
13	0.2510	9	0.2510				
14	0.1116			5			
15	0.04276		0.04276				
16	0.02049	10					

Table 4

Yankee Core I beginning-of-life reactivities compared with unit cell calculations

State		ρ	k_{eff} [a]
Cold, clean	Measured	-	-
	LASER		1.1840
Hot, clean, zero power	Measured	0.113 ± 0.003 [b]	1.1196 ± 0.0033
	LASER		1.1210
Hot, clean, full power	Measured	0.0985 ± 0.0073 [c]	1.1035 ± 0.0081
	LASER		1.1042
	CEB [d]		1.1114
Hot, equil. Xe and Sm, full power	Measured	0.0693 ± 0.008 [c]	1.0718 ± 0.0090
	LASER		1.0717
	CEB		1.0790

a) $k_{eff} = \exp(\rho)$ is applied (ref. 5).

b) Obtained from ref. 5.

c) Obtained from ref. 49.

d) 10 energy group treatment.

Table 5

Yankee core compositions

Region type	Number density [a] (10^{24} atoms/cm^3)
Zirconium followers	0.04298
Ag-In-Cd control rods	0.05480
Water gaps (268°C; 136 atm.)	0.02619
Core steel baffle	0.08538
Water reflector (268°C; 136 atm.)	0.02619

[a] Refers to cold dimensions.

Table 6

Yankee Core I average axial quarter core properties

Power density (MW/cm)		0.4244
Axial buckling B_z^2 (cm^{-2})		0.00015
DBU	Unit cell mass density (g U/cm^3)	3.3762
	Unit cell power density (W/cm^3)	63.3037
CDB	Fuel rod mass density (g U/cm)	3.912
	Dancoff factor for regular lattice	0.39402

Table 7

Yankee control rod composition

	w/o	Isotopes considered in natural abundance
Ag	80	107, 109
In	15	113, 115
Cd	5	110, 112, 114, 116 111, 113

Table 8

Infinite dilution resonance integrals

Element	RI_{RESAB} [a] (barns)	$RI_{measured}$ [a] (barns)
Ag	766	752 ± 40 (ref. 50)
In	3181	3235 ± 200 (ref. 50)

[a] RI includes 1/v absorption above 0.5 eV.

Table 9

Time step lengths and control rod patterns applied in average axial investigations

Phase I Reference power - 392 MWt		Phase II Reference power - 540 MWt	
Time step length (days)	Control rod pattern	Time step length (days)	Control rod pattern
initial	none	initial	none
0	none	0	none
0	1235	0	135
2	1235	2	135
14.6666	1235	14.6666	135
0	245	0	15
2	245	2	15
48	245	87.5833	15
0	135	0	2
2	135	2	2
50.0833	135	67.5	2
0	25	0	none
2	25	2	none
29.25	25	59.75	none
45.8333	25	66.0833	none
0	1		
2	1		
48	1		
0	2		
2	2		
31.3333	2		
0	none		
2	none		
52.6666	none		
59.2083	none		
59.2083	none		

Table 10

Yankee Core I beginning-of-life reactivities compared with unit cell and over-all calculations

Beginning-of-life state		k_{eff}
Hot, clean, full power	Measurement	1.1035 ± 0.0081 [a]
	LASER unit cell	1.1042
	DBU over-all	1.1037
Hot, equil. Xe and Sm, full power	Measurement	1.0718 ± 0.0090 [a]
	LASER unit cell	1.0717
	DBU over-all	1.0704

[a] See table 4.

Table 11

Yankee Core I end-of-life burn-up at normal operating conditions compared with unit cell and over-all calculations

End-of-life state		Burn-up (MWD/TU)
Hot, equil. Xe and Sm, full power	Measurement	6240 [a]
	LASER unit cell	7700
	DBU over-all	6250

[a] Obtained from ref. 5.

Table 12

Measured and calculated burn-ups normalized to core average of Yankee Core I spent fuel assemblies

Assembly location	Measurement	Relative error (%)	TURBO[a]	Deviation (%)	DBU	Deviation (%)	CDB[b]	Deviation (%)	CDB	Deviation (%)
G5			1.481		1.449		1.477		1.459	
F5 (E5)	1.395 ± 0.030	± 2.2	1.435	+ 2.9	1.418	+ 1.6	1.455	+ 4.3	1.431	+ 2.6
G4	1.415 ± 0.036	± 2.5	1.432	+ 1.2	1.423	+ 0.6	1.444	+ 2.0	1.431	+ 1.1
F4	1.356 ± 0.030	± 2.2	1.405	+ 3.6	1.396	+ 2.9	1.425	+ 5.1	1.407	+ 3.8
H4	1.272 ± 0.037	± 2.9	1.287	+ 1.2	1.284	+ 0.9	1.288	+ 1.3	1.286	+ 1.1
H5	1.278 ± 0.030	± 2.3	1.279	+ 0.1	1.290	+ 0.9	1.304	+ 2.0	1.299	+ 1.6
G3			1.269		1.266		1.271		1.268	
F3			1.258		1.266		1.281		1.274	
H3	1.036 ± 0.036	± 3.5	1.052	+ 1.5	1.057	+ 2.0	1.048	+ 1.2	1.052	+ 1.5
J5	1.014 ± 0.028	± 2.8	0.989	- 2.5	1.009	- 0.5	1.003	- 1.1	1.011	- 0.3
F2			0.984		1.002		0.999		1.005	
J4	0.937 ± 0.030	± 3.2	0.943	+ 0.6	0.956	+ 2.0	0.942	+ 0.5	0.951	+ 1.5
G2			0.933		0.946		0.934		0.941	
J3	0.596 ± 0.019	± 3.2	0.613	+ 2.3	0.600	+ 0.3	0.580	- 3.0	0.588	- 1.7
H2			0.608		0.597		0.578		0.585	
K5	0.643 ± 0.016	± 2.5	0.577	-10.3	0.584	- 9.2	0.566	-12.0	0.578	-10.1
F1			0.571		0.579		0.563		0.574	
K4	0.455 ± 0.016	± 3.5	0.457	+ 0.4	0.452	- 0.6	0.433	- 4.8	0.442	- 2.8
G1			0.451		0.447		0.430		0.438	

a) Obtained from ref. 41.

b) Non-uniform Doppler effect omitted.

Table 13

Uranium inventories of Yankee Core I spent fuel assemblies

Assembly location	U^{234} (kg) Measurement	U^{235} (kg) Measurement	CDB	U^{236} (kg) Measurement	CDB	U^{238} (kg) Measurement	CDB	Total U (kg) Measurement	CDB
G5			6.19		0.662		262.5		269.4
F5 (E5)	0.0450±0.0015	6.36±0.08	6.26	0.608±0.012	0.657	263.0±0.7	263.4	270.0±0.7	270.3
G4	0.0476±0.0017	6.43±0.10	6.25	0.609±0.016	0.655	263.9±0.7	263.4	271.0±0.7	270.3
F4	0.0455±0.0011	6.46±0.09	6.28	0.614±0.012	0.645	263.0±0.6	262.6	270.1±0.6	269.5
H4	0.0507±0.0040	6.59±0.13	6.48	0.606±0.022	0.605	263.2±1.3	262.8	270.4±1.3	269.9
H5	0.0466±0.0017	6.54±0.08	6.49	0.565±0.011	0.612	264.2±1.0	263.7	271.4±1.0	270.8
G3			6.52		*0.600*		*262.9*		270.0
F3		7.07±0.16	6.53		0.604		263.7		270.8
H3	0.0492±0.0018	7.02±0.10	6.94	0.492±0.024	0.525	264.5±0.6	264.2	272.1±0.6	271.7
J5	0.0499±0.0023		7.00	0.513±0.013	0.506	263.0±1.3	263.4	270.6±1.3	270.9
F2		7.17±0.12	7.02		0.507		263.4		270.9
J4	0.0516±0.0017		7.14	0.471±0.017	0.486	264.6±0.9	264.4	272.3±0.9	272.0
G2		7.83±0.09	7.15		0.485		264.4		272.0
J3	0.0541±0.0014		7.87	0.344±0.010	0.337	264.4±0.8	264.2	272.8±0.8	272.4
H2		7.81±0.09	7.88		0.335		264.2		272.4
K5	0.0499±0.0022		7.92	0.329±0.009	0.335	265.4±1.0	265.1	273.6±1.0	273.4
F1		8.15±0.13	7.94		0.333		265.1		273.4
K4	0.0554±0.0018		8.21	0.292±0.013	0.272	264.8±0.9	264.5	273.3±0.9	273.0
G1			8.22		0.270		264.5		273.0

Table 14

Plutonium inventories of Yankee Core I spent fuel assemblies

Assembly location	Pu^{239} (kg) Measurement	CDB	Pu^{240} (kg) Measurement	CDB	Pu^{241} (kg) Measurement	CDB	Pu^{242} (kg) Measurement	CDB	Total Pu (kg) Measurement	CDB
G6		1.37		0.231		0.121		0.0106		1.73
F5 (E5)	1.36 ±0.04	1.37	0.205 ±0.008	0.227	0.115 ±0.005	0.119	0.0123 ±0.0008	0.0102	1.69 ±0.04	1.72
G4	1.38 ±0.04	1.36	0.207 ±0.010	0.225	0.109 ±0.006	0.117	0.0108 ±0.0007	0.0100	1.71 ±0.04	1.71
F4	1.36 ±0.04	1.35	0.205 ±0.008	0.221	0.108 ±0.005	0.114	0.0104 ±0.0006	0.0097	1.68 ±0.04	1.69
E4	1.27 ±0.04	1.26	0.181 ±0.010	0.195	0.0966±0.0055	0.0940	0.0103 ±0.00074	0.0072	1.56 ±0.04	1.56
E5	1.35 ±0.04	1.29	0.190 ±0.008	0.200	0.0936±0.0047	0.0977	0.00697 ±0.00051	0.00755	1.64 ±0.04	1.60
G3		1.26		0.192		0.0913		0.00687		1.55
F3		1.27		0.195		0.0941		0.00711		1.57
E3	1.12 ±0.02	1.11	0.140 ±0.011	0.148	0.0641±0.0046	0.0615	0.00500 ±0.00044	0.00381	1.33 ±0.02	1.32
J5	1.17 ±0.05	1.09	0.136 ±0.007	0.142	0.0638±0.0050	0.0577	0.00541 ±0.00052	0.00342	1.38 ±0.05	1.29
F2		1.08		0.140		0.0570		0.00335		1.28
J4	1.05 ±0.03	1.03	0.126 ±0.008	0.128	0.0557±0.0033	0.0495	0.00410 ±0.00032	0.00274	1.24 ±0.03	1.21
G2		1.03		0.127		0.0484		0.00265		1.21
J3	0.776±0.022	0.695	0.0662±0.0066	0.0603	0.0220±0.0042	0.0154	0.00179 ±0.00044	0.000517	0.866±0.029	0.771
H2		0.692		0.0598		0.0152		0.000505		0.768
K5	0.715±0.024	0.710	0.0634±0.0025	0.0601	0.0220±0.0024	0.0115	0.000900±0.00010	0.000505	0.801±0.024	0.787
F1		0.704		0.0593		0.0152		0.000492		0.779
K4	0.557±0.027	0.550	0.0429±0.0059	0.0376	0.0120±0.0028	0.0074	0.000460±0.00013	0.000185	0.612±0.028	0.595
G1		0.545		0.0370		0.0072		0.000179		0.569

Table 15

Initial and final uranium and plutonium inventories of Yankee Core I spent fuel

	Measurement (kg)	Relative error (%)	Calculation CDB (kg)	Deviation (%)
Initial loading				
U^{234}	4.2		0	
U^{235}	711		711	
U^{236}	4.2		4.2	
U^{238}	20,189		20,189	
Total U	20,908		20,904	
Final loading				
U^{234}	3.78 ± 0.13	± 3.4	0	
U^{235}	539 ± 5	± 0.9	537	- 0.4
U^{236}	36.7 ± 1.3	± 3.5	37.7	+ 2.7
U^{238}	$20,040 \pm 20$	± 0.1	20,050	+ 0.05
Total U	$20,620 \pm 20$	± 0.1	20,625	+ 0.02
Pu^{239}	81.3 ± 2.0	± 2.5	79.1	- 2.7
Pu^{240}	10.3 ± 0.4	± 3.9	10.7	+ 3.9
Pu^{241}	4.94 ± 0.22	± 4.5	4.79	- 3.0
Pu^{242}	0.435 ± 0.03	± 6.9	0.351	- 19.3
Total Pu	97.0 ± 1.8	± 1.9	94.9	- 2.2
Burn-up (MWD/TU)	8440 ± 135 [a]	± 1.6	8498	+ 0.7

a) Average value inferred from calorimetric, isotopic and Cs^{137} measurements.

Table 16

Uranium and plutonium inventories of selected Yankee Core I spent fuel rods

Fuel rod	H3-C-f6				G4-C-f6				E5-C-a6(F5-C-f6)			
Mass (g)	Experiment[a]	Error (%)	CDB	Deviation (%)	Experiment	Error (%)	CDB	Deviation (%)	Experiment	Error (%)	CDB	Deviation (%)
U^{234}	0.163 ±0.008	4.9			0.156 ±0.012	7.7			0.149 ±0.007	4.7		
U^{235}	23.0 ±0.3	1.3	23.0	0	21.3 ±0.3	1.4	20.7	- 2.8	21.0 ±0.3	1.4	20.7	-1.4
U^{236}	1.63 ±0.03	1.8	1.68	+ 3.1	1.97 ±0.06	3.1	2.14	+ 8.6	1.97 ±0.04	2.0	2.13	+8.1
U^{238}	867.3 ±4.3	0.5	866.1	- 0.1	865.0 ±4.3	0.5	863.6	- 0.2	865.1 ±4.3	0.5	863.6	-0.2
Total U	892.1 ±4.3	0.5	890.8	- 0.1	888.4 ±4.3	0.5	886.4	- 0.2	888.2 ±4.3	0.5	886.4	-0.2
Pu^{239}	3.68 ±0.12	3.3	3.69	+ 0.3	4.55 ±0.13	2.9	4.58	+ 0.7	4.42 ±0.14	3.2	4.57	+3.4
Pu^{240}	0.461 ±0.020	4.3	0.473	+ 2.6	0.673 ±0.026	3.9	0.734	+ 9.0	0.667 ±0.029	4.4	0.727	+9.0
Pu^{241}	0.208 ±0.011	5.3	0.196	- 5.7	0.350 ±0.018	5.2	0.385	+10.0	0.352 ±0.019	5.4	0.383	+8.8
Pu^{242}	0.0145±0.0010	6.9	0.0115	-20.7	0.0315±0.0021	6.7	0.0318	+ 1.0	0.0326±0.0022	6.8	0.0316	-3.1
Total Pu	4.36 ±0.12	2.8	4.37	+ 0.2	5.60 ±0.13	2.3	5.73	+ 2.3	5.47 ±0.14	2.6	5.71	+4.4
Burn-up (MWD/TU)												
Isotopic	8720 ±350	4.0	8637	- 0.9	11280 ±510	4.5	11990	+ 4.2	11620 ±460	4.0	11920	+2.6
Cs^{137}	3440 ±340	4.0		+ 2.3	11640 ±460	4.0		+ 3.0	11710 ±470	4.0		+1.8

[a] Fuel rod average measurements and associated estimated 2-standard deviation precisions are obtained from ref. 34.

Table 17

Normalized uranium and plutonium inventories of a Yankee Core I spent fuel rod

Fuel rod core location: H3-C-f6					
Mass ratio	**Measurement[a)]**	**FLEF[b)]**	**Deviation (%)**	**CDB[c)]**	**Deviation (%)**
U^{235}/U^{238} x 10	0.265 ± 0.005	0.265 ± 0.005	0 ± 1.9	0.265 ± 0.005	0 ± 1.9
U^{236}/U^{238} x 100	0.188 ± 0.004	-	-	0.194 ∓ 0.008	$+ 3.2 \mp 6.4$
Pu/U x 100	0.490 ± 0.015	0.489 ∓ 0.020	$- 0.2 \mp 7.2$	0.490 ∓ 0.017	0 ∓ 6.5
Pu^{239}/Pu	0.844 ± 0.008	0.855 ± 0.007	$+ 1.3 \pm 1.8$	0.844 ± 0.008	0 ± 1.9
Pu^{240}/Pu	0.106 ± 0.007	0.100 ∓ 0.004	$- 5.7 \mp 10.4$	0.108 ∓ 0.004	$+ 1.9 \mp 10.4$
Pu^{241}/Pu x 10	0.477 ± 0.040	0.428 ∓ 0.030	-10.3 ∓ 14.7	0.449 ∓ 0.030	$- 5.9 \mp 14.7$
Pu^{242}/Pu x 100	0.333 ± 0.040	0.236 ∓ 0.030	-29.2 ∓ 21.0	0.263 ∓ 0.030	-21.0 ∓ 21.0
Burn-up (MWD/TU)					
Isotopic	8720 ± 350	8700 ∓ 700	$- 0.2 \mp 12.0$	8637 ∓ 585	$- 0.9 \mp 10.7$
Cs^{137}	8440 ± 340		$+ 3.1 \mp 12.0$		$+ 2.3 \mp 11.0$

a) The measured uncertainties are estimated in ref. 47.

b) Obtained from ref. 47.

c) The calculated uncertainties are caused by a displacement in the normalization of the U^{235}/U^{238} mass ratio within the experimental bounds.

Table 18

Normalized uranium and plutonium inventories of a Yankee Core I spent fuel rod

Fuel rod core location: G4-C-f8					
Mass ratio	Measurement[a]	FLEF[b]	Deviation (%)	CDB[c]	Deviation (%)
U^{235}/U^{238} x 10	0.246±0.005	0.246±0.005	0± 2.0	0.246±0.005	0± 2.0
U^{236}/U^{238} x 100	0.228±0.008	-	-	0.234∓0.010	+ 2.6∓ 7.9
Pu/U x 100	0.632±0.020	0.592∓0.030	- 6.3∓ 7.9	0.608∓0.028	- 3.8∓ 7.6
Pu^{239}/Pu	0.813±0.008	0.825±0.007	+ 1.5± 1.8	0.810±0.008	- 0.4± 2.0
Pu^{240}/Pu	0.120±0.007	0.114∓0.004	- 5.0∓ 9.2	0.123∓0.004	+ 2.5∓ 9.2
Pu^{241}/Pu x 10	0.625±0.050	0.566∓0.040	- 9.4∓14.4	0.616∓0.040	- 1.4∓14.4
Pu^{242}/Pu x 100	0.563±0.050	0.402∓0.050	-28.6∓17.7	0.472∓0.059	-16.2∓19.3
Burn-up (MWD/TU)					
Isotopic	11280±510	11000∓700	- 2.5∓10.6	11105∓625	- 1.6∓10.0
Cs^{137}	11640±460		- 5.5∓10.0		- 4.6∓ 9.3

a) The measured uncertainties are estimated in ref. 47.

b) Obtained from ref. 47.

c) The calculated uncertainties are caused by a displacement in the normalization of the U^{235}/U^{238} mass ratio within the experimental bounds.

Table 19

Normalized uranium and plutonium inventories of a Yankee Core I spent fuel rod

Fuel rod core location: E5-C-a6 (F5-C-f6)					
Mass ratio	Measurement[a]	FLEF[b]	Deviation (%)	CDB[c]	Deviation (%)
U^{235}/U^{238} x 10	0.243±0.005	0.243±0.005	0± 2.0	0.243±0.005	0± 2.0
U^{236}/U^{238} x 100	0.228±0.006	-	-	0.240∓0.010	+ 5.3∓ 7.0
Pu/U x 100	0.617±0.020	0.607∓0.030	- 1.6∓ 8.1	0.626∓0.028	+ 1.5∓ 7.8
Pu^{239}/Pu	0.808±0.008	0.821±0.007	+ 1.6± 1.9	0.808±0.008	- 0.2± 2.0
Pu^{240}/Pu	0.122±0.007	0.116∓0.004	- 4.9∓ 9.0	0.125∓0.007	+ 2.4∓11.5
Pu^{241}/Pu x 10	0.644±0.050	0.587∓0.040	- 8.9∓14.0	0.643∓0.040	- 0.2∓14.0
Pu^{242}/Pu x 100	0.596±0.050	0.432∓0.050	-27.5∓16.7	0.510∓0.060	-14.4∓18.4
Burn-up (MWD/TU)					
Isotopic	11620±460	11400∓700	- 1.9∓10.0	11505∓643	- 1.0∓ 9.5
Cs^{137}	11710±470		- 2.6∓10.0		- 1.8∓ 9.5

a) The measured uncertainties are estimated in ref. 47.

b) Obtained from ref. 47.

c) The calculated uncertainties are caused by a displacement in the normalization of the U^{235}/U^{238} mass ratio within the experimental bounds.

Table 20

Yankee Core I and II average axial assembly F5 properties

Average power density in Core I (MW/cm)		0.03116
Average power density in Core II (MW/cm)		0.03570
Buckling B^2 (cm^{-2})		0.0007
CDB	Fuel rod mass density (g U/cm)	3.912
	Dancoff factor for regular lattice	0.39402

Table 21

Normalized uranium and plutonium inventories of a Yankee Core I fuel rod recycled in Core II for extended burn-up

Fuel rod core location: F5-C-f6			
Mass ratio	Measurement	CDB	Deviation (%)
U^{235}/U^{238} x 10	0.191 ± 0.003	0.191 ± 0.003	0 ± 1.6
U^{236}/U^{238} x 100	0.337 ± 0.006	0.341 ∓ 0.006	+1.2 ∓ 3.6
Pu/U x 100	0.971 ± 0.023	0.933 ∓ 0.018	-3.9 ∓ 4.2
Pu^{239}/Pu	0.724 ± 0.033	0.724 ± 0.005	0 ± 5.2
Pu^{240}/Pu	0.154 ± 0.008	0.155 ∓ 0.002	+0.6 ∓ 6.5
Pu^{241}/Pu x 10	1.050 ± 0.060	1.060 ∓ 0.030	+1.0 ∓ 6.6
Pu^{242}/Pu x 100	1.655 ± 0.104	1.445 ∓ 0.070	-12.7 ∓ 10.5
Burn-up (MWD/TU)			
Isotopic	19750 ± 630	19280 ∓ 520	-2.4 ∓ 5.8
Cs^{137}	20500 ± 660		-6.0 ∓ 5.8

Table 22

Normalized uranium and plutonium inventories of some Yankee Core I fuel rods of which one has been recycled in Core II for extended burn-up

Location	E5-SW-a5			F5-SE-f5		
Mass ratio	Measurement	CDB	Deviation (%)	Measurement	CDB	Deviation (%)
U^{235}/U^{238} x 10	0.222±0.004	0.222±0.004	0 ± 1.8	0.158±0.003	0.158±0.003	0 ± 1.9
U^{236}/U^{238} x 100	0.271±0.007	0.267±0.007	-1.5± 5.2	0.380±0.008	0.384±0.005	+1.0± 3.4
Pu/U x 100	0.663±0.021	0.680±0.017	+2.6± 5.7	0.966±0.023	1.023±0.012	+5.9± 3.6
Pu^{239}/Pu	0.758±0.044	0.755±0.008	-0.4± 6.9	0.654±0.030	0.652±0.006	-0.3± 5.5
Pu^{240}/Pu	0.153±0.011	0.162±0.004	+5.9± 9.8	0.193±0.010	0.200±0.003	+3.6± 6.7
Pu^{241}/Pu x 10	0.782±0.061	0.754±0.032	-3.6±11.9	1.234±0.073	1.229±0.023	-0.4± 7.8
Pu^{242}/Pu x 100	1.003±0.096	0.840±0.069	-16.3±16.5	2.977±0.191	2.502±0.112	-16.0±10.2
Burn-up (MWD/TU)						
Isotopic	14000±560	14117±538	+0.8±7.8	24840±790	24674±556	-0.6±5.4
Cs^{137}	14560±580		-3.0±7.7	25720±820		-4.1±5.4

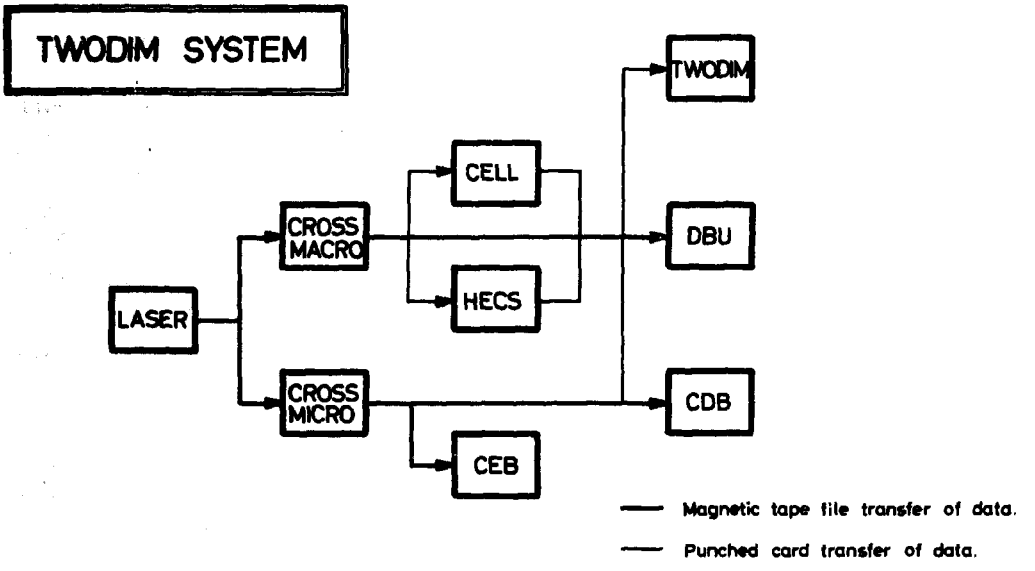

Fig. 1. The data flow in the TWODIM SYSTEM of programmes for nuclear light-water reactor calculations.

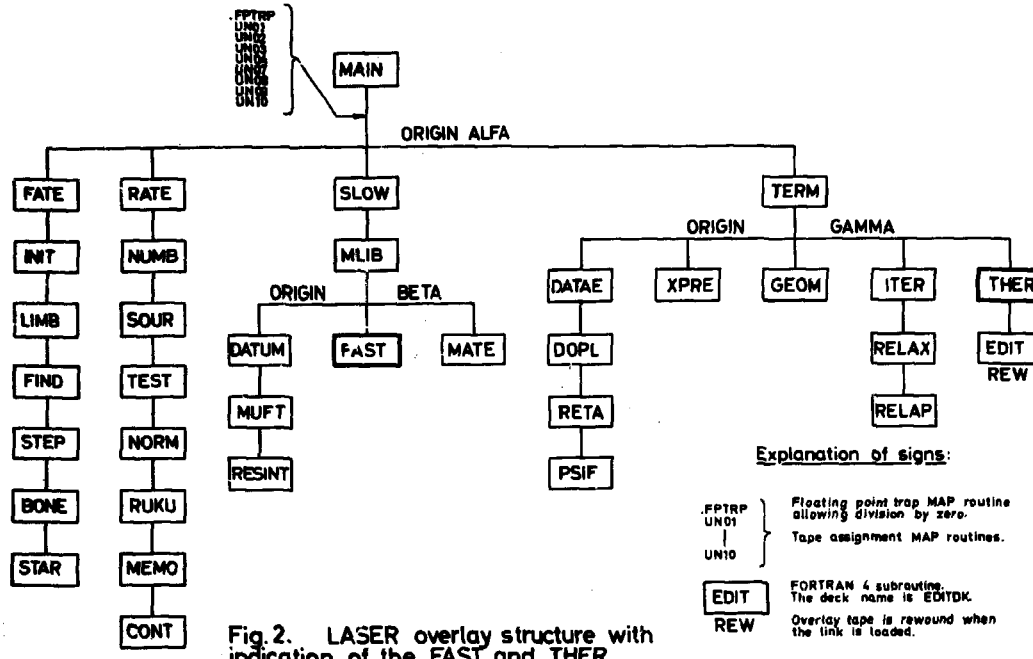

Fig. 2. LASER overlay structure with indication of the FAST and THER subroutines.

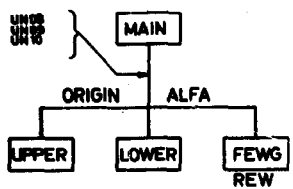

For explanation of signs see fig. 2.

Fig. 3. CROSS overlay structure.

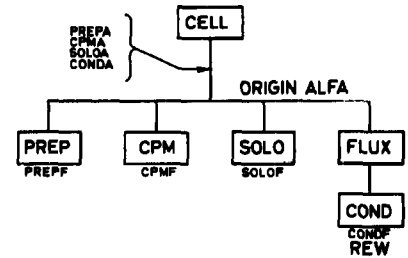

Explanation of signs

PREPA } Dynamic overlay FORTRAN 4 routine.

COND
CONDF
REW
ILLINOIS-ALGOL procedure
The deck name is CONDP.
Dynamic overlay MAP routine that loads the link.
Overlay tape is rewound when the link is loaded.

Fig. 4. CELL overlay structure.

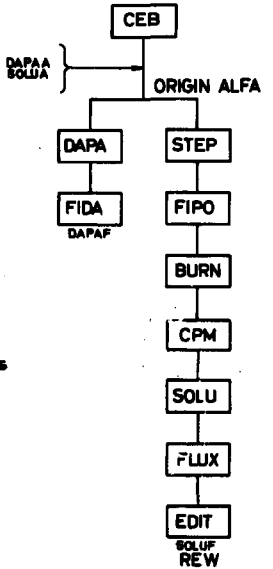

For explanation of signs see fig.4.

Fig. 5. CEB overlay structure.

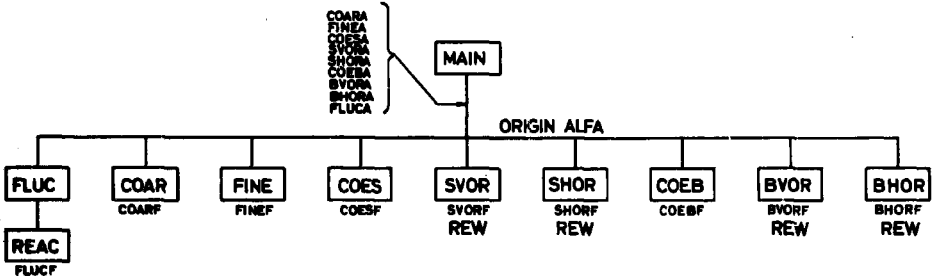

For explanation of signs see fig. 4.

Fig. 6. TWODIM overlay structure.

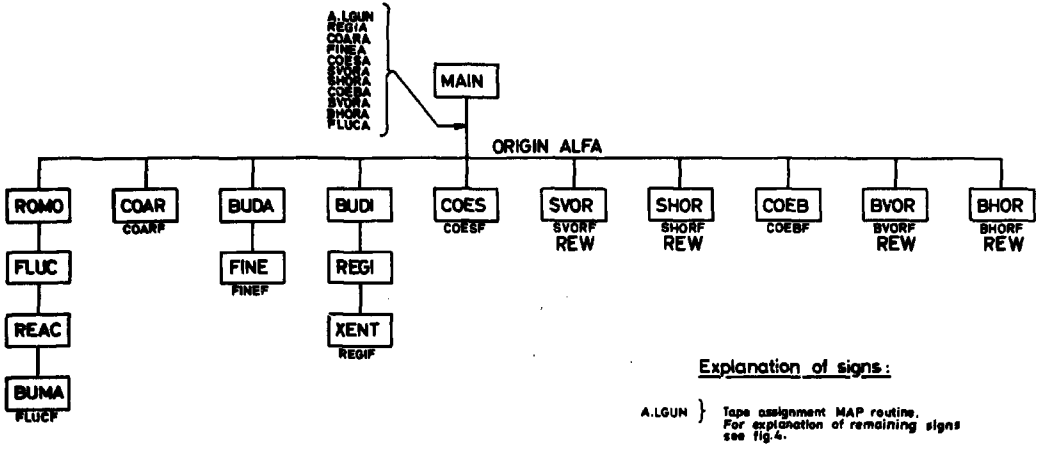

Fig.7. DBU overlay structure.

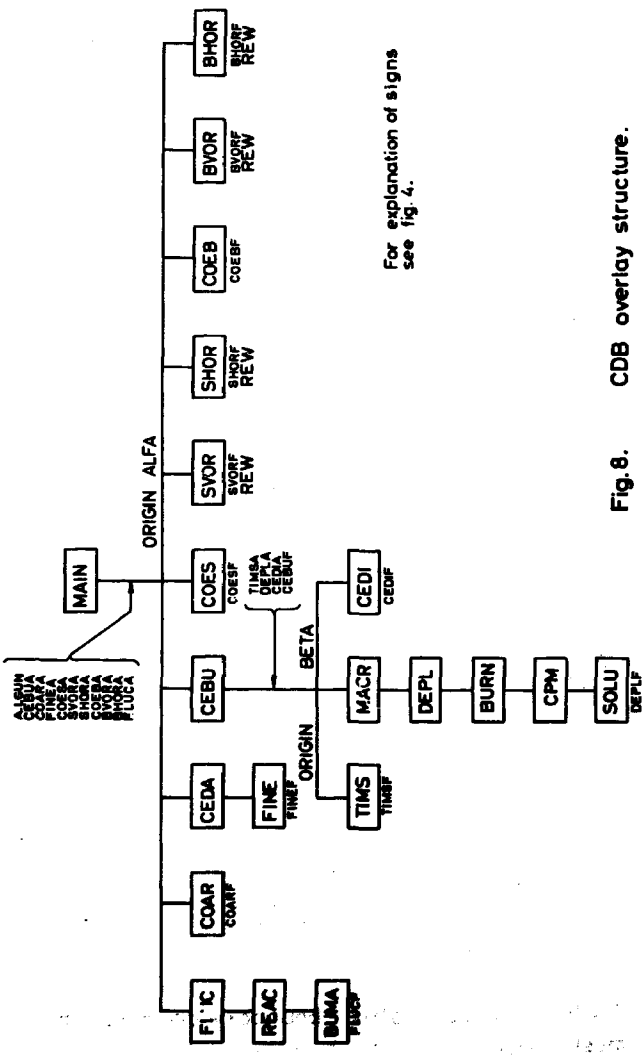

Fig.8. CDB overlay structure.

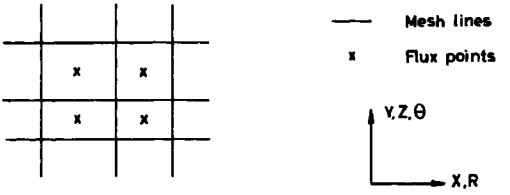

Fig. 9. Mesh description in TWODIM.

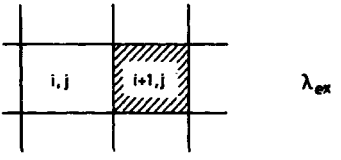

Fig. 10. Logarithmic boundary condition in mesh i+1, j.

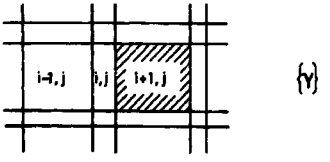

Fig. 11. Gamma - matrix boundary condition in mesh i+1, j.

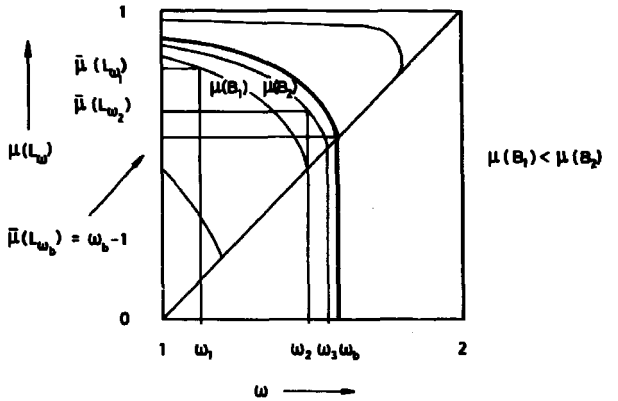

Fig. 12. $\mu(L_\omega)$ as a function of ω for various values of $\mu(B)$.

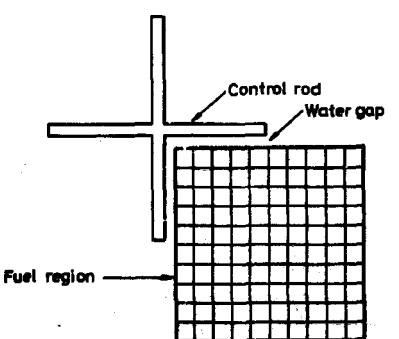

Fig. 13. Light-water fuel assembly.

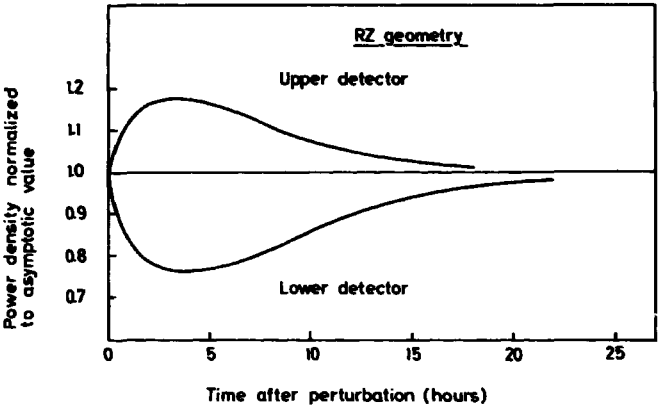

Fig. 14. Axial mode oscillation induced by insertion of four control rod rings.

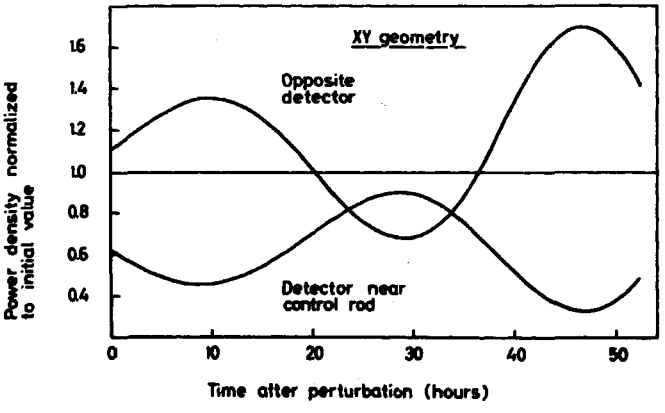

Fig. 15. Azimuthal mode oscillation induced by control rod insertion.

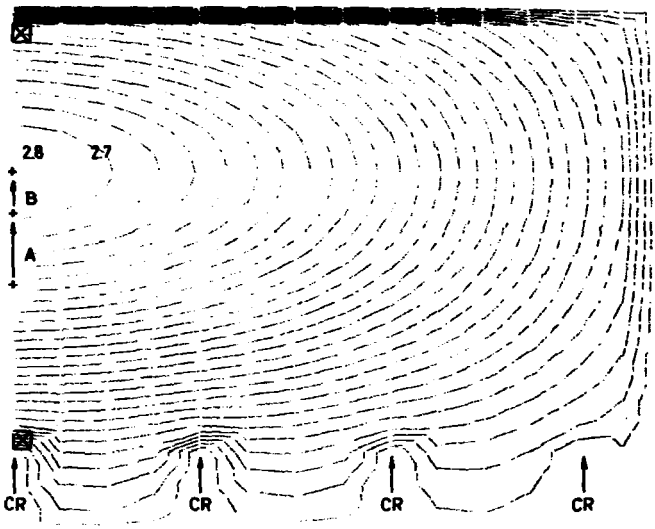

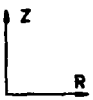

⊠ Detector

Some point to average power densities are indicated.

A) Power maximum movement owing to control rod insertion.

B) Power maximum movement three hours after control rod insertion owing to xenon effect.

Fig. 16. Power density map three hours after insertion of four control rod rings.

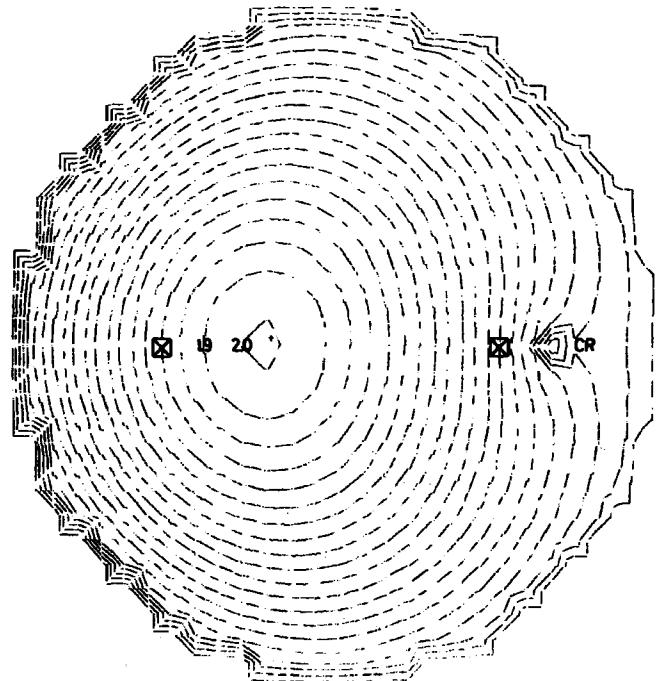

Y

X

Detector

Some point to average power densities are indicated.

Fig. 17. Azimuthal mode oscillation nine hours after perturbation.

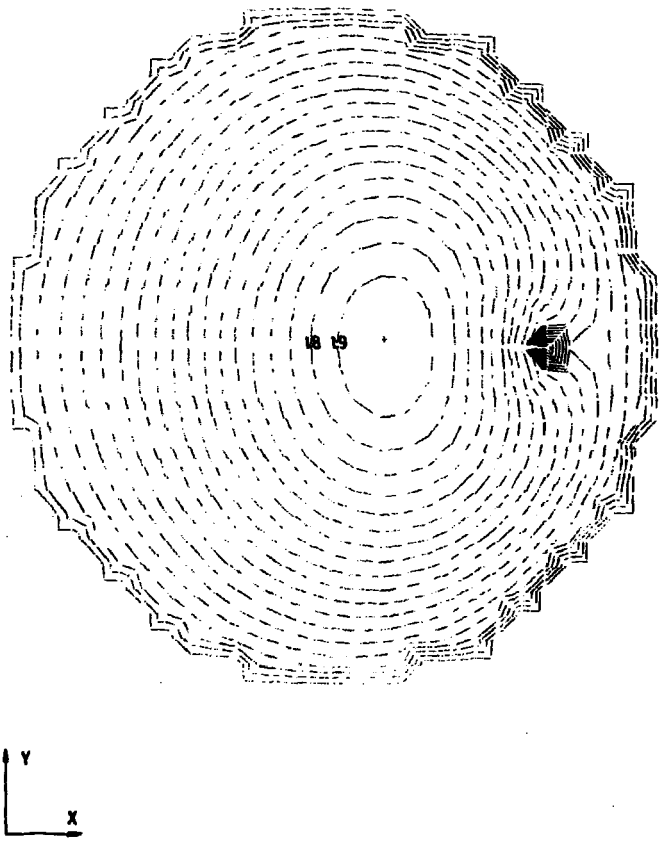

Fig. 18. Azimuthal mode oscillation thirty hours after perturbation.

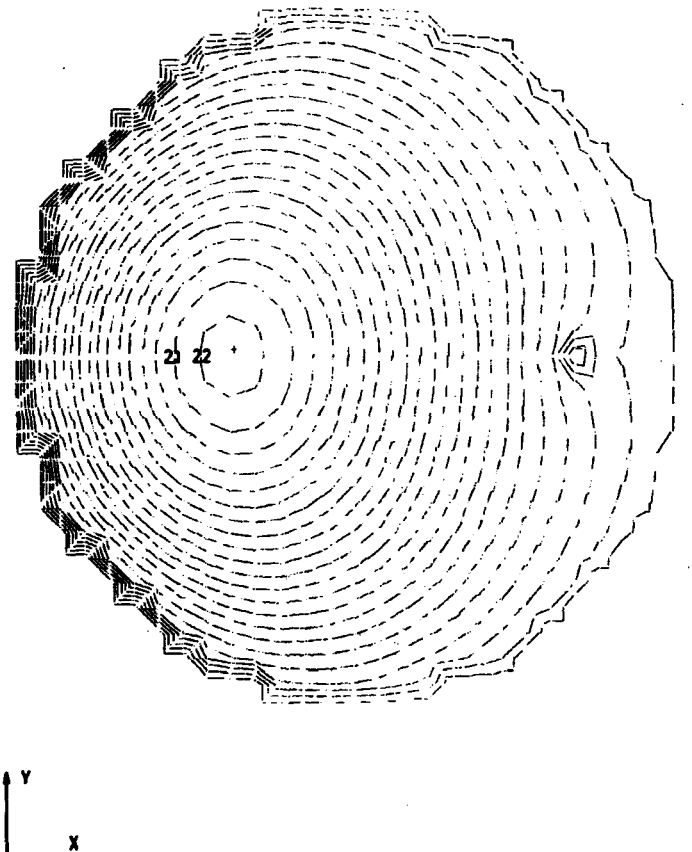

Fig. 19. Azimuthal mode oscillation forty-five hours after perturbation.

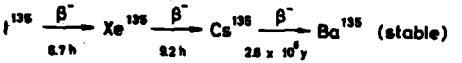

Fig. 20. Mass chain 135.

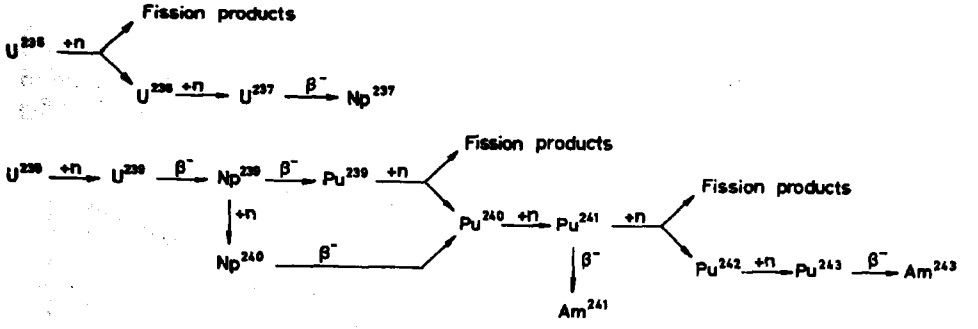

Fig. 21. The U^{235} - U^{238} Pu system.

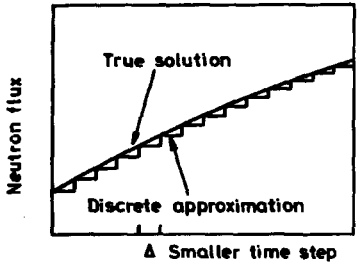

Fig. 22. Conventional flux normalization procedure in a larger time step.

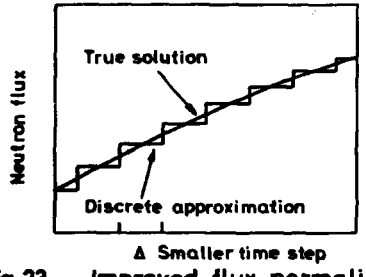

Fig. 23. Improved flux normalization procedure in a larger time step.

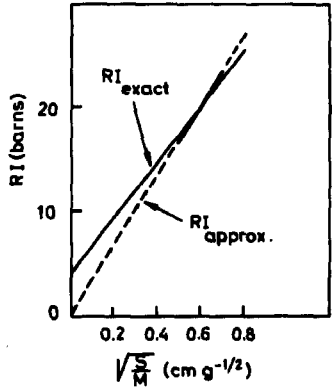

Fig. 24. Total resonance integral as a function of UO_2 fuel rod surface area to mass ratio.

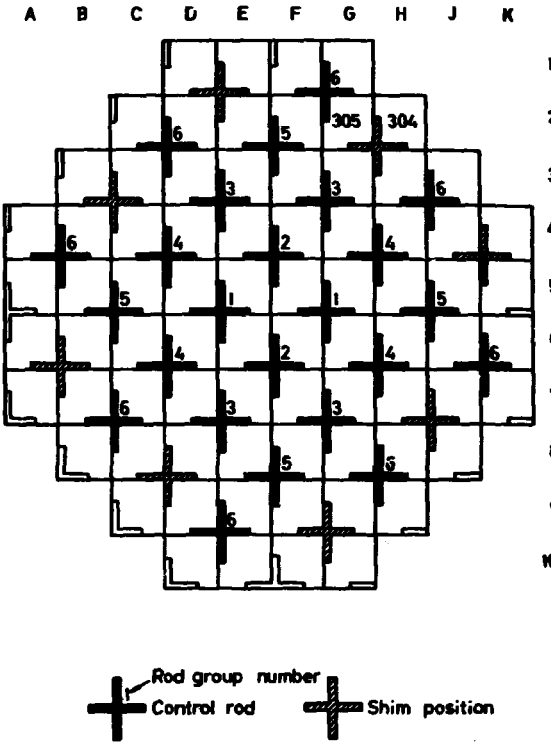

The positions of the 305 and 304 fuel rod assemblies are shown.

Fig. 25. Yankee core plan with control rod and assembly identifications.

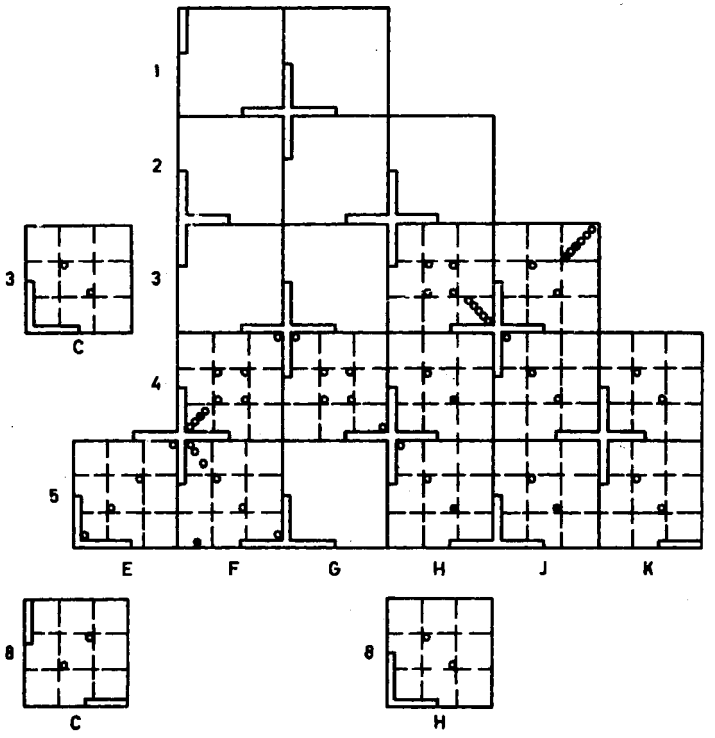

The rods indicated by open circles were sectioned for isotopic and radiochemical samples.

All Phase II fuel rods from assembly F 5.

Fig. 26. Core location of Phase I and Phase II fuel rods selected for post-irradiation analyses.

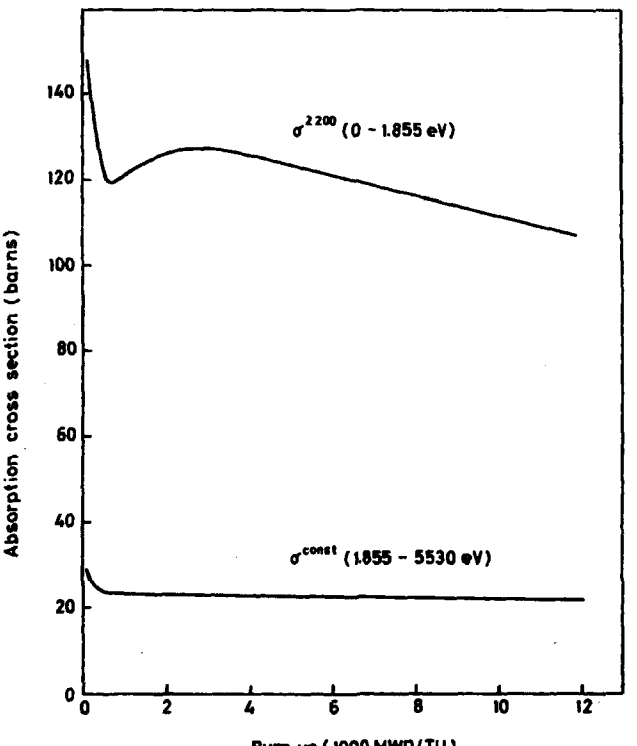

Fig. 27. Pseudo fission product cross sections for Yankee unit cell calculated with the FISS programme.

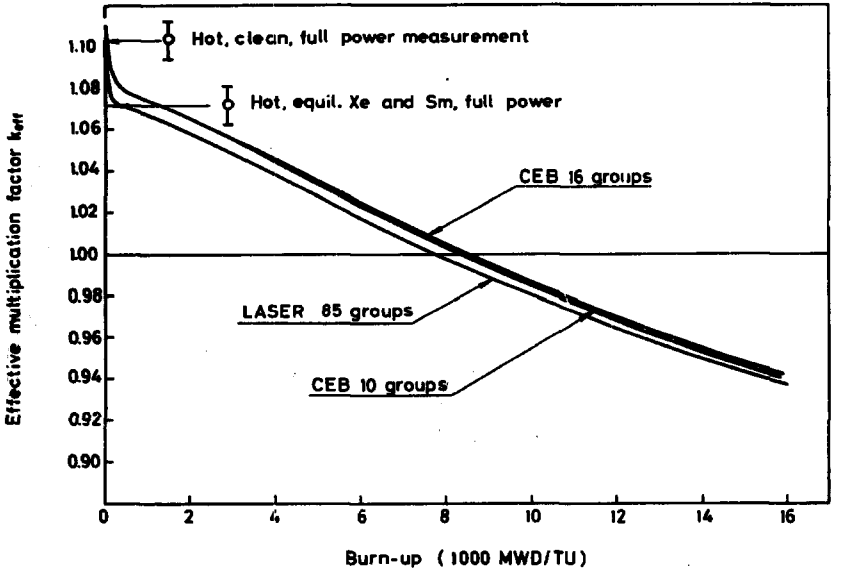

Fig. 28. Yankee Core I unit cell effective multiplication factor as a function of burn-up.

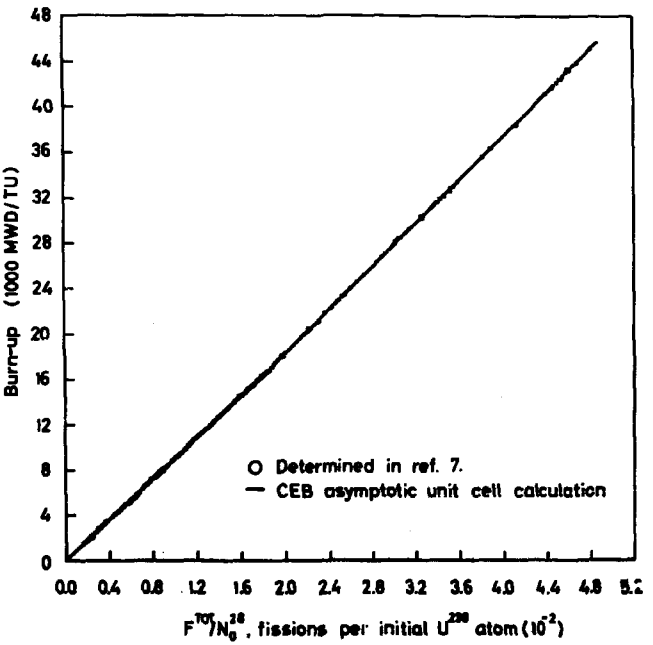

Fig. 29. Fuel burn-up versus total accumulated fissions.

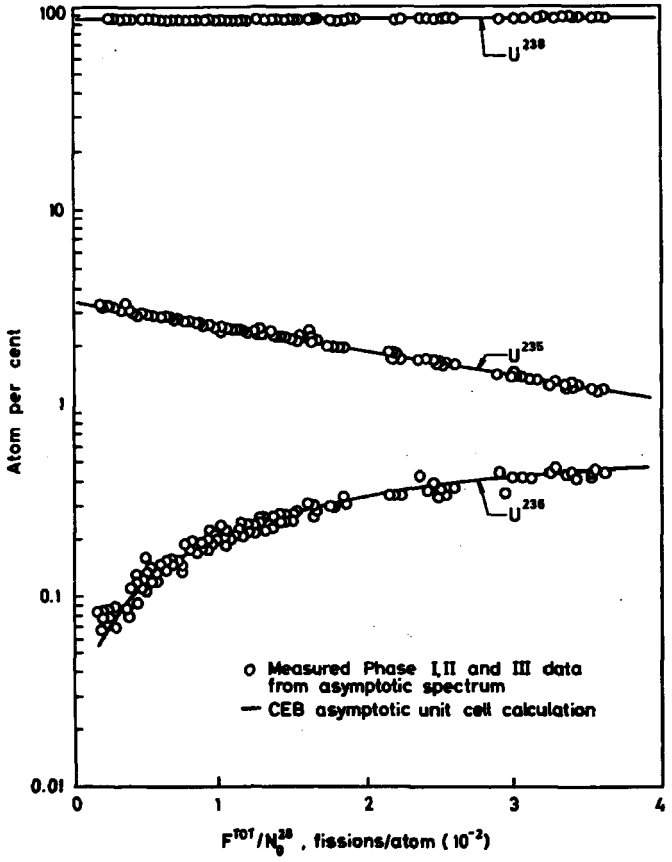

Fig. 30. Uranium isotopic abundance versus total fissions.

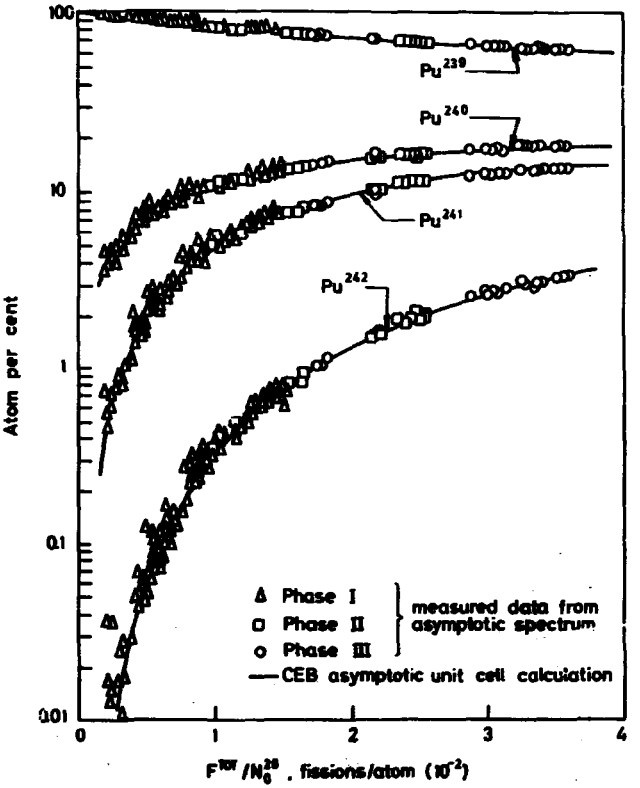

Fig. 31. Plutonium isotopic abundance versus total fissions

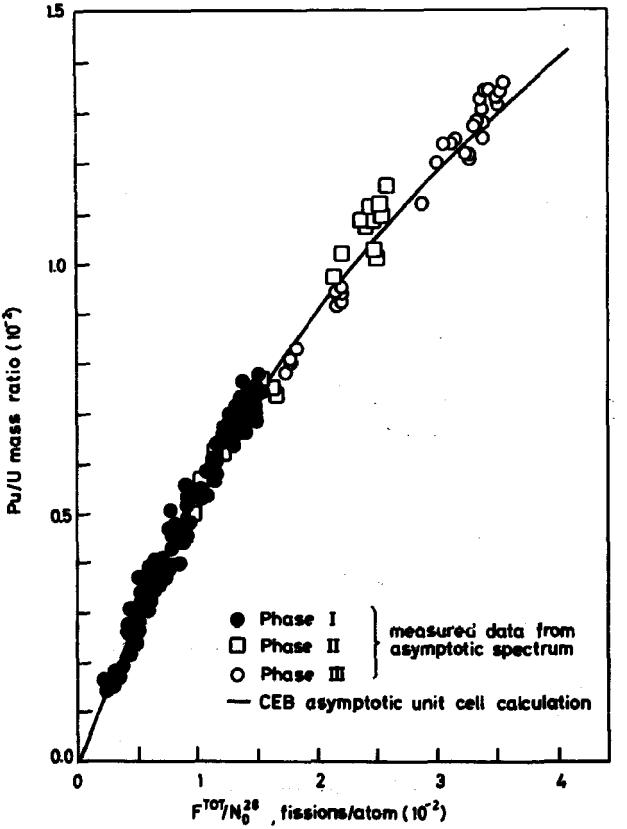

Fig. 32. Calculated and measured Pu/U mass ratio versus total fissions.

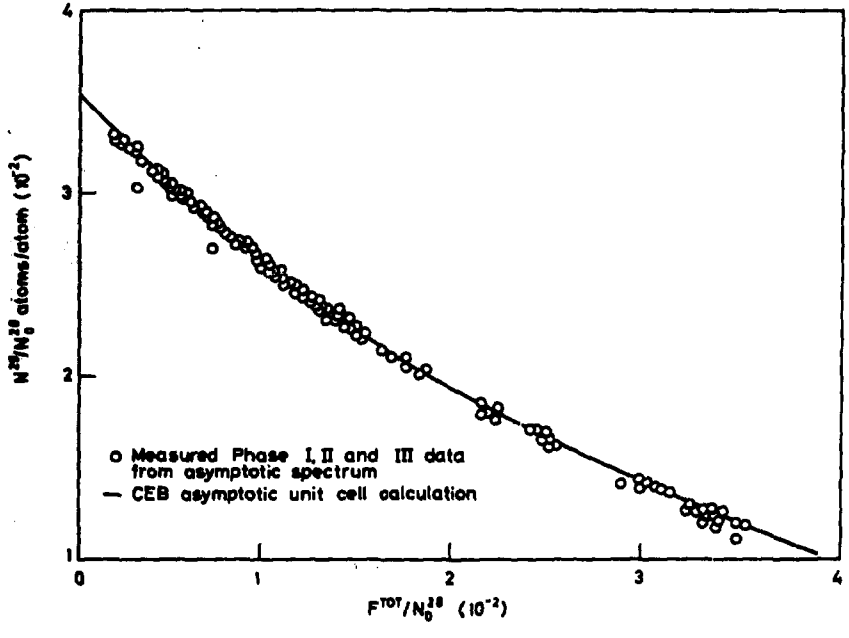

Fig. 33. U^{235} concentrations versus accumulated fissions.

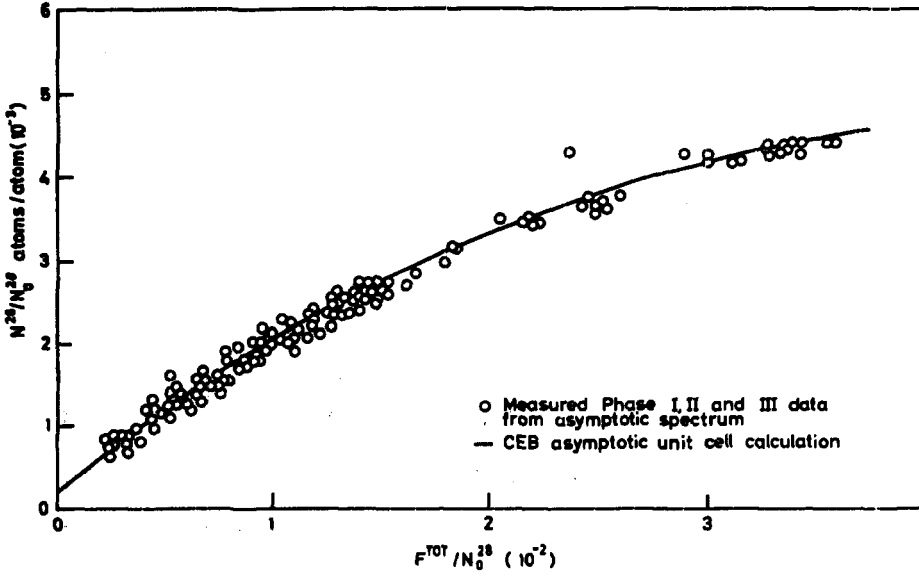

Fig. 34. U^{236} concentrations versus accumulated fissions.

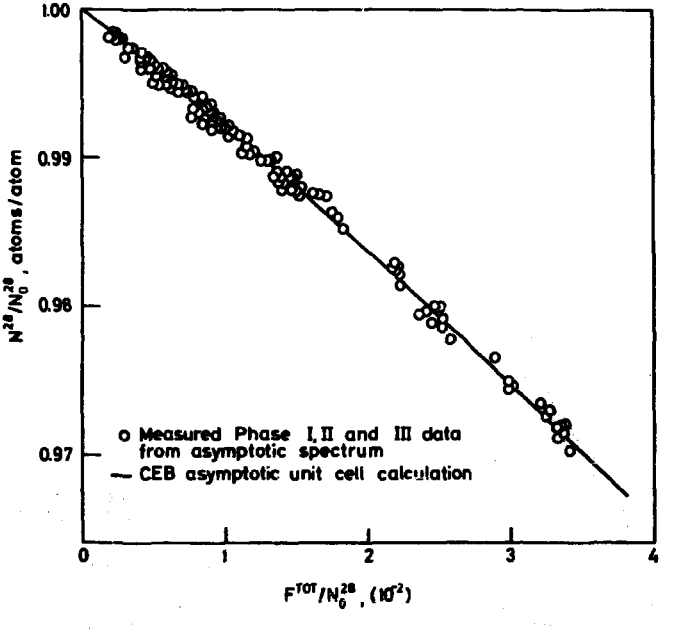

Fig. 35. U^{238} concentrations versus accumulated fissions.

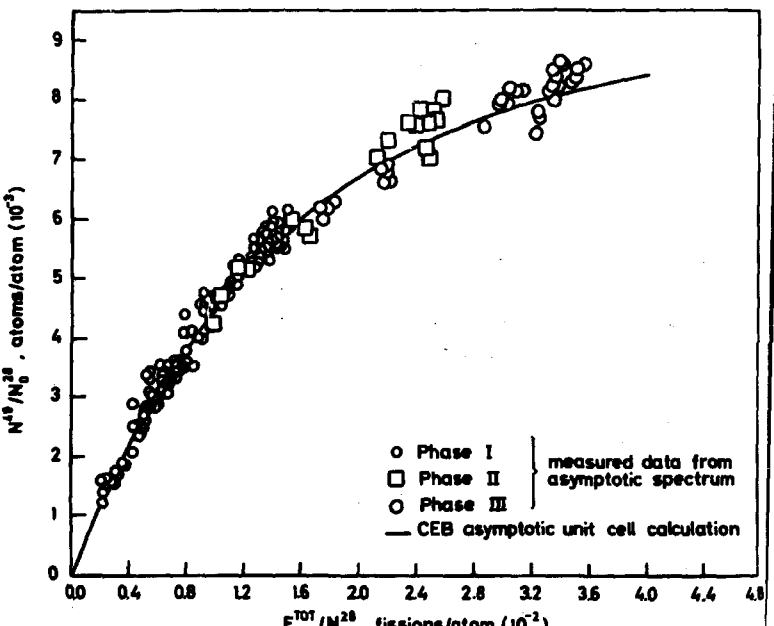

Fig. 36. Pu^{239} concentrations versus accumulated fissions.

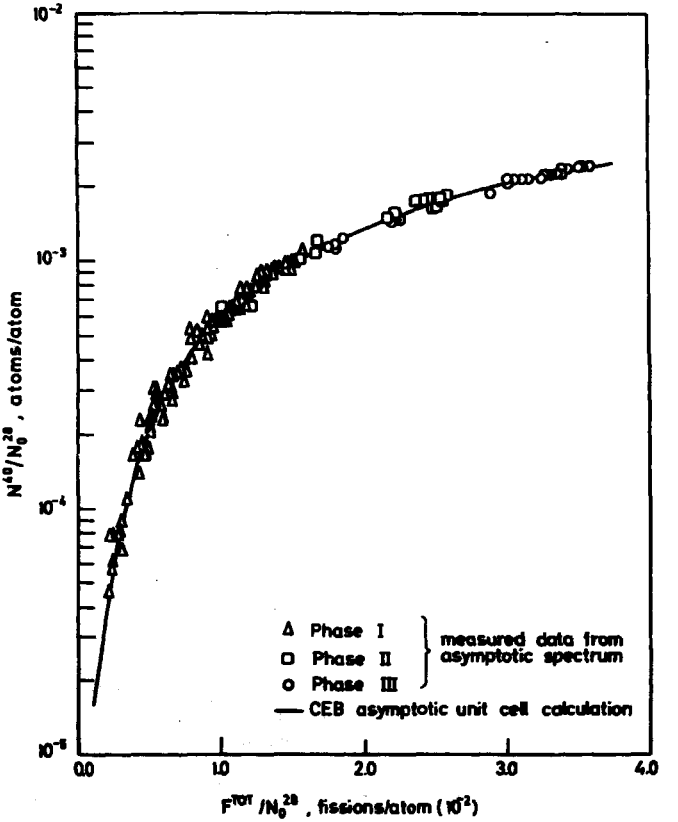

Fig. 37. Pu^{240} concentrations versus accumulated fissions.

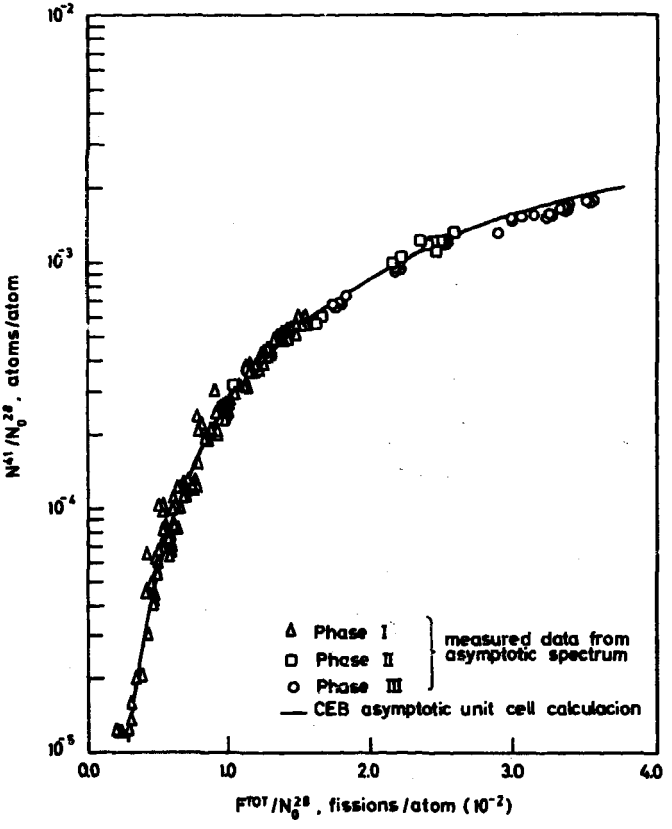

Fig. 38. Pu^{241} concentrations versus accumulated fissions.

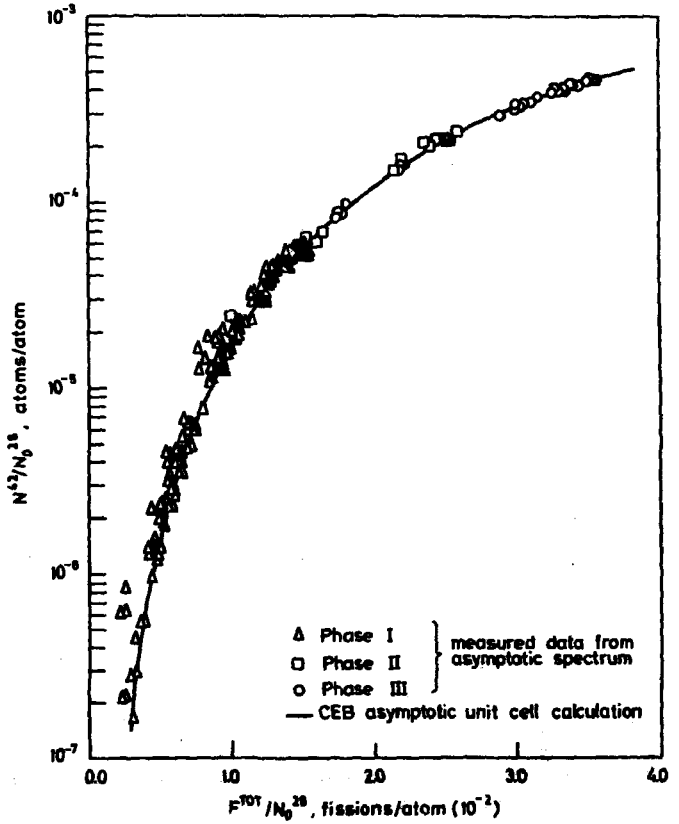

Fig. 39. Pu^{242} concentrations versus accumulated fissions.

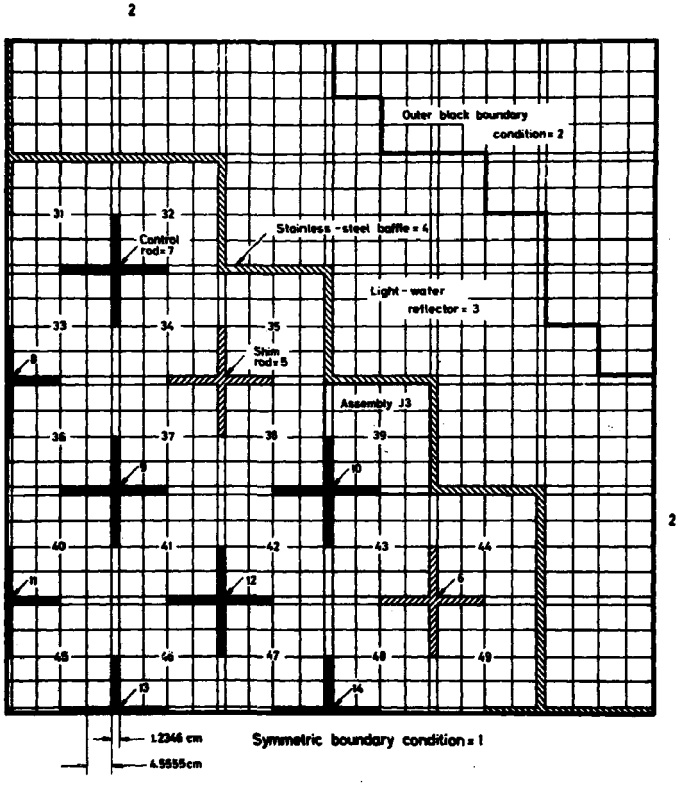

The composition numbers and the cold dimensions used are indicated.

Fig. 40. Mesh and burn-up region descriptions in average axial quarter core DBU and CDB investigations.

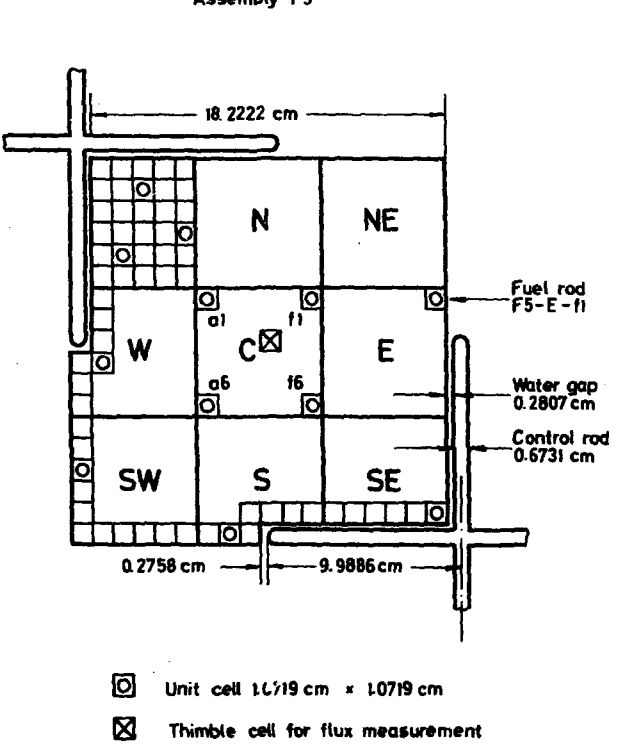

Fig. 41. Plan view of Yankee fuel assembly with cold dimensions and fuel rod core locations.

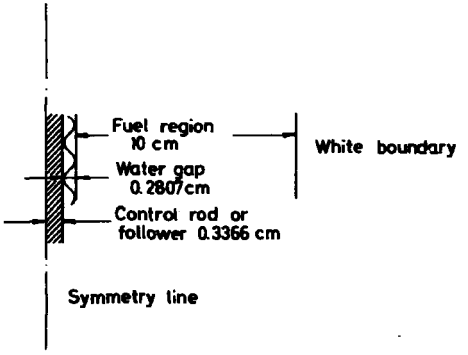

Fig. 42. Dimensions applied in control region calculations performed with CELL and HECS.

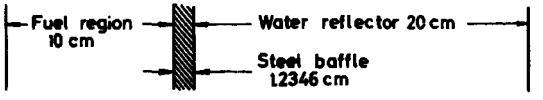

Fig. 43. Dimensions applied in core baffle calculations performed with CELL.

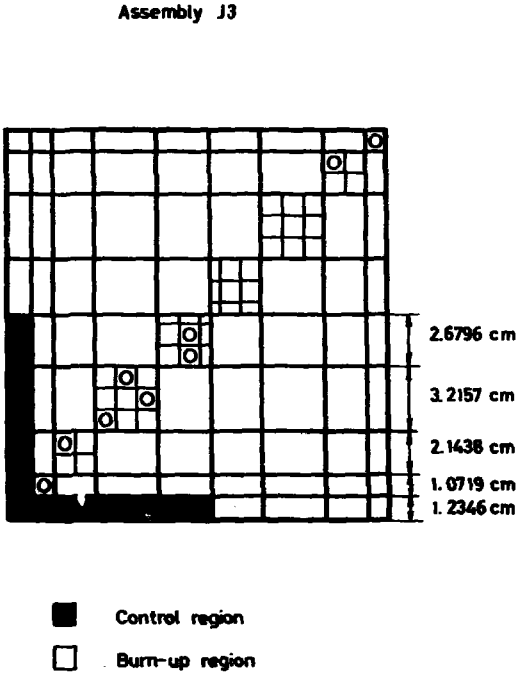

Fig. 44. Detailed mesh description within selected fuel assembly for application in average axial quarter core investigations.

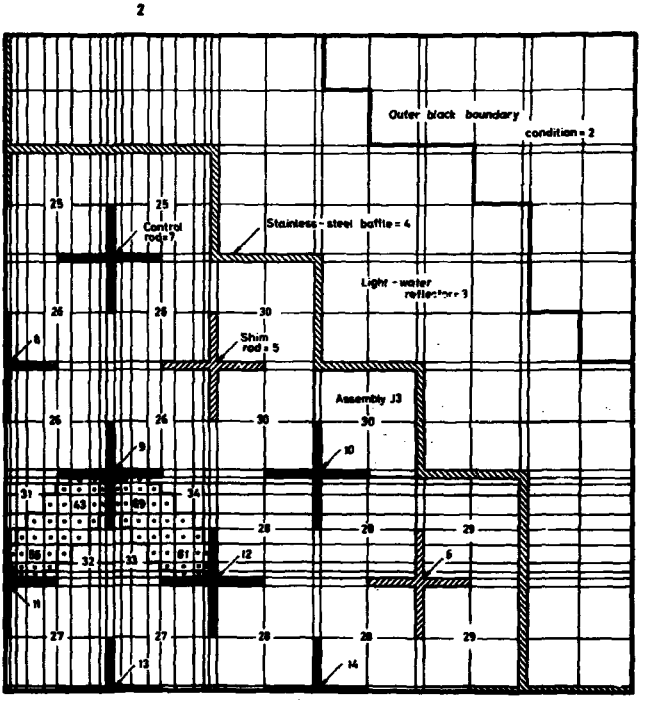

⊡ Refers to detailed burn-up calculation.
The composition numbers used are indicated.

Fig. 45. Mesh and burn-up region descriptions in average axial quarter core CDB investigation of the assemblies F4 and G4.

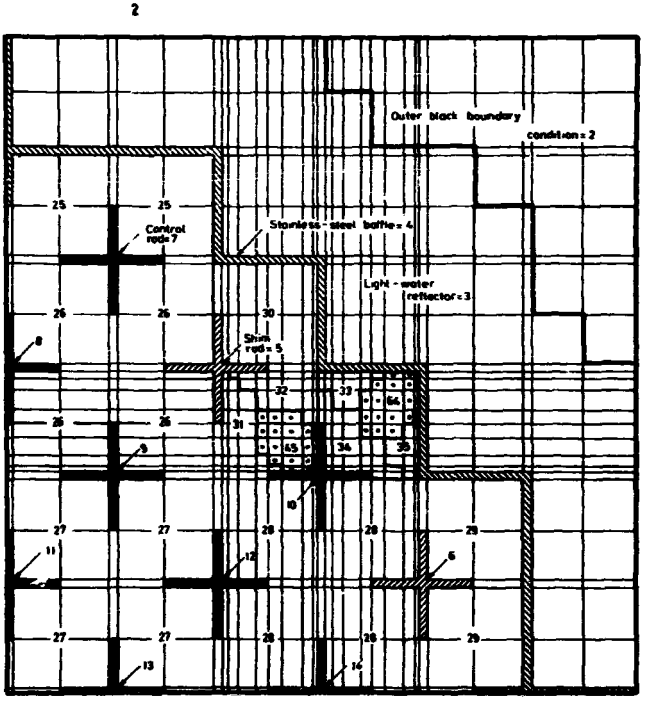

⊡ Refers to detailed burn-up calculation.
The composition numbers used are indicated.

Fig. 46. Mesh and burn-up region descriptions in average axial quarter core CDB investigation of the assemblies H3 and J3.

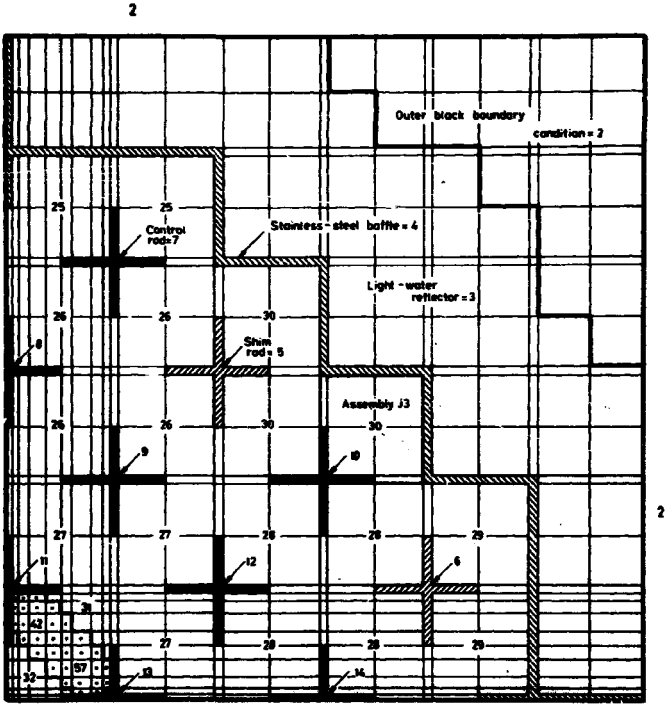

⊡ Refers to detailed burn-up calculation.
The composition numbers used are indicated.

Fig. 47. Mesh and burn-up region descriptions in average axial quarter core CDB investigation of the assembly F5.

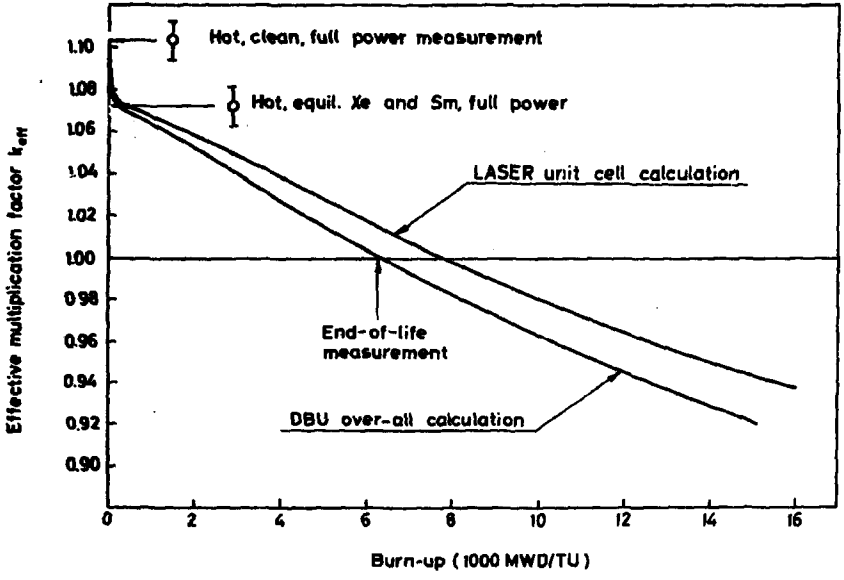

Fig. 48. Yankee Core I effective multiplication factor as a function of burn-up.

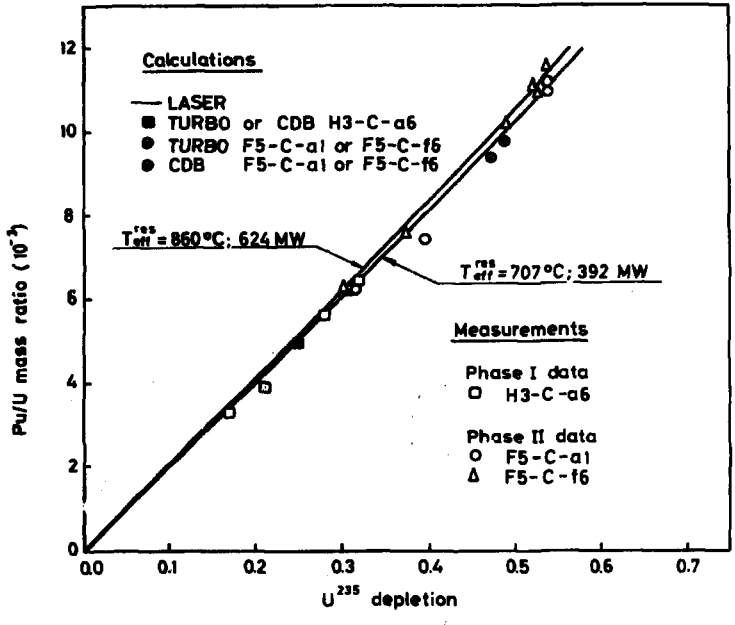

Fig. 49. Variation of plutonium with fuel depletion in asymptotic spectrum.

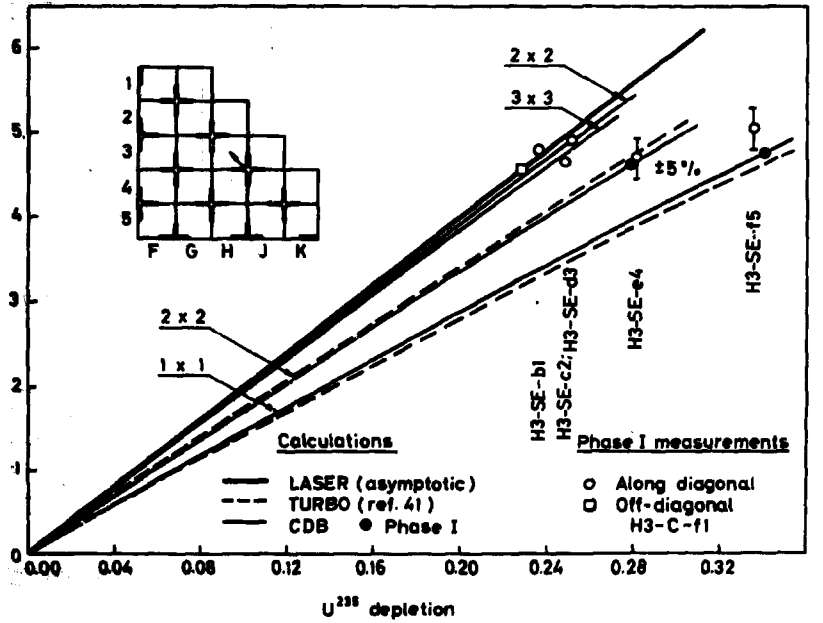

Fig. 50. Average axial net plutonium along the diagonal from zirconium follower to assembly centre of H3 as function of fuel depletion.

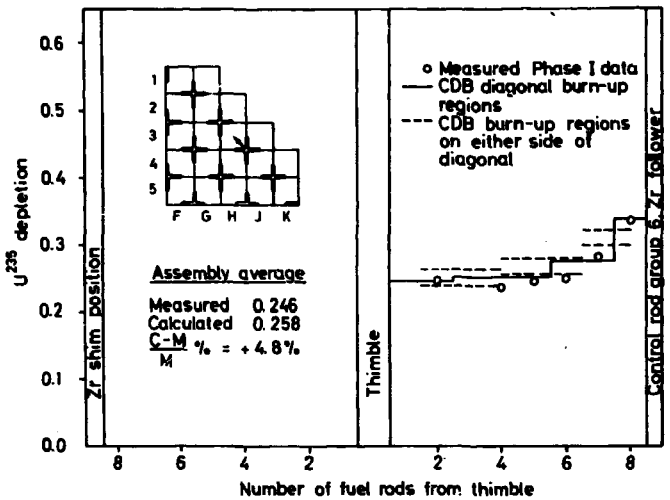

Fig. 51. Average axial fuel depletion across assembly H3.

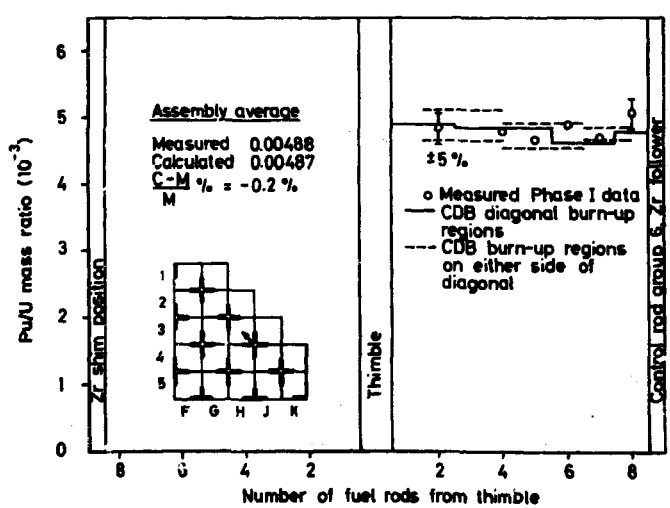

Fig. 52. Average axial plutonium across assembly H3.

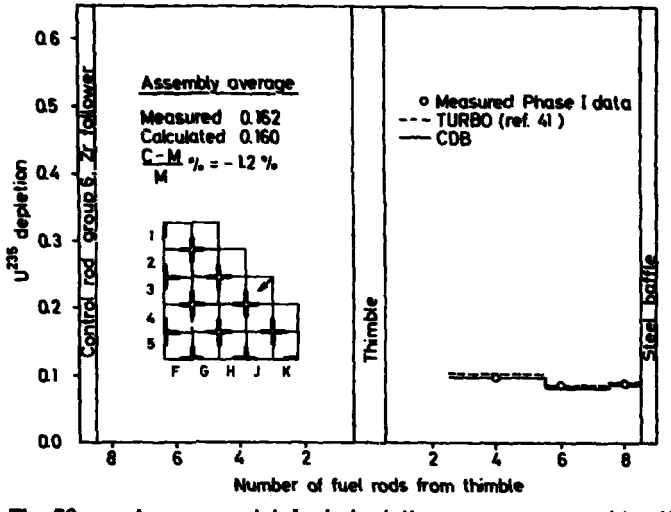

Fig. 53. Average axial fuel depletion across assembly J3.

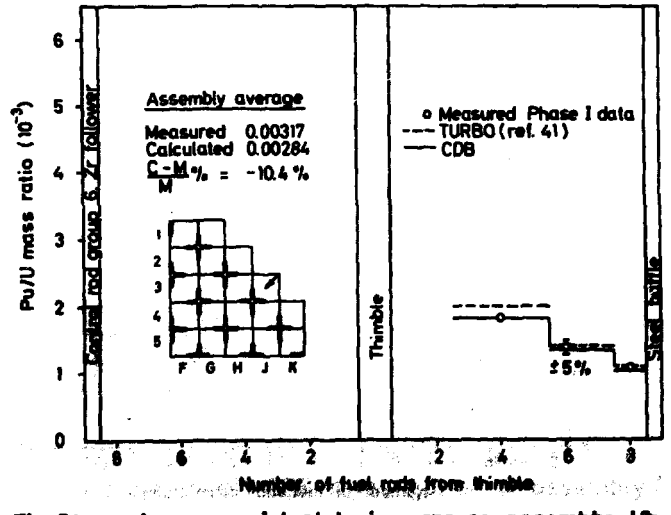

Fig. 54. Average axial plutonium across assembly J3.

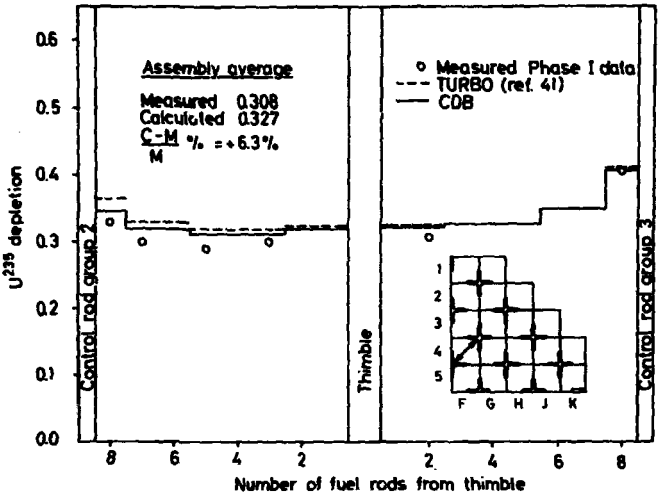

Fig. 55. Average axial fuel depletion across assembly F4.

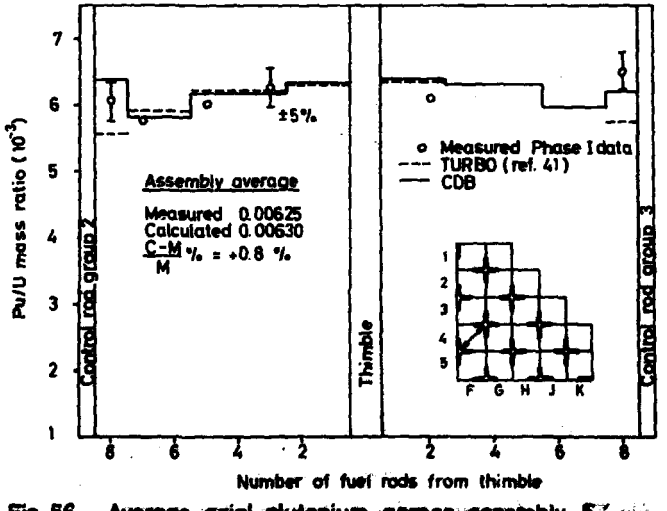

Fig. 56. Average axial plutonium across assembly F4.

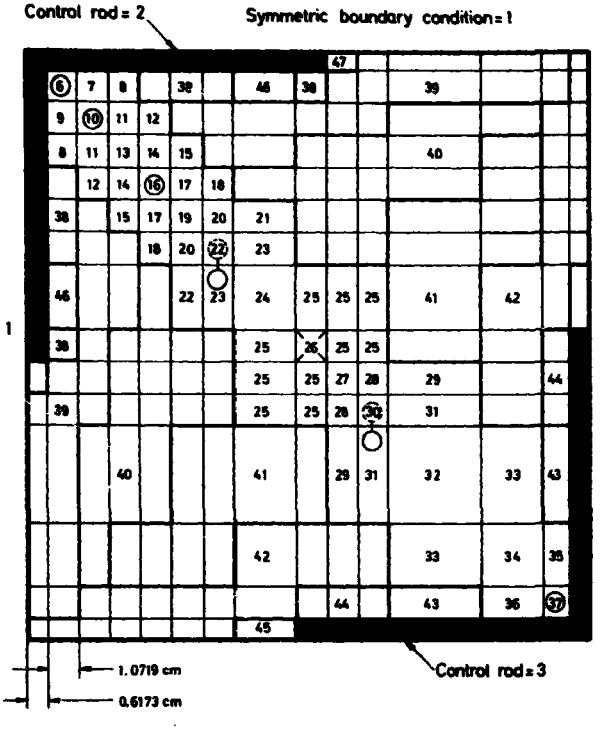

[12] Refers to detailed burn-up calculation.

(16) Location of measured fuel rod.

The composition numbers and the cold dimensions used are indicated.

Fig. 57 Mesh and burn-up region descriptions in average axial CDB investigation of assembly F5.

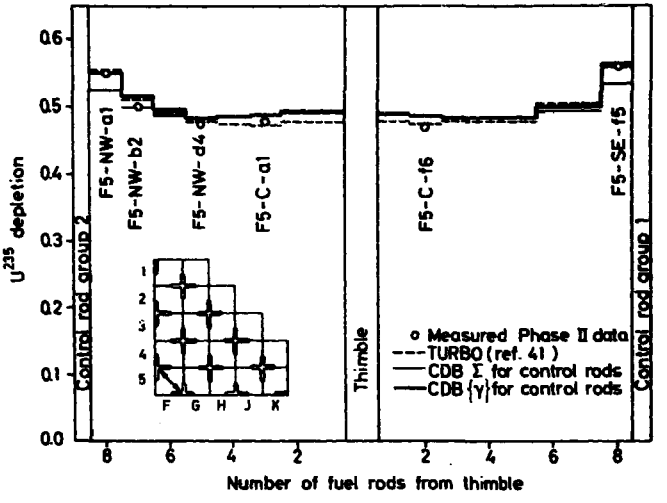

Fig. 58. Distribution of fuel depletion across assembly F5.

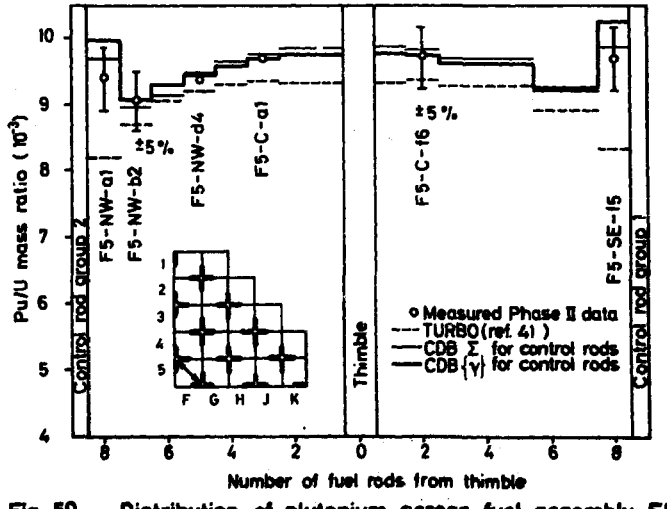

Fig. 59. Distribution of plutonium across fuel assembly F5.

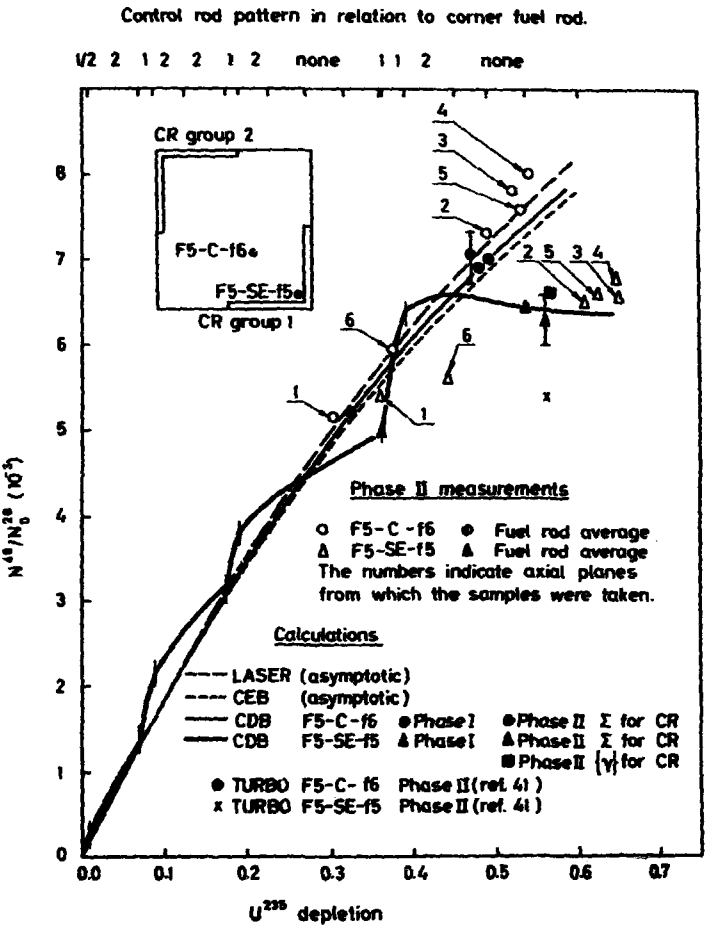

Fig. 60. Variation in Pu^{239} with fuel depletion.

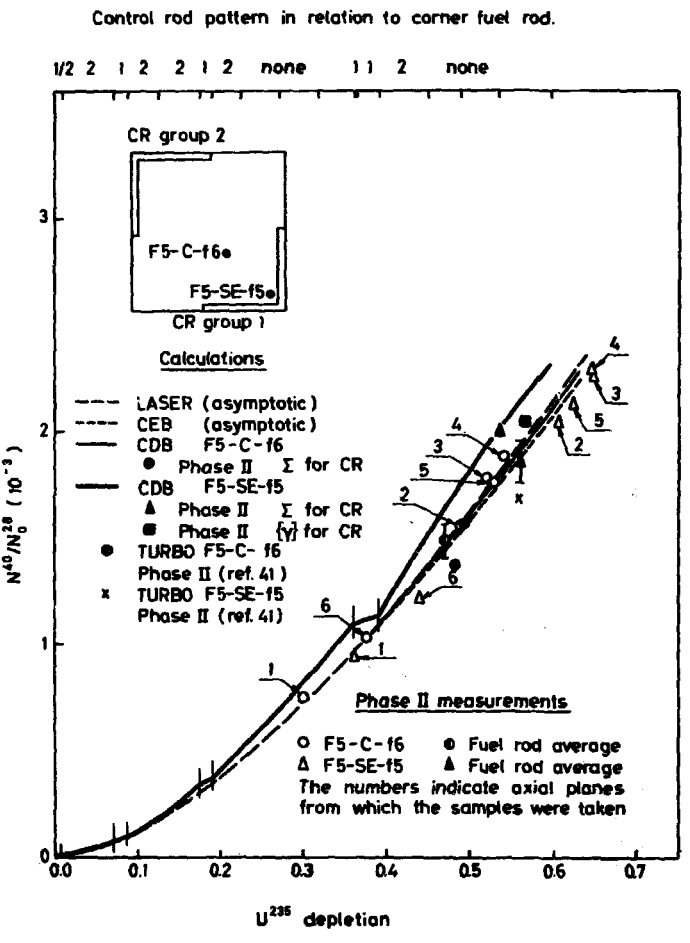

Fig. 61. Variation in Pu^{240} with fuel depletion.

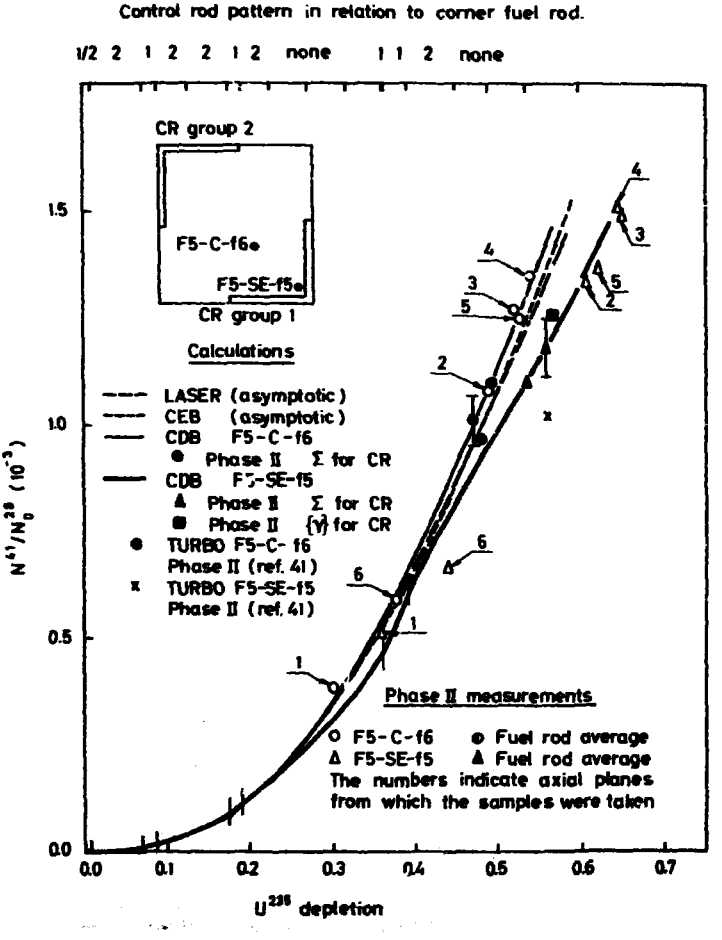

Fig. 62. Variation in Pu^{241} with fuel depletion.

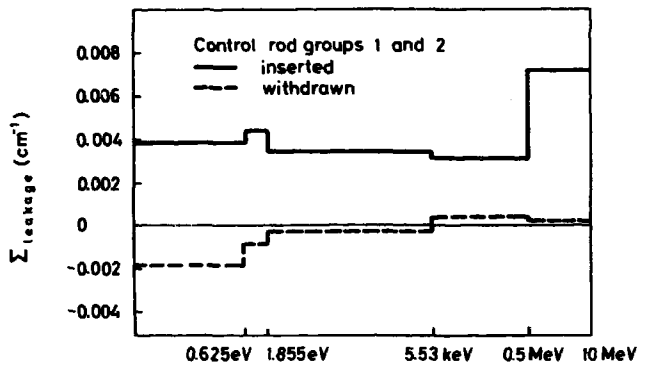

Fig. 63. Typical leakage spectra for an asymptotic fuel rod

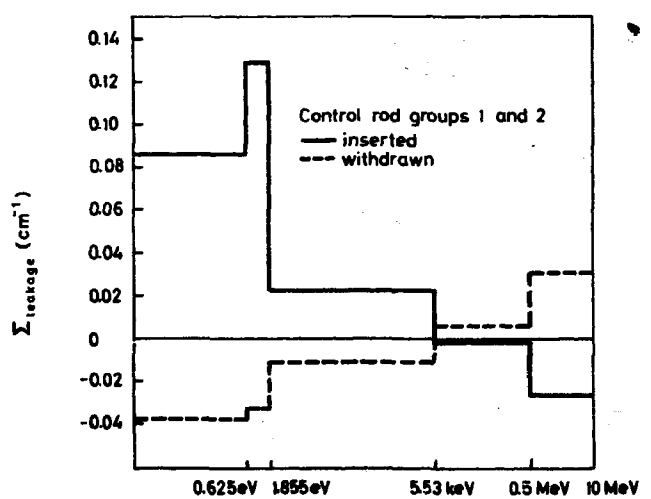

Fig.64. Typical leakage spectra for a corner fuel rod.

Fig. 65. **LASER -**

unit cell burn-up.
Binary deck set-up.

```
            $*TAPE 20520    A9R      RISOE LIBRARY
            $*TAPE 20012    B8R      LASER LIBRARY
            $*TAPE 21077    B9W      CROSS LIBRARY
            $PAUSE
            OPER. ACTION PAUSE

            ..CONTINUING

            $ATTACH         A9
            $AS             SYSLB2
            $REWIND         SYSLB2
            $EXECUTE        IBJOB
IBJOB VERSION 5 HAS CONTROL.
$IBJOB          ALTIO,ALGOLF
$IEDIT          SYSLB2,SCHF13
$IBLDR .FPTRP
$IBLDR UN01
$IBLDR UN02
$IBLDR UN03
$IBLDR UN04
$IBLDR UN07
$IBLDR UN08
$IBLDR UN09
$IBLDR UN10
$IBLDR MAINDK
$ORIGIN         ALPHA
$IBLDR INITDK
$IBLDR FATEDK
$IBLDR LIMBDK
$IBLDR FINDDK
$IBLDR STEPDK
$IBLDR BONEDK
$IBLDR STARDK
$ORIGIN         ALPHA
$IBLDR RATEDK
$IBLDR NUMBDK
$IBLDR SOURDK
$IBLDR TESTDK
$IBLDR NORMDK
$IBLDR RUKUDK
$IBLDR MEMODK
$IBLDR CONTDK
$ORIGIN         ALPHA
$IBLDR SLOWDK
$IBLDR MLTBDK
$ORIGIN         BETA
$IBLDR DATUMD
$IBLDR MUFTDK                                   (continued)
$IBLDR RESONI
```

```
$ORIGIN         BETA
$IBLDR MATEDK
$ORIGIN         BETA
$IBLDR FASTDK
$ORIGIN         ALPHA
$IBLDR TERMDK
$ORIGIN         GAMMA
$IBLDR DATAED
$IBLDR DOPLDK
$IBLDR RETADK
$IBLDR PSIFDK
$ORIGIN         GAMMA
$IBLDR XPREDK
$ORIGIN         GAMMA
$IBLDR GEOMDK
$ORIGIN         GAMMA
$IBLDR ITERDK
$IBLDR RELAXD
$IBLDR RELAPD
$ORIGIN         GAMMA,REW
$IBLDR THERDK
$IBLDR EDITDK
```

Fig.66. **CROSS-**

data processing.
Binary deck set-up.

```
        $*TAPE 21077    B9R     CROSS LIBRARY
        $*TAPE 20425    A6W     CEB LIBRARY
        $PAUSE
        OPER. ACTION PAUSE

        ..CONTINUING

        $EXECUTE        IBJOB
IBJOB VERSION 5 HAS CONTROL.
$IBJOB          ALTIO
$IBLDR UN08
$IBLDR UN09
$IBLDR UN10
$IBLDR MAINDK
$ORIGIN         ALPHA
$IBLDR UPPERD
$ORIGIN         ALPHA
$IBLDR LOWERD
$ORIGIN         ALPHA,REW
$IBLDR FEWGDK
```

Fig. 67. **CELL -**

cross section condensation.
Binary deck set-up.

```
          $*TAPE 20520   A9R      RISOE LIBRARY
          $PAUSE
          OPER. ACTION PAUSE

          ..CONTINUING

          $ATTACH        A9
          $AS            SYSLB2
          $REWIND        SYSLB2
          $EXECUTE       IBJOB
IBJOB VERSION 5 HAS CONTROL.
$IBJOB         ALTIO
$IEDIT         SYSLB2,SCHF4
$IBLDR CELL
$IBLDR PREPA
$IBLDR CPMA
$IBLDR SOLOA
$IBLDR CONDA
$ORIGIN        ALFA
$IBLDR PREPP
$IBLDR PREPF
$ORIGIN        ALFA
$IBLDR CPMP
$IBLDR CPMF
$ORIGIN        ALFA
$IBLDR SOLOP
$IBLDR SOLOF
$ORIGIN        ALFA,REW
$IBLDR FLUXP
$IBLDR CONDP
$IBLDR CONDF
```

Fig. 68. **CEB -**

fast unit cell burn-up.
Binary deck set-up.

```
            $*TAPE 20520    A9R      RISOE LIBRARY
            $*TAPE 20425    A6R      CEB LIBRARY
            $ATTACH         A9
            $AS             SYSLB2
            $PAUSE
            OPER. ACTION PAUSE

            ..CONTINUING

            $REWIND         SYSLB2
            $EXECUTE        IBJOB
IBJOB VERSION 5 HAS CONTROL.
$IBJOB          ALTIO
$IEDIT          SYSLB2,SCHF3
$IBLDR CEB
$IBLDR DAPAA
$IBLDR SOLUA
$ORIGIN         ALFA
$IBLDR DAPAP
$IBLDR FIDAP
$IBLDR DAPAF
$ORIGIN         ALFA
$IBLDR STEPP
$IBLDR FIPOP
$IBLDR BURNP
$IBLDR CPMP
$IBLDR SOLUP
$IBLDR FLUXP
$IBLDR EDITP
$IBLDR SOLUF
```

Fig.69. **TWODIM -**

over-all flux solution.
Binary deck set-up.

```
          $*TAPE 20520    A9R      RISOE LIBRARY
          $ATTACH         AS
          $AS             SYSLB2
          $REWIND         SYSLB2
          $PAUSE
          OPER. ACTION PAUSE

          ..CONTINUING

          $EXECUTE        IBJOB
IBJOB VERSION 5 HAS CONTROL.
$IBJOB          ALTIO
$IEDIT          SYSLB2,SCHF2
$IBLDR MAIN
$IBLDR COARA
$IBLDR FINEA
$IBLDR COESA
$IBLDR SVORA
$IBLDR SHORA
$IBLDR COEBA
$IBLDR BVORA
$IBLDR BHORA
$IBLDR FLUCA
$ORIGIN         ALFA
$IBLDR FLUCP
$IBLDR REACP
$IBLDR FLUCF
$ORIGIN         ALFA
$IBLDR COARP
$IBLDR COARF
$ORIGIN         ALFA
$IBLDR FINEP
$IBLDR FINEF
$ORIGIN         ALFA
$IBLDR COESP
$IBLDR COESF
$ORIGIN         ALFA,REW
$IBLDR SVORP
$IBLDR SVORF
$ORIGIN         ALFA,REW
$IBLDR SHORP
$IBLDR SHORF
$ORIGIN         ALFA
$IBLDR COEBP                                  (continued)
$IBLDR COEBF
```

```
$ORIGIN         ALFA,REW
$IBLDR BVORP
$IBLDR BVORF
$ORIGIN         ALFA,REW
$IBLDR BHORP
$IBLDR BHORF
```

Fig. 70. **DBU-**

over-all burn - up.
Binary deck set - up.

```
          $*TAPE 20520   A9R      RISOE LIBRARY
          $*TAPE SCRATCH A6W
          $PAUSE
          OPER. ACTION PAUSE

          ..CONTINUING

          $ATTACH        A9
          $AS            SYSLB2
          $REWIND        SYSLB2
          $EXECUTE       IBJOB
IBJOB VERSION 5 HAS CONTROL.
$IBJOB          ALTIO
$IBLDR MAIN
$IBLDR REGIA
$IBLDR A.LGUN
$IEDIT          SYSLB2,SCHF2
$IBLDR COARA
$IBLDR FINEA
$IBLDR COESA
$IBLDR SVORA
$IBLDR SHORA
$IBLDR COEBA
$IBLDR BVORA
$IBLDR BHORA
$IBLDR FLUCA
$ORIGIN         ALFA
$IEDIT          SYSIN1
$IBLDR ROMOP
$IEDIT          SYSLB2,SRCH
$IBLDR FLUCP
$IBLDR REACP
$IBLDR RUMAP                                  (continued)
$IBLDR FLUCF
```

```
$ORIGIN         ALFA
$IBLDR COARP
$IBLDR COARF
$ORIGIN         ALFA
$IBLDR BUDAP
$IBLDR FINEP
$IBLDR FINEF
$ORIGIN         ALFA
$IBLDR BUDIP
$IBLDR REGIP
$IEDIT          SYSIN1
$IBLDR XENTP
$IEDIT          SYSLB2,SRCH
$IBLDR REGIF
$ORIGIN         ALFA
$IBLDR COESP
$IBLDR COESF
$ORIGIN         ALFA,REW
$IBLDR SVORP
$IBLDR SVORF
$ORIGIN         ALFA,REW
$IBLDR SHORP
$IBLDR SHORF
$ORIGIN         ALFA
$IBLDR COEBP
$IBLDR COEBF
$ORIGIN         ALFA,REW
$IBLDR BVORP
$IBLDR BVORF
$ORIGIN         ALFA,REW
$IBLDR BHORP
$IBLDR BHORF
```

Fig.71. **CDB-**

combined unit cell and over-all burn-up.
Binary deck set-up.

```
            $*TAPE 20520   A9R      RISOE LIBRARY
            $*TAPE 20425   B6R      CDB LIBRARY
            $*TAPE SCRATCH A6W
            $PAUSE
            OPER. ACTION PAUSE

            ..CONTINUING

            $ATTACH        A9
            $AS            SYSLB2
            $REWIND        SYSLB2
            $EXECUTE       IBJOB
IBJOB VERSION 5 HAS CONTROL.
$IBJOB          ALTIO,MAP
$IBLDR MAIN
$IBLDR CEBUA
$IBLDR A.LGUN
$IEDIT          SYSLB2,SCHF2
$IBLDR COARA
$IBLDR FINEA
$IBLDR COESA
$IBLDR SVORA
$IBLDR SHORA
$IBLDR COEBA
$IBLDR BVORA
$IBLDR BHORA
$IBLDR FLUCA
$ORIGIN         ALFA
$IBLDR FLUCP
$IBLDR REACP
$IBLDR BUMAP
$IBLDR FLUCF
$ORIGIN         ALFA
$IBLDR COARP
$IBLDR COARF
$ORIGIN         ALFA
$IEDIT          SYSIN1
$IBLDR CEDAP
$IEDIT          SYSLB2,SRCH
$IBLDR FINEP                                    (continued)
$IBLDR FINEF
```

```
$ORIGIN         ALFA
$IEDIT          SYSIN1
$IBLDR CEBUP
$IBLDR TIMSA
$IBLDR DEPLA
$IBLDR CEDIA
$IBLDR CEBUF
$ORIGIN         BETA
$IBLDR TIMSP
$IBLDR TIMSF
$ORIGIN         BETA
$IBLDR MACRP
$IBLDR DEPLP
$IEDIT          SYSLB2,SCHF3
$IBLDR BURNP
$IBLDR CPMP
$IBLDR SOLUP
$IEDIT          SYSIN1
$IBLDR DEPLF
$ORIGIN         BETA
$IBLDR CEDIP
$IBLDR CEDIF
$ORIGIN         ALFA
$IEDIT          SYSLB2,SCHF2
$IBLDR COESP
$IBLDR COESF
$ORIGIN         ALFA,REW
$IBLDR SVORP
$IBLDR SVORF
$ORIGIN         ALFA,REW
$IBLDR SHORP
$IBLDR SHORF
$ORIGIN         ALFA
$IBLDR COEBP
$IBLDR COEBF
$ORIGIN         ALFA,REW
$IBLDR BVORP
$IBLDR BVORF
$ORIGIN         ALFA,REW
$IBLDR BHORP
$IBLDR BHORF
```